Characterisation and Production of Small Extracellular Vesicles from Human Bone Marrow Mesenchymal Stromal Cells



Rui Lei

St Hugh's College

University of Oxford

A thesis submitted for the degree of

Doctor of Philosophy in Engineering Science

Hilary 2023

Contents

Acknowledgements 4
List of Publications 5
Abstract 6
List of Figures 9
List of Tables 11
List of Abbreviations 13
Chapter 1 Introduction 16
1.1 Background 16
1.2 Knowledge Gap and Research Questions 17
1.3 Aims and Objectives 20
1.4 Thesis Structure 21
Chapter 2 Literature Review 23
2.1 Bone Marrow Mesenchymal Stromal Cells Derived Small Extracellular Vesicles 23
2.2 Functional Studies and Applications of MSC-sEVs 28
2.3 Characterisation of sEVs 33
2.4 Production of sEVs 33
2.5 Isolation and Purification of sEVs 40
2.6 Challenges in Clinical Applications of MSC-sEVs 47
Chapter 3 Characterisation and Functional Studies of Small Extracellular Vesicles from Human Bone Marrow Mesenchymal Stromal Cells on Skin Regeneration 51
3.1 Abstract 52
3.2 Introduction 54
3.3 Materials and Methods 58
3.4 Results 69
3.5 Discussion 78
3.6 Supplementary Information 85
Chapter 4 An Automated, High-throughput, Hollow Fibre Bioreactor System for Production of Mesenchymal Stromal Cells Derived Small Extracellular Vesicles 95
4.1 Abstract 96

4.2 Introduction 98
4.3 Materials and Methods 102
4.4 Results 113
4.5 Discussion 121
Chapter 5 Purification of Mesenchymal Stromal Cell derived Small Extracellular Vesicles Using Ultrafiltration 128
5.1 Abstract 129
5.2 Introduction 131
5.3 Materials and Methods 134
5.4 Results 142
5.5 Discussion 158
5.6 Supplementary Information 169
Chapter 6 Conclusions and Future Work 175
6.1 Conclusions 175
6.2 Limitations and Future Work 178
References 181

Acknowledgements

I would like to express my deepest gratitude to my supervisors, Professor Zhanfeng Cui and Professor Cathy Ye, for their guidance, support, and encouragement throughout my PhD journey. Their expertise, patience, and insightful feedback have been invaluable in shaping my research.

I would like to extend my thanks to all members of the Tissue Engineering group, for their support and camaraderie. Thanks to Shuai, Simge, Li, Nianlin, Tamiris, their presence and sense of humor have made the PhD journey a much more enjoyable experience. I am also grateful to the colleagues from the Oxford Suzhou Centre for Advanced Research (OSCAR), especially Dr Hui Wang, Yida, Binbin, Jiachen, Weizhi, for their welcome and support during my visit to OSCAR.

My particular thanks go to my boyfriend Haodong He, for his unfailing support and continuous encouragement throughout my PhD journey. Thank you, for your love, company and understanding.

Finally, I would like to express my deepest appreciation to my parents and my grandma, for their unwavering love, support, and patience. Their encouragement and understanding have been crucial in enabling me to pursue my academic aspirations. Special thanks and love to my late grandfather, I know he would be proud of me.

Thank you all for being part of this journey with me. I could not have done it without your support.

List of Publications

The work reported in this thesis has produced the following publications:

1. Risto, M., **Lei, R.**, Zeng, Y., Zhu, J., Chang, H., Ye, H., Cui, Z. Membrane Applications in Autologous Cell Therapy. *Membranes* 12, no. 12: 1182 (2022). [Co-first author]
2. **Lei, R.**, Wang, H., Cui, Z., Ye, H. Characterisation and Functional Studies of Small Extracellular Vesicles from Human Bone Marrow Mesenchymal Stromal Cells on Skin Regeneration. *To be submitted.*
3. **Lei, R.**, Zeng, Y., Cui, Z., Ye, H. An Automated, High-throughput, Hollow Fibre Bioreactor System for Production of Mesenchymal Stromal Cells Derived Small Extracellular Vesicles. *To be submitted.*
4. **Lei, R.**, Ren, S., Ye, H., Cui, Z. Purification of Mesenchymal Stromal Cells Derived Small Extracellular Vesicles Using Ultrafiltration. *To be submitted.*

Rui Lei is an inventor of the following patent:

1. A novel cell reactor and cell production method thereof, Patent Application No. CN202211437349.2, filed on 17th November 2022

Abstract

Small extracellular vesicles (sEVs) released by mesenchymal stromal/stem cells (MSCs) have been broadly reported to be the key paracrine mediators that trigger the therapeutic action of MSCs in various diseases and tissue regeneration processes. Therefore, human MSC derived sEVs (MSC-sEVs) can serve as a promising cell-free therapeutic alternative to the MSC therapy in regenerative medicine. To achieve widespread clinical applications of MSC-sEVs, the development of a reliable functional identification tool set to quantify their physiological and biological effects and a robust method for the scaled production of high-end MSC-sEVs is critical.

In this project, a methodology to harvest, separate and characterise MSC-sEVs was established. A normal human dermal fibroblast (NHDF) based wound healing model was developed for functional identification and assessment of MSC secretome, including MSC-sEVs. The proliferation and migration of NHDFs were quantified with or without the treatment of various secretome from different cells. Based on experimental data, a comprehensive comparison in terms of the wound healing potential was conducted between different MSC secretome fractions, suggesting that MSC-sEV might be the most effective fraction in promoting NHDF migration, and also outperformed the corresponding sEV fraction from the recipient NHDFs. The developed NHDF-based wound healing model was proved to be a useful tool for in vitro functional identification and assessment of cellular secretome.

After confirming the promising regenerative effects of MSC-sEVs on skin regeneration, an automated enclosed hollow fibre bioreactor (HFBR) based cell expansion system (CES) was established to produce MSC-sEVs at scale. The developed HFBR-based CES was shown to be a practical method for industrial-scale production of MSC-sEVs with advantages of automatic processes, acceptable cost, high reproducibility and biosafety, which enabled a continuous production of high quality MSC-sEVs for 13 days, and achieved a 250-fold higher yield of purer MSC-sEVs than the conventional flask approach.

Ultrafiltration was also explored to separate and purify the produced MSC-sEV at scale. The impacts of membrane pore size and various operational parameters on the membrane separation of sEVs were investigated. Then, a fed-batch ultra-diafiltration (UF/DF) protocol with optimised filtration parameters was designed accordingly for the isolation and purification of MSC-sEVs, that is, operating at lower transmembrane pressure using a 500 kDa molecular weight cut-off membrane, with the assistance of moderate stirring speed and at least 6 diafiltration steps. Evidence confirmed that the subsequently developed fed-batch UF/DF protocol can achieve MSC-sEV preparations with a 3-fold higher yield and nearly doubled purity, in comparison to the common ultracentrifugation method. With advantages including high recovery, efficient production, excellent scalability, process automation, and cost-effectiveness, the proposed fed-batch UF/DF protocol could be an attractive method for both small lab-scale separation and industrial scale manufacture of MSC-sEVs.

Overall, by providing viable solutions to the current challenges of functional characterisation, scaled production and efficient purification, the outcome of this thesis could pave the way for rapid development of the MSC-sEV based therapeutics and progress in clinical applications.

List of Figures

Figure 2.1 Biogenesis of extracellular vesicles.....27

Figure 3.1 Flow chart of the fractionation protocol of secretome fractions. 61

Figure 3.2 Characterisation of MSC-sEV and HDF-sEV 70

Figure 3.3 The effect of cellular secretome at different concentration (represented as C) on migration of NHDFs 73

Figure 3.4 The effect of cellular secretome at different concentration (represented as C) on proliferation of NHDFs.....77

Figure 4.1 Detail information of the modified Oxford MEStar Cell Expansion System 104

Figure 4.2 Glucose and lactate level in the CES during the 13-day cell culture. 114

Figure 4.3 Characterisation of Flask-sEV and CES-sEV 115

Figure 4.4 The yield and purity of sEVs produced by traditional flask method and CES method.....118

Figure 4.5 Functional potency of sEVs.....120

Figure 5.1 Experimental set-up for stirred cell ultrafiltration system.....137

Figure 5.2.The effects of membrane pore size on sEV isolation 143

Figure 5.3 The effects of stirring speed on sEV isolation process.....147

Figure 5.4 The effects of applied pressure on sEV isolation 149

Figure 5.5 The effects of direct dilution and diafiltration on sEV isolation 151

Figure 5.6 Flow chart of the fed-batch UF/DF process and ultracentrifugation process. 154

Figure 5.7 Characterisation of UF-sEV and UC-sEV 156

Supplementary Figure 3.1 Original images from the western blot data shown in Figure 3.2d 85

Supplementary Figure 3.2 Bright field images of NHDFs treated with different secretome fractions at 0 h, 6 h and 18 h. 86

Supplementary Figure 5.1 Computational fluid dynamics simulation 171

Supplementary Figure 5.2 The effects of stirring speed on the properties of the sEV preparations 172

Supplementary Figure 5.3 The effects of direct dilution and diafiltration on particle recovery and isolation process 173

List of Tables

Table 2.1 Pros and cons of common sEV isolation methods. 41

Table 4.1 Comparison of traditional flask method and CES method for sEV production. 116

Table 5.1 Calculation of average shear rate at different stirring speeds 146

Table 5.2 Comparison of fed-batch UF/DF method and UC method for sEV isolation. 157

Supplementary Table 3.1 GLM ANOVA results for migration (cell covered area of the gap in μm2) of NHDFs in response to factors of migration time (Hour), three secretome fraction types from MSC (Treatment) and concentration of secretome (Concentration) 87

Supplementary Table 3.2 Results of Tukey's post-hoc multiple comparisons between different secretome fractions of MSC at different concentrations (e.g. MSC-sEV-1 means the group treated with MSC-sEV at 1 μg/mL) for their effects on migration behaviour of NHDFs 88

Supplementary Table 3.3 GLM ANOVA results for migration (cell covered area of the gap in μm2) of NHDFs in response to factors of migration time (Hour), two secretome fraction types from MSC (Treatment) and concentration of secretome (Concentration) 89

Supplementary Table 3.4 Results of Tukey's post-hoc multiple comparisons between two secretome fractions of MSC at different concentrations (e.g. MSC-CM-1 means the group treated with MSC-CM at 1 μg/mL) for their effects on migration behaviour of NHDFs 90

Supplementary Table 3.5 GLM ANOVA results for migration (cell covered area of the gap in μm2) of NHDFs in response to factors of migration time (Hour), cell source of sEVs (sEV type) and concentration of sEVs (Concentration) 91

Supplementary Table 3.6 Results of Tukey's post-hoc multiple comparisons between different sEV types at different concentrations (e.g. MSC-sEV-0.01 means the group treated with MSC-sEV at 0.01 μg/mL) for their effects on migration behaviour of NHDFs 92

Supplementary Table 3.7 GLM ANOVA results for proliferation (Folds of OD450 at Day 0) of NHDFs in response to factors of treatment time (Day), cell source of secretome (Cell Source) and secretome fraction type (Treatment) at concentration ≤ 30 μg/mL 93

Supplementary Table 3.8 Results of Tukey's post-hoc multiple comparisons between different secretome fraction types at different concentrations (e.g. MSC-sEV-1 means the group treated with MSC-sEV at 1 μg/mL) for their effects on proliferation behaviour of NHDFs 94

List of Abbreviations

AD-MSC-sEV	Adipose mesenchymal stromal cell derived small extracellular vesicle
AKI	Acute kidney injury
BCA	Bicinchoninic acid
BM-MSC	Bone marrow mesenchymal stromal cell
BM-MSC-sEV	Bone marrow mesenchymal stromal cell derived small extracellular vesicle
CCK-8	Cell Counting Kit-8
CKD	Chronic kidney disease
CES	Cell expansion system
CES-MSC	Mesenchymal stromal cells cultured in cell expansion system
CES-sEV	Small extracellular vesicles produced by cell expansion system-cultured mesenchymal stromal cells
CFD	Computational fluid dynamics
CM	Conditioned medium
CVD	Constant volume diafiltration
DC	Differential centrifugation
DF	Degree of freedom
DGC	Density gradient centrifugation
DMEM	Dulbecco's Modified Eagle Medium
DOE	Design of Experiments
DV	Diafiltration volume
ECS	Extracapillary space
ECS CIRCULATION	Extracapillary space circulation line
ECS FEED	Extracapillary space feed line
EV	Extracellular vesicle
FBS	Fetal bovine serum
FBS-EV	Fetal bovine serum derived extracellular vesicle
Flask-MSC	Mesenchymal stromal cells cultured in flasks
Flask-sEV	Small extracellular vesicles produced by flask-cultured mesenchymal stromal cells

GLM	General linear model
GMP	Good manufacturing practice
hBM-MSC	Human bone marrow mesenchymal stromal cell
HDF-CM	Conditioned medium of normal human dermal fibroblasts
HDF-NsEV	Non-small extracellular vesicle fraction of HDF-CM
HDF-sEV	Normal human dermal fibroblasts derived small extracellular vesicle
HFBR	Hollow fibre bioreactor
hTERT-MSC	hTERT-immortalized bone marrow mesenchymal stromal cell
ICS	Intracapillary space
ICS CIRC.	Intracapillary space circulation line
ICS FEED	Intracapillary space feed line
ILV	Intraluminal vesicle
ISEV	International society for extracellular vesicles
mAb	Monoclonal antibody
MF	Microfiltration
MHC	Major histocompatibility complex
MSC	Mesenchymal stromal/stem cell
MSC-CM	Conditioned medium of mesenchymal stromal cells
MSC-NsEV	Non-small extracellular vesicle fraction of MSC-CM
MSC-sEV	Mesenchymal stromal cell derived small extracellular vesicle
MVB	Multivesicular body
MWCO	Molecular weight cut-off
NHDF	Normal human dermal fibroblast
NsEV	Non-small extracellular vesicle
NTA	Nanoparticle tracking analysis
OD	Optical Density
OD 450	Optical Density assessed at 450 nm
PBS	Phosphate buffered saline
PEG	Polyethylene glycol
PROSPR	Protein organic solvent precipitation
PVDF	Polyvinylidene fluoride
qPCR	Quantitative polymerase chain reaction
SD	Standard deviation

SEC	Size exclusion chromatography
sEV	Small extracellular vesicle
TEM	Transmission electron microscopy
TFF	Tangential flow filtration
TMP	Transmembrane pressure
UC	Ultracentrifugation
UC-MSC-sEV	Umbilical cord mesenchymal stromal cell derived small extracellular vesicle
UF	Ultrafiltration
UF/DF	Ultra-diafiltration, ultrafiltration combined with diafiltration

Chapter 1 Introduction

1.1 Background

Human bone marrow mesenchymal stromal cells (hBM-MSCs) have originally been thought to be an effective therapeutic tool in the field of tissue engineering and regenerative medicine via cell replacement and multipotential differentiation [1,2]. However, Mesenchymal stromal/stem cell (MSC) therapy is accompanied with a series of risk considerations, including immune rejection and tumorigenic potential during the treatment, as well as technical challenges such as cell handling, harvesting, preservation, etc [3]. More recently, it was shown that MSCs had a low rate of engraftment but long-lasting curative effects following transplantation, indicating that engraftment and differentiation may not be the primary mechanism of action [4]. Extensive studies suggested that MSCs displayed their regenerative effects largely via paracrine signalling [5–7], by secreting numerous bioactive factors including soluble molecules [8] like cytokines, growth factors, chemokines, and extracellular vesicles (EVs) [9] into the extracellular environment, i.e. the conditioned medium of MSCs (MSC-CM), to interact with the target cells or tissues.

Small extracellular vesicles (sEVs) refer to cell naturally secreted, non-replicable, bilipid membranous nanoparticles which are smaller than 200 nm in diameter [10,11]. It has been widely established that sEVs secreted by their parent cells can play a crucial role in various physiological and pathological processes by transporting preassembled

biological information (such as genetic materials, proteins, and lipids) to the target cells for cellular communication and behaviour alteration [12–15]. As a result, sEVs can serve as a promising tool for disease diagnostics [16], drug delivery [17], tissue regeneration [18] and immunomodulation [19]. The small extracellular vesicles secreted by MSCs (MSC-sEV) have drawn increasing attention recently as they are believed to be responsible for the beneficial paracrine effects of MSC therapy [20–22]. Particularly, a growing amount of evidence has shown that MSC-sEVs are the vital paracrine mediators that trigger the therapeutic action of MSCs in a variety of tissue regeneration processes of nervous systems, heart, bone, cartilage, kidney, liver, lung, muscle, skin, etc [23]. Increasing interest has been attracted to MSC-sEVs for their role as an appealing cell-free therapeutic strategy which could also bypass the risk issues associated with live MSC therapy in regenerative medicine.

1.2 Knowledge Gap and Research Questions

Production and clinical applications of high-end MSC-sEV products has been severely hampered by a lack of functional identification platform. It is conceivable that the secretome in the conditioned medium of MSCs may involve both useful components, like soluble proteins and sEVs, as well as unfavourable factors, such as metabolic waste that may induce conflicting effects. However, there has been little research that quantitatively compare the functional potency between the MSC-sEV, the non-sEV fraction of MSC secretome (MSC-NsEV), and the complete MSC-CM, which could be confounding in subsequent research and applications. Additionally, the

corresponding secreted compounds of the recipient cells should also be taken into account as a control group but were rarely studied in previous research. Thus, it is especially crucial to develop a reliable bioassay-based detection tool for identification and evaluation of the functional alterations stimulated by different fractions of MSC secretome, for the purpose of precise clinical research and applications.

The scale production of high quality MSC-sEVs is the technical foundation for the clinical translation of MSC-sEV therapy [24]. However, the low yield of sEV production is a major obstacle to the implementation of MSCs-sEV product in therapeutic applications [25]. The current method of producing sEVs relies on the harvest of conditioned medium from conventional method using flasks or dishes, where the cell culture and the subsequent sEV yield are constrained by the limited cell growth area [26]. In order to address this technical challenge, the most direct approach is to expand the cell culture platform to accommodate more cells for large-scale manufacture of sEV-based products [27]. For instance, multilayer Nunc™ Cell Factory [28], microcarriers in stirred tank bioreactors [29], and hollow fibre membrane based bioreactors (HFBR) [30,31] have been applied to increase the cell culture area for cell expansion and sEV manufacture. Among previous methods, the hollow fibre bioreactor emerges as a powerful sEV production system, due to the ability of continuously producing and concentrating cell secreted products, as well as its scalability. However, this HFBR-based method has been largely restricted to manually operated and poorly monitored lab-scale test with high dependence on good manufacturing practice (GMP) facilities.

Therefore, a highly automated, scalable and closed HFBR-based system need to be developed to achieve efficient and economical production of high quality MSC-sEVs at scale.

The technological difficulties involved in isolating and purifying sEVs are also a barrier to the conversion of MSC-sEVs into therapeutic products. To meet the high demand of MSC-sEVs with satisfied purity and properties for the downstream therapy, a robust, productive and scalable sEV isolation and purification method is essential to separate MSC-sEVs from highly heterogeneous MSC conditioned medium [27,32,33]. There are several commonly used techniques available for sEV separation and purification, each with benefits and drawbacks. Among various sEV isolation approaches, ultracentrifugation is the most frequently used method in the lab, which is capable for the treatment of the conditioned medium up to several hundred mL [34]. However, it comes with drawbacks of low scalability [48], mechanical damage to sEVs [35], high cost of the facilities, and labour intensive [36]. Other methods such as affinity-based capture [37], precipitation [38], and size exclusion chromatography [39] are also associated with disadvantages of high expenses, the introduction of undesired reagents, and limited working capacity, respectively, which hinders their use for the wide scale isolation of sEVs for clinical therapy [40]. By contrast, ultrafiltration has recently become a favoured technology for the industrial scale sEV separation, which attributes to its advantages of high throughput, excellent scalability, remarkable recovery, effective process, and relative low cost [27]. While it is true that ultrafiltration is a promising

method that is widely recognised for sEV isolation, the interaction between sEVs and membranes during the filtration process is not fully understood. The impacts of membrane pore size and different filtration parameters on the recovery, purity, and productivity of MSC-sEVs need further investigation, and a novel ultrafiltration-based isolation method should be developed and optimised accordingly for the industrial scale manufacture of MSC-sEV products.

1.3 Aims and Objectives

The overall aim of this thesis is to develop robust characterisation and production methods for potential clinical applications of small extracellular vesicles derived from the human bone marrow mesenchymal stromal cells. Specific objectives are outlined as follows:

1) To develop a robust bioassay-based detection platform for bioactivity comparison and functional identification of MSC secretome to support precise medical research and clinical applications of MSC-sEV products.
2) To develop an automated, high-throughput and regulation complying method and device for culturing the interested cells to meet the needs of a cost-effective, scalable production of high quality MSC-sEVs.
3) To develop and optimise a robust, effective and scalable ultrafiltration-based protocol for isolation and purification of MSC-sEVs.

1.4 Thesis Structure

This thesis is structured into six chapters.

Chapter 1 introduces the research background, explains the research questions, states the aims of this DPhil project, and presents an overview of the thesis structure.

Chapter 2 reviews the existing literature in the relationship between bone marrow mesenchymal stromal cell, its secretome and released small extracellular vesicles, the functional applications of the MSC-sEVs, as well as the current characterisation, production, isolation and purification methods of sEVs. The challenges in clinical applications of MSC-sEVs are also presented.

Chapter 3 shows a comprehensive, quantitative functional comparison between the MSC-sEV fraction, non-sEV fraction and the whole MSC conditioned medium on wound healing, with the corresponding control groups from the recipient cells.

After confirming the promising regenerative effects of MSC-sEVs on skin regeneration, Chapter 4 presents an optimised, automated and bio-safe hollow fibre bioreactor-based cell expansion system that is feasible for industrial scale production of high quality MSC-sEVs.

Chapter 5 looks into the development and optimisation of membrane filtration method for MSC-sEV isolation, investigates the impacts of various filtration parameters on the recovery, purity and productivity of sEVs, and then presents a fed-batch ultra-diafiltration protocol with optimised filtration parameters for the isolation and purification of MSC-sEVs.

Chapter 6 concludes the thesis with the summary of the key findings, contributions and limitations of the work, and provides the perspectives for the future research direction.

Chapter 2 Literature Review

This chapter presents an update to the following published article:

Risto, M., Lei, R., Zeng, Y., Zhu, J., Chang, H., Ye, H., Cui, Z. Membrane Applications in Autologous Cell Therapy. Membranes 12, no. 12: 1182 (2022).

2.1 Bone Marrow Mesenchymal Stromal Cells Derived Small Extracellular Vesicles

2.1.1 Bone Marrow Mesenchymal Stromal Cells

Mesenchymal stromal cells, also known as mesenchymal stem cells, are self-renewing stromal cells with fibroblast-like spindle morphology after adherent culture, exhibiting multilineage differentiation into a variety of mesodermal cell types [41]. According to the definition given by the International Society for Cellular Therapy, MSCs must show adherence to plastic surface under standard culture conditions, express cell markers CD73, CD90 and CD105 but negative to CD14, CD34 and CD45, and meanwhile show in vitro differentiation ability into osteoblasts, chondroblasts and adipocytes [42]. MSCs have been considered as a powerful tool for tissue regeneration and organ repair in various human diseases due to their vast differentiation potential and the immunomodulatory capacities [1].

MSCs can be extracted from several sources such as bone marrow, adipose tissue, umbilical cord, placenta, etc [43]. Bone marrow was the default source where the MSCs were first discovered [44], and it is also the most commonly used and studied source for human MSCs, as it is abundantly available and easily harvestable, and thought to be renewable [45]. Bone marrow mesenchymal stromal cells (BM-MSCs) have been shown to play a vital role in the field of tissue engineering and regenerative medicine [46,47], including topics of bone regeneration [48], cartilage repair [49], nervous system rebuilding [50], myocardium restoration [51], liver regeneration [52], skin regeneration [53], etc.

The early paradigm of cell replacement and multipotential differentiation of MSCs into the functional cells after transplantation were thought as a therapeutic mechanism of action, while more recently, it was reported by several studies that the mechanism of transdifferentiation could be very inefficient, which occurred in a too limited frequency to be regarded as principal mechanism [54]. In addition, MSCs showed a low engraftment rate and poor survival in the injured area but long-remained therapeutic effects after transplantation, suggesting that engraftment and differentiation may not be the main contributor [4]. Therefore, the emphasis has shifted towards the paracrine secretions of the MSCs that stimulate tissue repair response over the past decade [5,55].

2.1.2 Secretome of Bone Marrow Mesenchymal Stromal Cells

Paracrine signaling represents the phenomenon that cells produce signals by secreting various molecules, which could travel over a distance to the recipient cells for cellular communication and alter their behaviours. In recent years, contrary to

engraftment and differentiation, paracrine effects of MSCs have been increasingly accepted to bear the prime responsibility for mediating the regenerative effects of MSCs [9]. More and more evidence showed that MSCs produce a variety of bioactive factors, i.e. the secretome, and display their therapeutic effects largely via this paracrine signalling mechanism [7,9]. Secretome is defined as a complex group of factors that are secreted by the living cells or shed from the cell membrane surface to the extracellular space [6]. It consists of soluble proteins [8] such as cytokines, growth factors, chemokines, extracellular vesicles [9], and probably free nucleic acids and lipids [56]. The composition of cell secretome may vary from different cell types, and can also change with the cell conditions under various physiological or pathological states [56]. Conditioned medium (CM) is the entire milieu of the secretome consisting of soluble molecules and vesicular particles [56]. A growing effort has been made by the scientific community to investigate the reparative potential of the MSC secretome or the MSC-CM in regenerative medicine over the past few years [6]. For example, CM harvested from BM-MSCs were reported to have promising pharmaceutical potentials in cutaneous regeneration and wound healing in skin models [57–61]. The secreted proteins in the MSC-CM might play an important role in coordinating some of the biological therapeutic effects of the MSCs. A great amount of research has been conducted using proteomic methods, aiming at the characterisation and functional studies of the associated cytokines, growth factors, chemokines for a deeper insight into the mechanism of action. In spite of the functional potential that might be induced by the soluble components of the MSC-CM, increasing

interest has been focussed on the extracellular vesicles, especially exosomes or those with a size range of 30–200 nm, as they have been proposed to deliver complex biological information to mediate the positive paracrine effects of MSC therapy [20–22].

2.1.3 Extracellular Vesicles

Extracellular vesicles (EVs) are non-replicable, bilipid membrane-bound nanovesicles naturally released by most cells, and usually with spherical shape, showing cup shape with clear membrane structure under transmission electron microscopy [10,62]. There are three major types of EVs according to the biogenesis pathway. Exosomes and microvesicles are two main subtypes that differ in the way of formation and size distribution [36,63]. Exosomes are nanovesicles with the size distribution of 30-150 nm, produced by endocytosis (reverse-budding). First of all, early endosomes are formed through the internalisation of the plasma membrane, and then they mature into multivesicular bodies (MVBs) by inward budding, leading to the formation of intraluminal vesicles (ILVs) inside the MVB cargo. Finally, MVBs fuse with the plasma membrane to release the ILVs to the extracellular space [63], which are known as exosomes. Microvesicles are particles with the size range of 100-1000 nm, produced by blebbing of the plasma membrane, which is generally less well investigated compared to exosomes. The third one is called apoptotic bodies (100-5000 nm) that originate from apoptotic cells [64].

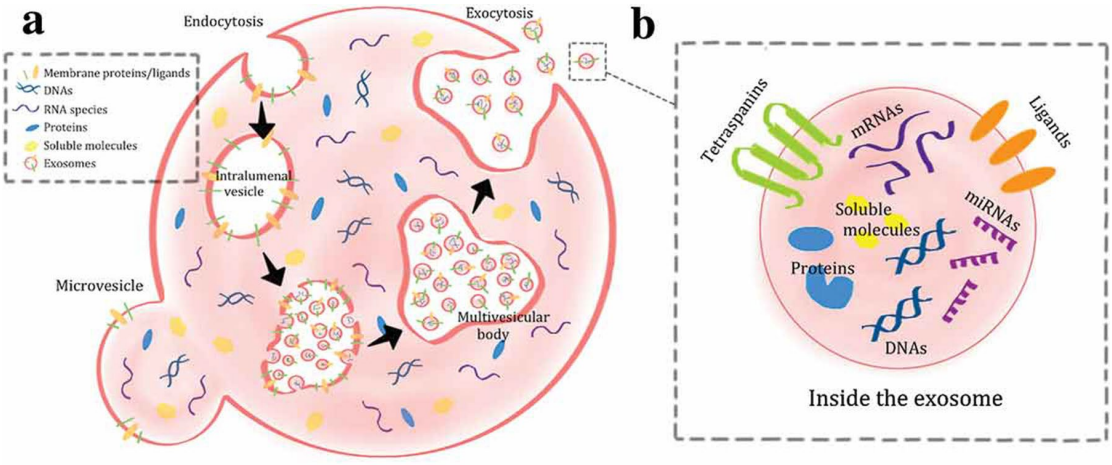


Figure 2.1 Biogenesis of extracellular vesicles. (a) Biogenesis of microvesicles and exosomes. (b) The contents of the exosomes. Reprinted from "Engineering mesenchymal stem cells to improve their exosome efficacy and yield for cell-free therapy," by Phan et al., 2018, Journal of Extracellular Vesicles, Volume 7. Copyright 2018 by authors.

2.1.4 Small Extracellular Vesicles

Since wide agreement on the specific EV subtype markers has not been reached yet, it is incredibly challenging to assign an EV to a particular biogenesis route. As a result, the International Society for Extracellular Vesicles (ISEV) recommended researchers to consider the usage of operational terminology for EV subtypes that associated with the physical properties such as size (small/medium/large EVs) or density (low/middle/high density EVs), biochemical composition (e.g. positive to a certain antibody/marker), or cell origin/conditions, rather than terms like exosome and microvesicle which might be inappropriately used historically regarding the erroneous expectations of unique biogenesis and the overlap of the EV characteristics [10]. Small extracellular vesicles (sEVs), which refer to the EVs < 200 nm in diameter [11], is the major and the most popular EV subtype that has been widely studied for their role as significant cell-cell communication mediators [12]. Particularly, sEVs derived from

mesenchymal stromal/stem cells (MSC-sEVs) have emerged as key paracrine mediators that induce the curative functions of MSCs, and therefore can serve as critical cell-free therapeutic tool in regenerative medicine [21,65].

2.2 Functional Studies and Applications of MSC-sEVs

2.2.1 Functions of EVs

EVs were originally regarded as the "dumpster" of cells for disposal of cellular waste [12,40]. They have now been considered to play their function role as a significant cell-cell communication mediator in numerous physiological and pathological processes [66–70]. EVs carry preassembled complex biological information (including proteins, nucleic acids and lipids) in their cargoes, protect them from the degrading enzymes by lipid membrane, travel over a distance to interact with recipient cells to achieve intercellular communication, and thereby have their functional role [71–78]. After being secreted into the extracellular environment, EVs could interact with target cells by three means: i) EVs directly fused with the cell membrane; ii) Cells uptake EVs via endocytosis; iii) EVs adhere to the cell surface and deliver the information through the lipid–ligand receptor interaction [79].

EVs can serve as a promising therapeutic strategy and have huge potential in the application of disease diagnostics [16], drug delivery vehicles [17], immunomodulation [19], and tissue regeneration [18]. First of all, the cargoes of EVs can be considered as the fingerprint of the type and conditions of their parent cells. As a result, with the intrinsic

characteristics of naturally biogenesis and systematically distribution, EVs can serve as circulating biomarkers, indicating specific cell physiology and playing a vital role in diagnostic, prognostic and prediction of therapeutic outcomes [80–82]. In addition, with the properties of immune tolerance, low toxicity, great stability, as well as the abilities of substances encapsulation and permeability to physiological barriers [25], EVs can be attractive candidates for drug delivery vehicles. They can be designed with particular loading or targeting capabilities, delivering exogenous therapeutic reagents such as siRNA, microRNA, DNA, proteins, small molecules and chemotherapeutic drugs to the specific target cells or tissues for treatment [83]. Moreover, due to the immunomodulating potency [70] and regenerative activity, EVs produced by different types of stem cells may serve as promising bio-therapeutic agents in regenerative medicine. Especially, MSC-sEVs have been broadly reported to be a cell-free therapeutic alternative to the MSC based therapy for various disease and tissue regeneration, for example in wound healing [84,85], heart [86], kidney [87], liver [88], cartilage [89], etc [23].

2.2.2 Therapeutic Effects of MSC-sEVs

2.2.2.1 Wound Healing

Wound healing is a complex process comprising four overlapping phases; haemostasis, inflammation, cellular migration and proliferation, and finally tissue remodelling [90]. Recent studies showed that sEVs isolated from the conditioned medium of BM-MSCs displayed regeneration effects on skin wound healing resembling their parental cells, especially in promoting proliferation and migration of skin cells,

accelerating angiogenesis, granulation tissue formation, increasing re-epithelialisation, collagen synthesis and immune regulation [57,63,91–93]. Shabbir et al. demonstrated a dose-dependent enhancement of proliferation and migration of fibroblasts treated with human bone marrow mesenchymal stromal cell derived sEVs (BM-MSC-sEVs) by activating several important signalling pathways (Akt, ERK, and STAT3) in wound healing [94]. Another in vitro study suggested that the treatment of human adipose mesenchymal stromal cell derived sEVs (AD-MSC-sEVs) promote the collagen and elastin synthesis of photo-damaged skin cells [95]. AD-MSC-sEVs were also reported to increase the secretion of collagen I and III of fibroblasts in the early stage but diminish collagen synthesis in the late stage to reduce scar formation in a mouse skin incision model [96]. Additionally, it has been shown that human umbilical cord mesenchymal stromal cell derived sEVs (UC-MSC-sEVs) actively accelerate the second-degree burn wound healing in vivo by activating the Wnt/β-catenin signalling pathway, leading to the promotion of dermal fibroblast proliferation, angiogenesis, and inhibition skin cell apoptosis [93,97,98].

2.2.2.2 Heart Regeneration

MSC-sEVs have great clinical potential for the treatment of cardiovascular diseases by reducing the infarct size, promoting angiogenesis and improving cardiac functions. Lai et al. demonstrated that the treatment of MSC-sEVs reduced the size of infarction by 40% in a mouse myocardial infarction model [99]. The tube formation of placental microvascular endothelial cells was also induced in a dose-dependent trend

by the administration of placental MSCs-sEVs produced under hypoxic conditions, which may due to potency of the hypoxia inducible factor family of proteins [100]. Similar findings were also reported by Bian et al. that hypoxic MSC-sEVs stimulate the migration of human umbilical vein endothelial cell and promote tube formation in vitro [101]. Additionally, human UC-MSC-sEVs can also be loaded to hydrogel for controlled and sustained drug administration, which has been proved to ameliorate inflammation, fibrosis and cell apoptosis as well as induce angiogenesis in infarcted area of the rat model, and subsequently improve the myocardial function [102].

2.2.2.3 Kidney Regeneration

A growing number of research utilising MSC-EVs for amelioration of acute kidney injury (AKI) and chronic kidney disease (CKD). It has been reported that BM-MSC-sEVs delivered certain genetic material to the injured renal cells, and thereby accelerated cell proliferation, reduced apoptosis of tubular cells, ameliorated fibrosis, contributed to anti-inflammatory and angiogenesis as well as supported renal functional recovery in AKI [103–105]. In a mouse diabetic nephropathy model, BM-MSC-EVs reduced fibrosis and stopped its progression through the action of miRNAs that can suppress profibrotic genes [106]. In a CKD mice model, BM-MSC-EVs were also reported to reduced fibrosis and tubular atrophy, offered protection against renal damage both in vitro and in vivo [107,108].

2.2.2.4 Liver Regeneration

Several models of acute and chronic liver diseases have revealed the value of MSC-sEVs [88]. Human MSC-EVs were reported by a significant number of research to

increase hepatocyte proliferation, reduce hepatocyte apoptosis [109], promote angiogenesis, diminish oxidative stress [110], inhibit liver fibrosis [111], and thereby induce hepatic repair.

2.2.3 Advantages of Using MSC-sEVs

MSC-sEVs generated in a well-defined culture environment could be a powerful therapeutic agent and a promising cell-free alternative to current MSC-based therapy to bypass a series of risk factors accompanied with MSC treatment, such as tumorigenesis, immune rejection and other technical issues [3,79,112–114].

On the intrinsic side, tumorigenesis may happen during the MSC therapy due to the multipotency of MSCs and the dysfunction in regulation of cell proliferation or differentiation. Immune rejection is another issue that could occur after administration of living MSCs, which might affect their therapeutic potency. Therapy based on MSC-sEVs could be safer because of the inability to directly form tumours [3,40] and the lower immunogenicity than MSCs due to the less amount of the major histocompatibility complex (MHC) molecules on the membrane surface [112–114].

Extrinsic factors including cell handling, manufacturing, harvesting, storage, transportation and clinical treatment procedure may also add extra risk to the MSC therapy. On the contrary, using MSC-sEVs products present considerable advantages of relatively straightforward collection and separation procedures. Moreover, compared with living MSC products, sEVs are thought to be easier to preserve bioactivity throughout storage[112–114] and transportation [115]. And with a greater potential of being a

ready-to-go biologic product, MSC-sEVs may provide simpler administration for patients during the treatment [116].

2.3 Characterisation of sEVs

Characterisation of sEVs using a variety of complementary techniques is crucial for sEV research and applications. A wide range of methodologies and technologies have been developed and implemented to analyse the biochemical and physical properties of sEVs. However, no single technique has yet demonstrated the ability to fully reveal the whole spectrum of sEV characteristics. Furthermore, due to the high heterogeneity of sEV populations, it is not likely to obtain an accurate results from the bulk characterisation method alone. Therefore, techniques that enable the identification and characterisation of single sEV are adopted together with the bulk characterisation techniques. Indeed, several complementary techniques are commonly used: the particle quantification and size distribution of sEVs are normally assessed by nanoparticle tracking analysis (NTA); the protein amount is measured by bicinchoninic acid (BCA) protein quantification method; the expression of sEV markers are usually tested by immunoblotting; the morphology is confirmed by transmission electron microscopy [117].

2.4 Production of sEVs

2.4.1 Traditional sEV Production Method

The translation of MSC-sEV therapy is based on the mass production of high quality MSC-sEVs to satisfy the requirement of clinical studies and applications [24].

However, the advancements of MSC-sEV based products is considerably hampered by the extremely low production yield of sEVs and thus the high expenses [25]. The current approach of sEV production relies on the manual operations to collect the conditioned medium from the classic batch cell cultivation in flasks or dishes, where the total yield of sEVs is limited by the restricted growth of the adherent MSCs within the small surface area [26]. In addition, the whole process is highly labour-intensive, time consuming, and associated with high chances of human error and batch variability. In order to achieve wide-scale clinical application of MSC-sEV therapy, the technical challenges and the prohibitively high cost associated with these therapies must be addressed through creative engineering.

2.4.2 Novel sEV Production Method

To overcome this technical bottleneck, various approaches have been recently proposed mainly in three directions [27]. One method is based on increase of sEV secreation per cell by applying stimulation, including starvation [118], pH shift [119], temperature change [120], oxidative stress [121], chemical treatment [122], and physical stress [123]. However, a concern may be raised that this stimulation might induce the alteration of cell status or phenotype, leading to the change of the physiochemical properties and the functional potency of sEVs. Cell membrane fragmentation has also been reported to produce large quantities of vesicles that can mimic the structure and composition of sEVs, although the difference between these vesicles and the naturally released sEVs might exist and further evaluation is required [124]. As sEVs are secreted products of cells,

the total yield of sEVs is partially dependent on the number of the producer cells [125]. In addition to the previous two methods, the most straightforward approach for large scale production of sEV-based products is to scale up the platform for cell culture to accommodate the maximal cell number, allow expansion of cells and meanwhile preserve their quality and functions. Bioreactors for cell expansion soon appeared as a key requirement in sEV production. For example, by increasing the surface area, multilayer cell culture flasks like Nunc™ Cell Factory™ Systems [28], stirred tank bioreactors with microcarriers [29], and perfusion hollow fibre bioreactors [30,31] have been tested to replace the traditional single layer flask-based cell culture for sEV manufacture. While multiplate system, stirred tank and packed bed bioreactor systems go some way in achieving this goal, the drawbacks of labour intensive tissue culture practices and low yields inhibit their wide spread commercial success [126].

2.4.3 Hollow Fibre Membrane Bioreactor Method for sEV Production

Membranes can be a disruptive technology to reshape the bioprocessing and manufacture of cellular products and significantly reduce the associated cost. Membranes offer a physical barrier with selective transport properties and different surface properties and can be used to solve some key issues in biomanufacture. Membrane based technologies such as perfusion hollow fibre bioreactors (HFBRs) have been applied towards the culture and expansion of adherent cell types, as well as isolation of small extracellular vesicles. Since their first use in the expansion of human choriocarcinoma cells, HFBRs have been used to culture many adherent cell types, for

research and clinical applications, including, but not exclusively, endothelial cells, satellite cells, leukaemia cells, human cord blood derived mononuclear cells, and erythroid cells. HFBRs have also shown great promise in culturing MSC [127–132], the stem cells that are more readily for clinical applications.

The clear need for HFBRs for regenerative medicine has naturally drawn great attention from industry and various commercial systems have been developed. For example, Terumo, FibreCell Systems, Cell Culture Company, and Oxford Mestar now offer a range of HFBR solutions for bioprocessing applications [133–137]. Each of these companies has targeted slightly different markets. Terumo provides a wholistic end to end cell culture solution for the expansion of cells in the form of the Quantum platform. With full control of media flow rate, temperature and gas compositions afforded by the automatically fed cabinet, the Quantum system facilitates reduced manual operations thereby reducing the chance of contamination while improving reproducibility. To date the platform has been used for, the expansion of $CD3^+$ T-cell [138], MSCs [139], adipose stromal cells [140], neural stem cells [126], and induced pluripotent stem cellss [141]. The DUET pump platform developed by FibreCell Systems is intended for laboratory scale HFBR systems. Depending on the intended application, a range of different membrane modules may be used, each produced with a range of membrane materials and pore sizes. It is the relatively low cost and flexibility, compared to complete cell expansion systems, associated with the FibreCell Systems platform that make it so attractive to researchers. The DUET platform has consequently been used in the investigation of

immune regulatory effect of MSCs [142], the production of EVs at a GMP standard [24], the interaction of endothelial cells and myeloid leukaemia [143], and even in the investigation of stem cell health in microgravity conditions onboard the international space station [144]. The Cell Culture Company has produced several platforms suitable for a wide range of applications and scales of operation. At the smallest scale, intended for use in a standard tissue culture incubator, the HF Primer system is most suitable for research applications. Increasing in size, the AutovaxID is a standalone system intended as a pilot scale platform to bridge the gap between R&D and production scale. Finally, the AcuSyst-Maximizer and AcuSyst-Xcellerator provide a scale-up pathway intended for production applications of between 500–2000 L fed-bed equivalent in size. The RegenMed Solution system developed by Oxford Mestar is a modular system integrating cell seeding, expansion, harvest, and final formulation together, and has proved successful in CAR-T culture and human MSC expansion.

As previously discussed HFBRs may yield large numbers of adherent stem cells in a small 3D space, and consequently, may be used to increase the yield of sEVs. More recently, HFBR has been increasingly used in the field of MSC-sEV production, because of its advantages of maximising surface area, continuous production, pre-concentration ability of the cell secreted products and excellent scalability. The main body of the hollow fibre bioreactor is a cartridge cylinder which is divided into two compartments called extracapillary space (ECS) and intracapillary space (ICS) by a bundle of hollow fibres with extremely large surface area and a certain molecular

weight cut-off (MWCO). With continuous feeding of the fresh medium to the cell culture compartment and the circulation of the flow in the system, gas, nutrients and metabolite wastes are exchanged between ECS and ICS through the porous structure of the fibres. As a result, cells can be cultured outside of the tube-like, semi-permeable hollow fibre membrane for several weeks or months without passage [24,128,129], and the sEVs can be continuously produced in the ECS. A key practical advantage that HFBR systems offer is that they may also function as a part of the downstream process. Owing to the semi-permeable nature, membranes with suitable pore size allow the retention of sEVs. Through this means, sEV products can accumulate and be preliminarily concentrated within the cell culture compartment of an HFBR to produce a more EV-enriched conditioned medium. This in turn is beneficial for downstream purification processes as the smaller start volume makes subsequent liquid handling easier [130]. The less open culture procedure in HFBR also reduce the contamination risks. Recently, Mendt et al. demonstrated the Terumo Quantum platform may be used as an effective platform for the production of sEVs. The sEVs produced in turn were shown to increase the rate of survival from pancreatic cancer [145]. Furthermore, Williams et al. and Potter et al. demonstrated that MSC-sEVs could be successfully obtained from Quantum cell expansion system, while preserving their therapeutic effects [146,147]. Similarly, Cobin et al. demonstrated that sEVs could be produced efficiently and reproducibly by MSCs derived from multiple human donors using a HFBR platform from FibreCell Systems, while preserving the phenotype and functionality [24]. However, the risk of phenotypic

alterations of cells due to environmental change is an issue when moving from static 2D cultures to dynamic 3D environments with shear stress caused by flow circulation, oxygen sparging, etc.[125] It should be noted that sEVs reflect the state of the cells from which they originate, and their content can be considered as a fingerprint of the type and status of their parent cells. Thus, the main technical limitation of hollow fibre bioreactor systems is the need to control environmental parameters for cell culture without altering the cell phenotype and the functionality of sEV products. In order to ensure that the sEVs harvested from HFBR are of desired type, quality, and function, it is vital to continuously monitor the status of the cells in the bioreactor as previously mentioned. Currently, sterile sampling of metabolic products and macromolecular biomarkers is readily achievable to monitor the cell condition through the use of membrane probes. However, it is very challenging to achieve direct online monitoring of the status and functions of the parent cells, and so far there is no existing method that would allow direct characterisation of sEVs within the bioreactors during the cell culture, due to the limitation of current characterisation method. Therefore, it is also essential to characterise both the phenotype of their parent cells after the culture in the bioreactor and the isolated sEV sample itself in terms of size, morphology, expression of sEV markers and functional potency, prior to the next stage research and application.

2.4.4 EV-depleted Fetal Bovine Serum (FBS) for sEV Production

The cultivation of MSCs and the manufacture of sEVs heavily rely on the use of FBS as nutrients for cell growth. However, it is essential to know that the FBS contains

large quantities of endogenous serum EVs, which could be regarded as a contaminant to the targeted MSC-derived sEVs, and subsequently influence the profile of the final MSC-sEV product [148,149], increase the inconsistency of the functional potency [150], and result` in failure at the regulatory and clinical levels [115]. As a result, four options are recommended to avoid contamination of exogenous EVs to MSC-sEVs [148,149]: i) Harvesting sEVs under serum-free conditions if possible. ii) If it is unavoidable to use the serum during cell culture, sEVs should be collected using EV-depleted medium (FBS derived EVs are pre-depleted by ultracentrifugation at 100,000 x g for 16 hours [132]) during the production period. iii) Using the bovine serum albumin as an alternative to the FBS [151–153]. iv) Using the commercial EV free medium [10,150,154].

2.5 Isolation and Purification of sEVs

2.5.1 Importance of sEV Isolation

Robust isolation and purification of MSC-sEVs from MSC-CM, which is a complex mixture of cell secretome with high heterogeneity [32], is a key technical process to ensure the application of high quality MSC-sEVs with a consistent properties, purity and yield for the downstream therapy [27,33]. For EV research, the existence of different EV subtypes may confound the results of studies. It is obvious that the biology and functionality of EVs cannot be properly understood until the EV subgroups are successfully recognised and separated for downstream investigation [36]. For clinical applications, the purity of the sEVs must be confirmed to prevent potential negative

effects from using impure samples and to achieve the clinical requirement [36]. In addition, to meet the high demand of MSC-sEVs in their clinical translation and commercialisation, excellent scalability is an essential characteristic of the separation method employed.

2.5.2 Current sEV Isolation Method

Several common methods are available for sEV isolation and purification, the pros and cons of which can be seen in Table 2.1.

Table 2.1 Pros and cons of common sEV isolation methods.

Method	Principle	Throughput	Scalability	Cost	Operation	Effects on EVs
Ultracentrifugation	Sequential centrifugation step, separated EVs based on size and density	Large	Low	High equipment cost	Manual labour intensive, time intensive, batch variability	Mechanical damage
Affinity capture	Capture EVs based on their surface markers	Low	Medium	High cost for antibodies	Require a pre-concentration step, time consuming	Reversible step required
Precipitation	Use precipitating agent to induce the pelleting of EVs	Low	Medium	Medium/Low	Further purification required to remove the precipitating agents	Introduction of synthetic precipitating agents
Size exclusion chromatography	Separated EVs based on size with a packed column of with fine, porous beads	Medium	Medium	Medium	Require concentration step before and after	Minimal detrimental effects
Membrane filtration	Separated EVs based on size with filters	Large	High	Medium/Low	Time-efficient	Less detrimental effects

2.5.2.1 Ultracentrifugation (UC)

Differential centrifugation (DC) is a method that fractionate particles based on their size and density by escalating the centrifugal force in stages to 100,000 x g [40]. It has been considered as the most commonly used approach for laboratory scale sEV

separation, which allows the isolation process from a relatively large volume (about several hundred mL) of the conditioned medium [34]. Large EVs are collected at lower gravitational force than small EVs. However, because this approach cannot specifically distinguish between EVs and other particles of similar physical properties, issues such as sample heterogeneity and nonselectivity exist [36]. As a result, co-isolation of non-EV contaminants such as lipoprotein complexes [64], protein aggregates [155] happens during DC. Additional procedures such as the use of a column, density gradient method or ultrafiltration may be required if a more homogenous population is expected [82,115,156,157]. It may also cause mechanical damage to EV populations due to high shear force during ultracentrifugation [35] and therefore may lead to the loss of bioactivity and functionality. Other drawbacks of DC includes poor accessibility of the ultracentrifuges and rotors owing to their high cost, and labour intensive [36]. The commercial rotor-dependant working capacity and the batch process also largely limit the scalability of the UC method [31,115,125,158]. As a result, DC is not suitable for sEV isolation for clinical purposes.

Density gradient centrifugation (DGC) using a discontinuous density gradient of solutions such as sucrose or iodixanol to separate samples based on their buoyant density, in which EVs will travel to the part with equilibrium density [36,115]. DGC could produce purer EV fractions with less protein contaminants and minimise the mechanical damage to EVs [159,160]. However, the drawbacks including co-isolation of non-EV particles with overlap buoyant densities (e.g. lipoproteins), sample loss during

separation process,[36,159,161] labour intensive, time-consuming, and low throughput hamper the use of DGC method in clinical settings [115].

2.5.2.2 Affinity Capture

Affinity capture is a method that discriminates EVs from impurities based on their biochemical and biophysical properties using beads [39,159,162], plates or chips[163] with affinity tags[40,115], such as monoclonal antibodies (mAbs) against a targeted sEV surface antigen [159,161,164–170], and specific peptide [171]. Compared to the ultracentrifugation method, affinity capture is efficient and highly selective.[63,164] But the drawback is that it may depend on the availability of a suitable sEV surface marker and could be very expensive.[36,115] Also, because of its low starting sample volumes, an extra pre-concentration step is required for large volume of biofluid or cell conditioned medium, which makes it more suitable for purification step [35,38,148,172]. Moreover, a reversible step should also be taken into account to release targeted EVs.

2.5.2.3 Precipitation Reagents

The precipitation of EVs from conditioned medium and biofluids can be caused by the retraction of solvent after adding the water-soluble polymer, which leads to the concentration of EVs and subsequently clumping of EVs when their solubility is reached [173–175]. Polyethylene glycol (PEG) is one of the commonly used precipitation regents and a modified PEG-based method is reported to give a higher EV yield [176,177]. Acetone is a reagent used in Protein Organic Solvent Precipitation (PROSPR), where soluble proteins are removed via precipitation in cold acetone, leaving EVs behind in suspension. As a result, higher purity EVs are generated and can be obtained through

filtration or ultracentrifugation methods[178]. EVs with the presence of the negatively charged phosphatidylserine can also be precipitated from cell conditioned medium using acetate. The surface charge of EVs can be neutralised by acetate, leading to hydrophobic interactions and thus aggregation and precipitation of EVs [38]. Precipitation is regarded as a rapid concentration method with high EV recovery. However, co-isolation of nonvesicular contaminants is still an issue [36]. In addition, it is not suitable for clinical applications due to its low starting volume, influence of the precipitating agents on EV bioactivity [35,38,148,172]. Moreover, any materials introduced during manufacture must be removed from the final therapeutic sEV product to meet the clinical standards. The introduction of extra synthetic reagents to the sample leads to additional depletion steps and unavoidably increases processing time and costs as well as product loss due to multiple steps [35], no mention the biological activity retained [179].

2.5.2.4 Size Exclusion Chromatography (SEC)

SEC enables separation of molecules based on size using a single column with porous matrix. Molecules or particles smaller than the size cut-off enter the pores temporarily, whereas larger particles pass by the pores and elute earlier [35,36,38,148,172]. The performance is related to the column height, the pore size, and the column packing, etc. The use of SEC reduces the EV aggregates [35,38,148,172], isolates purer samples with less protein contaminants [180], and has minimal detrimental effects on EVs, leading to the separation of biophysically and functionally intact sEVs [35,180,181]. In addition, SEC is relatively inexpensive [182], which makes SEC a good candidate for clinical-oriented

EV separation. However, a major drawback is that the eluted EV samples could be very dilute [180], which required a subsequent reconcentration step [162,183]. Some non-EV contaminants above the size cut-off may also co-isolated.

2.5.2.5 Membrane Filtration

Among these EV isolation methods, ultracentrifugation, affinity capture, precipitation, and size exclusion chromatography have limitations of poor scalability, high cost, introduce unwanted agents and requiring extra concentration steps, respectively [40]. In contrast, membrane filtration is capable for high throughput, more readily scalable, faster, less labour intensive, and requires less capital investment for equipment. Consequently, it is a very promising separation method for large-scale manufacture of sEVs intended for clinical applications.

Microfiltration (MF) and ultrafiltration (UF) can readily be used for EV isolation and purification. MF with membrane pore sizes ranging between 0.1-0.8 μm is normally used to remove larger particles from the target EV fraction [184]. Track-etched polycarbonate membranes with pore sizes from 30-600 nm have been utilized for fast EV isolation or detection in specialized filtration devices, e.g. a cyclic tangential flow filtration (TFF) system [185], a TFF based microfluidic chip [186], an integrated double-filtration microfluidic device [187], an exosome total isolation chip [188], a lab-on-a-disc integrated with two nanofilters [189]. EVs can also be separated by ultrafiltration (membrane filter with pressure applied) [40]. Particles or soluble molecules smaller than the MWCO are pushed through the membrane [115]. Ultrafiltration may be superior to

other isolation methods in large-scale production as it is compatible for large volumes of samples [115]. It is often used together with other techniques. A considerable group of researchers agree with the opinion that membrane filtration coupled with SEC may be the favoured method for EV isolation [183,190,191]. Commercial centrifugal ultrafiltration filters with multiple membrane materials and MWCO ranging from 10-300 kDa are used for volume reduction of a large amount of biofluids and conditioned medium before EV isolation [192], or as an additional concentration step for the relatively dilute EVs from other isolation steps, for example, size exclusion chromatography (SEC) [193]. The problems may happen during fractionation is that deformable particles larger than the size cut-off may pass the filter with the help of applied external force[115], and trapping/binding of EVs on the porous membrane may lead to EV sample loss. Thus, choice of membrane and filter units (e.g., vertical versus tangential), as well as the operating parameters for filtration process are important [36,40]. It was reported by Vergauwen et al. that the most popular membrane type for EV concentration is regenerated cellulose with MWCO of 100 kDa, based on the records in the EV-TRACK knowledgebase [194]. UF-TFF can also be applied to EV isolation and purification. In TFF with a suitable choice of membrane MWCO, EVs larger than the pore sizes can be retained, concentrated and recirculated in the capillary space where biofluid or cell conditioned medium is continuously pumped in, while smaller molecules, such as small proteins, salts, and solvents can travel through the pores on the membrane and be removed in the permeate [195,196]. Structural and functional integrity of EVs can be

retained by a relatively gentle filtration. In addition, to increase the purity of EV products, diafiltration can be operated in TFF systems. Small molecules are further removed or lowered by adding fresh exchange buffer at the same rate as the permeate flow rate. Compared to conventional batch-wise dead-end filtration, TFF is superior as it reduces the formation of filter cake and can operate large-scale EV isolation and purification in a continuous process. Choi et al. successfully isolated EVs from human adipose derived stem cells by TFF with a 500 kDa MWCO membrane filter capsule, confirming the functional recovery in photo-damaged human dermal fibroblasts after EV treatments [95]. Higher purity might be obtained by combining different techniques with UF, although UF alone is applicable for EV isolation and purification [197]. EVs were reported to have been concentrated 50-fold through TFF with a 100 kDa MWCO membrane, followed by purification using chromatography column and further concentrated by 100 kDa MWCO centrifugal filter [198]. Finally, Hydrostatic filtration dialysis, a filtration technique which consists of filtration, concentration and dialysis using hydrostatic pressure of the fluid, has also been employed to isolate EVs from urine using dialysis membranes with 1000 kDa MWCO [199].

2.6 Challenges in Clinical Applications of MSC-sEVs

Overall, EV research is still at its infancy. Mechanisms of EV biogenesis such as cargo selection, packaging and release pathway as well as the mechanism on how EVs function in the paracrine system including targeting and information delivery are not well understood [40]. In addition, further investigation on specific EV biomarker and their

universal applicability is in urgent need for defining the EV subpopulations. Molecular characterisation like protein and genetic profiles for the EV composition is also a research focus [36].

The clinical applications of MSC-sEVs are full of challenges. Lack of functional clarification tool has been a major bottleneck for producing high-end MSC-sEV products. A robust bioassay-based detection platform for bioactivity comparison and functional identification is required to support precise medical research and application. To overcome this bottleneck, gene markers for specific function pathways are needed to report the functional alternations induced by MSC-sEV. Although biomarkers are widely used in molecular and cell biology, it appeared that a generic biomarker assay for MSC-sEV functions is still to be developed. By combining in vitro recipient cell assay, comparative transcriptome analysis, biomarker development, and quantitative polymerase chain reaction (qPCR), a set of functional biomarkers can be established to support qPCR detection of functional alternations in cells treated by MSC-sEV and thus facilitate function clarification of MSC-sEV products for clinical applications.

On the engineering side, the development and standardisation of methods for large-scale MSC-sEV production, isolation, purification and preservation need to be addressed for the manufacture of high-end sEV products. Clinical-grade MSC-sEVs are in high demand for the transition from bench to clinical settings due to the noticeable advancement of MSC-sEVs in regenerative treatments [125], but the low sEV yield in routine production method largely limits the use of MSC-EVs [40]. In addition, a robust

MSC-sEVs isolation and purification method with excellent scalability is a key technical process to ensure the application of high quality MSC-sEVs with a consistent properties, purity and yield for the downstream therapy [27,33]. Bioprocessing and manufacture of the cell secreted products account for a large fraction of the cost. Hence, in order to achieve cost-effective production, it is crucial to establish the engineering foundation and develop standard manufacturing processes early in the development cycle [125]. Current processing technologies are largely based on mimicking laboratory cell culture and sEV production with different degrees of automation [200]. By scaling up the cell culture methods for upstream sEV production and isolation and purification method for downstream sEV processing, a sufficient amount of sEVs with satisfied bioactivity, functionality and increasing consistency are expected to be produced. Infrastructure investment to create ultraclean environments is necessary for the "open operation" where the product or component are exposed to the operational environment. There is an urgent need for novel bioprocessing technologies, new equipment, and new devices, to form a fully enclosed, automatic, and single use system, to perform all the processing steps in hospitals without the need for dedicated GMP facilities. Furthermore, attention must also be paid to the preservation, formulation, and cold chain technologies for sEVs. Reliable preservation strategies need to be developed to enhance long term stability of MSC-sEVs for clinical use. The technological breakthrough in scalable production and long-term preservation of sEVs would

significantly contribute to the progress of the clinical translation and commercialisation of MSC-sEV products.

Chapter 3 Characterisation and Functional Studies of Small Extracellular Vesicles from Human Bone Marrow Mesenchymal Stromal Cells on Skin Regeneration

This chapter presents the following article:

Lei, R., Wang, H., Cui, Z., Ye, H. Characterisation and Functional Studies of Small Extracellular Vesicles from Human Bone Marrow Mesenchymal Stromal Cells on Skin Regeneration. To be submitted.

Author contributions:

Z.C. and H.Y. defined the project scope and provided research funding. H.Y., H.W. and R.L. designed the experiments. R.L. performed the experiments, analysed data, and drafted the manuscript. Z.C., H.Y. and H.W. reviewed the manuscript.

3.1 Abstract

A panoply of studies showed that mesenchymal stromal cells (MSCs), also termed as mesenchymal stem cells, could secrete a variety of bioactive substances into the culture medium and display various therapeutic effects. Small extracellular vesicles, a type of membrane-bound vesicles produced by cells, might be the key role in MSC secretome that responsible for the beneficial paracrine effects of MSC therapy. In this study, we harvested the conditioned medium (CM) from both human bone marrow mesenchymal stromal cells (hBM-MSCs) and normal human dermal fibroblasts (NHDFs), fractionated CM of each into small extracellular vesicle (sEV) fraction and non-small extracellular vesicle (NsEV) fraction, respectively, and compared their functions on NHDF-based migration and proliferation assay. Our findings indicate that there might be multiple active components but also defective components in the conditioned medium from hBM-MSCs (MSC-CM) for the proliferation and migration of skin cells. Both sEV and NsEV from hBM-MSCs (referred as MSC-sEV and MSC-NsEV) as well as MSC-CM itself showed an overall promotive effect on migration behaviour of NHDFs, but MSC-sEV seems to be more potent for NHDF migration among different MSC secretome fractions and is also superior in effect to the corresponding sEVs produced by the recipient NHDFs. Our study provided referential significance for the choice of cellular secretome fractions to be used as skin regeneration strategies. It also offers specific fractionation and functional comparison

strategy of different secretome fractions on cell-based model, which would be a useful tool for comprehensive functional evaluation of cellular secretome.

3.2 Introduction

Mesenchymal stromal cells (MSCs), also termed as mesenchymal stem cells, are self-renewing multipotent cells exhibiting multilineage differentiation and has been considered as a powerful tool for various human diseases [1,2]. Bone marrow derived mesenchymal stromal cells (BM-MSCs) has been regarded as a promising source of human MSC-based therapeutic strategies in the field of tissue engineering and regenerative medicine [46,47]; however, challenges associated with MSC-based therapy relating to cell origin, tumorigenic potential, differentiation and proliferation capacity, cell handling, storage and transport conditions are considered [3]. The early paradigm of cell replacement and multipotential differentiation of MSCs were thought as a therapeutic mechanism of action, while more recently, it was reported by several studies that MSCs showed a low engraftment rate in injured area but long-remained therapeutic effects after implantation, suggesting that the paracrine mechanism might be the principal mechanism that contributes to tissue repair [4,54]. Therefore, the emphasis has shifted towards the paracrine secretions of the MSCs over the past decade [5,6]. More and more evidence showed that MSCs secrete a variety of bioactive molecules including cytokines, growth factors and chemokines into the conditioned medium (CM) and displayed their therapeutic effects largely via their paracrine signalling mechanism [7,9]. Particularly, CM harvested from BM-MSCs (MSC-CM) were reported to have promising pharmaceutical potentials in cutaneous regeneration and wound healing in skin models [57–61].

Small extracellular vesicles (sEVs), a type of membrane-bound vesicles with a diameter of 30-200 nm secreted by most cells, were originally regarded as the "dumpster" secreted by cells [40]. However, with the report of its significant role in cell-cell communication, it has been emerged that sEVs are the key secretory products that responsible for the beneficial paracrine effects of MSC therapy, and thus increasing attention was invested to investigate the biological activity of MSC derived sEVs (MSC-sEV) [15–17]. Recent studies showed that sEVs isolated from the conditioned medium of BM-MSCs displayed regeneration effects on skin wound healing resembling their parental cells, especially in promoting proliferation and migration of skin cells, angiogenesis, granulation tissue formation, collagen synthesis and immune regulation [57,63,91,92].

Given that sEVs play a role in different physiological processes, it is of paramount importance to assess their potency using cell assays. For this purpose, wound healing was chosen as a model to evaluate the potency of sEVs in this study. Wound healing is a complex process comprising four overlapping phases; haemostasis, inflammation, cellular migration and proliferation, and finally tissue remodelling [90]. It has been established that dermal fibroblasts are stimulated to proliferate and migrate under the stress condition of wound healing, and play a vital role in both inflammatory and proliferative phase by secreting a variety of signalling molecules and extracellular matrix proteins, e.g., fibronectin, type I collagen and type III collagen [201–203]. Due to its significant role in wound healing process, dermal fibroblast-based skin model was

widely used to test the therapeutic effects of cellular secretome on skin wound healing. For example, it was reported that the MSC-CM promoted proliferation of dermal fibroblasts, enhancing wound closure and collagen density [204]. Shabbir et al. demonstrated a dose-dependent enhancement of proliferation and migration of fibroblasts treated with human bone marrow mesenchymal stromal cell derived sEVs by activating several important signalling pathways (Akt, ERK, and STAT3) in wound healing [94].

It is reasonable to hypothesize that the MSC secretome may contain both beneficial factors including soluble proteins and sEVs but also deleterious factors such as metabolism waste that may mediate contradictory effects, and among those beneficial factors, MSC-sEV may be more favourable in tissue repair and wound healing. However, among previous functional studies of MSC secretome, few of them compared the function of MSC-sEV with the whole MSC-CM in a quantitative way simultaneously and a perspective also lacked in these studies that whether other secreted substances in the non-sEV fraction (NsEV) of conditioned medium (the left-over of MSC-CM during the isolation process of sEVs, hereinafter called MSC-NsEV) would display any positive or negative therapeutic effects. In addition, secreted substances of the recipient cells itself may also play a functional role and should be considered as a control group for the secretome of the parental cells, but was rarely investigated parallelly in previous research. Therefore, it is necessary to conduct a comprehensive and rigorous comparison of the functions between different fractions of

MSC conditioned medium (MSC-sEV and MSC-NsEV) and the whole MSC-CM itself on tissue repair and wound healing in a quantitative way, with the parallel control of corresponding secretome fractions from recipient cells, to fill the knowledge gap.

Here we produced conditioned medium by incubating human (h)BM-MSCs in DMEM with EV-depleted fetal bovine serum. The conditioned medium of MSCs was fractionated into sEV fraction and non-sEV fraction. Normal human dermal fibroblasts (NHDFs) were chosen as recipient cells as they play an important role in tissue repair and wound healing. A proper control of CM and corresponding fractions derived from the recipient NHDFs were produced under the same conditions (Figure 3.1). In this study, we investigate the functions of different secretome fractions (CMs, sEVs and NsEVs) from both hBM-MSCs (the parental cell) and NHDFs (the recipient cell) on NHDF-based migration and proliferation assay, giving a comprehensive comparison of their wound healing potential in vitro and providing referential significance for the choice of cellular secretome fractions to be used as skin regeneration strategies. In addition, our skin cell-based model together with the rigorous experiment setting would be a useful tool for comprehensive in vitro functional evaluation of cellular secretome under a sensible environment without interference from additives.

3.3 Materials and Methods

3.3.1 Cell Cultivation

Human Bone Marrow derived Mesenchymal Stem Cells (hBM-MSCs) (Cat.: C-12974, Lot.: 438Z012.1) and Normal Human Dermal Fibroblasts (NHDFs) (Cat.: C-12302, Lot.: 412Z029.2) at passage 2 (P2) were purchased from PromoCell, Germany. The hBM-MSCs were subcultured at a seeding density of 5000 cells/cm^2 to passage 9 (P9) in PromoCell mesenchymal stem cell growth medium (Cat.: C-28009, Lot.: 466M132, PromoCell, Germany) with supplement (Cat.: C-39809, Lot.: 465M187, PromoCell, Germany) and 1% Anti-Anti (Cat.: 15240-062, Lot.: 2257209, Gibco, USA), and NHDFs were subcultured at a seeding density of 5000 cells/cm^2 to passage 10 (P10) in PromoCell fibroblast growth medium (Cat.: C-23020, Lot.: 466M324, PromoCell, Germany) with supplement (Cat.: C-39325, Lot.: 468M030, PromoCell, Germany) and 1% Anti-Anti. Cell morphology was observed by OLYMPUS CKX53 optical microscope (OLYMPUS, Japan)

3.3.2 Depletion of Extracellular Vesicle (EV) from Fetal Bovine Serum (FBS)

Fetal bovine serum derived extracellular vesicles (FBS-EV) were depleted from FBS (Cat.: 10099-141C, Lot.: 2139378CP, Gibco, USA) by ultracentrifugation at 120,000 × g, 4℃ for 18 hours using Himac CP70NE Ultracentrifuge (Himac, Japan) with P28S Rotor (Himac, Japan). The supernatant was collected and sterilized by

filtering through 0.22 μm vacuum filter apparatus (Cat.: 431097, Corning, USA). The sterile EV-depleted FBS was obtained and stored at -80 ℃ before use.

3.3.3 Preparation of Conditioned Medium of hBM-MSCs and NHDFs

The hBM-MSCs (P9) and NHDFs (P10) were cultured in multilayer cell culture flasks (Cat.: 353144, Corning, USA) at a seeding density of 14285 cells/cm^2 (equal to 2.5 x 10^6 cells per T175 flask area), using 20 mL of corresponding PromoCell complete medium per T175 flask area at 37℃ in a humidified incubator containing 5% CO2, respectively. After 24 hours of attachment, cells were gently washed twice with Phosphate Buffered Saline (PBS, Cat:10010-031, Lot: 2192549, Gibco, USA) and replaced with 25 mL EV-depleted medium consist of Dulbecco's Modified Eagle Medium (DMEM), Low Glucose, Pyruvate (Cat:11885-084, Lot: 2192435, Gibco, USA), supplemented with 1% Penicillin-Streptomycin (Cat:15140-122, Lot: 2257223, Gibco, USA) and 10% EV-depleted FBS per T175 flask area. After incubation for further 48 hours, the conditioned medium derived from hBM-MSCs and NHDFs were harvested, respectively, centrifuged at 300 × g, 4℃ for 15 min using Eppendorf 5810R Centrifuge (Eppendorf, Germany) with A-4-81 Rotor (Eppendorf, Germany) to remove the dead cells and cell debris. 10 mL of the centrifuged conditioned medium from hBM-MSCs (MSC-CM) and NHDFs (HDF-CM) were taken, respectively, and stored at 4℃ before use (applied to NHDF-based assay within 2 days). The rest of MSC-CM and HDF-CM were used to prepare sEV/non-sEV fractions.

3.3.4 Preparation of sEV Fraction and Non-sEV Fraction of hBM-MSCs and NHDFs

sEVs were isolated by differential centrifugation from MSC-CM (MSC-sEV) and HDF-CM (HDF-sEV) as previously described by Thery et al [205] with modification. The protocol includes 2000 × g for 30 min using Eppendorf 5810R Centrifuge with A-4-81 Rotor, 10,000 × g for 40 min using with FA-45-6-30 Rotor (Eppendorf, Germany), 100,000 × g ultracentrifugation for 90 min using Himac CP70NE Ultracentrifuge (Himac, Japan) with P70AT Rotor (Himac, Japan). All the discards from MSC-CM and HDF-CM in the above three steps were collected as non-sEV fraction, respectively, known as MSC-NsEV and HDF-NsEV. The crude pellets from MSC-CM and HDF-CM after the first-round 100,000 × g ultracentrifugation were washed with PBS at 100,000 × g and 4 ℃ for 45 min using Optima™ MAX-TL Ultracentrifuge (Beckman Coulter, USA) and TLA-120.2 Rotor (Beckman Coulter, USA), respectively. The pellets after second-round ultracentrifugation from MSC-CM and HDF-CM were resuspended in 400 µL PBS, respectively, known as MSC-sEV and HDF-sEV. A flow chart of the fractionation protocol of secretome fractions was shown in Figure 3.1.

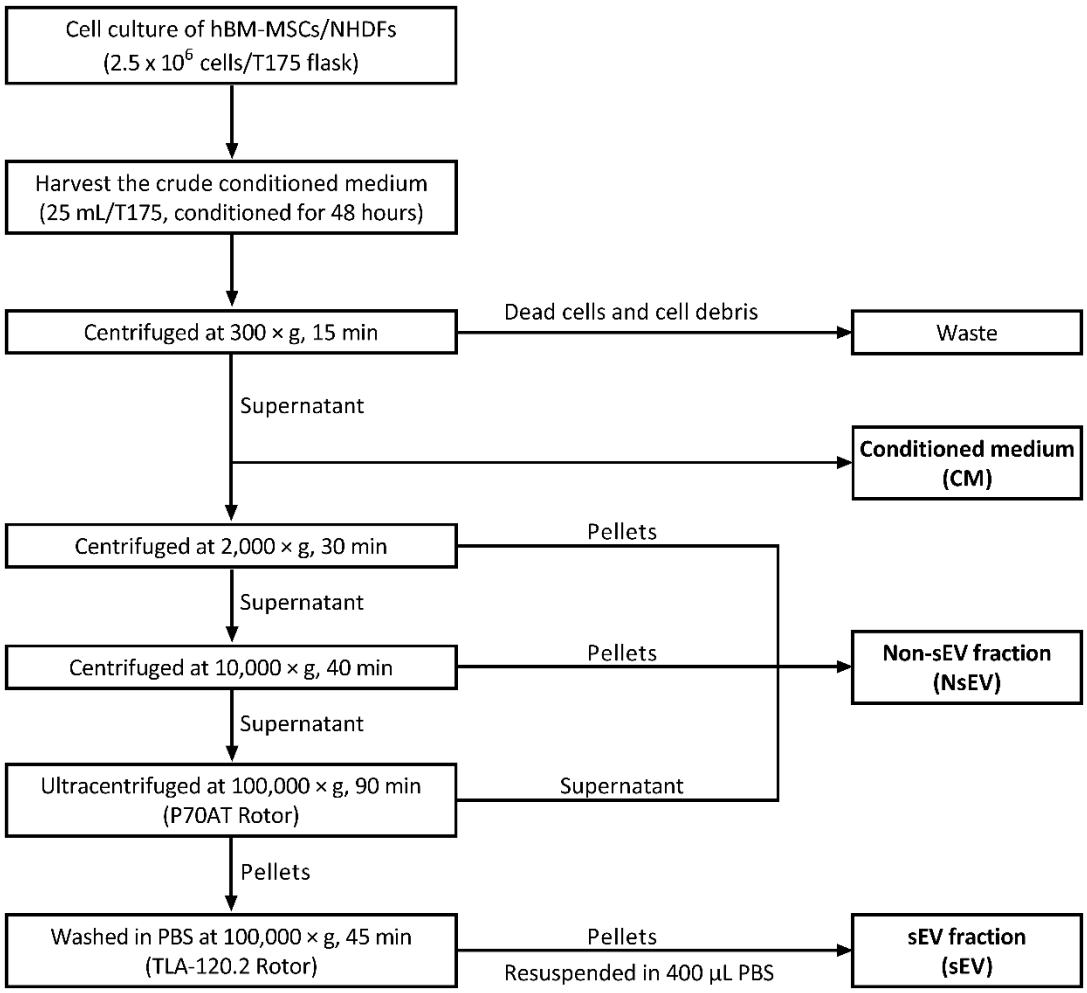


Figure 3.1 Flow chart of the fractionation protocol of secretome fractions.

3.3.5 Nanoparticle Tracking Analysis (NTA)

sEV samples were diluted 100-fold with PBS before measurement. The movement of the particles were recorded for 5 x 60s at camera level 13 by NanoSight NS300 (Malvern Panalytical Ltd, UK) and analysed by NTA 3.2 software (Malvern Panalytical Ltd, UK) at detect threshold 7 for EV concentrations and size distributions.

3.3.6 Protein Extraction and Quantification

After the collection of conditioned medium, hBM-MSCs (P9) and NHDFs (P10) were trypsinised with 5 mL of 0.05% trypsin-EDTA solution (Cat.: 25300-054, Lot.:

2185895, Gibco, USA) per T175 flask area for 2 min, respectively, inactivated with 10 mL completed medium per T175 flask area and centrifuged at 300 × g, 20℃ for 5 min to get the cell pellets. The cell pellets of hBM-MSCs (P9) and NHDFs (P10) were lysed by adding Pierce™ RIPA buffer (Cat.: 89901, Lot.: VI311555, Thermo Fisher Scientific, USA) with freshly added cOmplete™, Mini, EDTA-free Protease Inhibitor CocktailTM (Cat.: 04693159001, Lot.: 43002700, Roche, Switzerland), respectively. The mixture was incubated on ice for 30 min, and then centrifuged at 12000 rpm, 4℃ for 20 min using Eppendorf 5810R Centrifuge with FA-45-30-11 Rotor (Eppendorf, Germany), respectively. The supernatant was taken as MSC-lysate and HDF-lysate. sEV fraction, non-sEV fraction and the whole conditioned medium were lysed by adding RIPA buffer with freshly added protease inhibitor and incubating on ice for 30 min. Protein concentration of the cell lysate, sEV fraction, non-sEV fraction and the whole conditioned medium from hBM-MSCs and NHDFs were quantified using QuantiPro™ BCA Assay Kit (Cat.: QPBCA-1KT, Lot.: SLCH0421, Sigma-Aldrich, USA).

3.3.7 Western Blot

Cell lysate and sEV lysate of hBM-MSCs and NHDFs were normalised to the same protein concentration by PBS, based on the protein quantification results. The lysates were mixed with 4x Laemmli sample buffer (Cat.: 1610747, Lot.: 64351030, Bio-Rad, USA) and NuPAGE sample reducing agent (Cat.: NP0004, Lot.: 2205873, Thermo Fisher Scientific, USA) depend on the type of antibody, and then boiled at 95℃ for 5

min. The lysates and Precision Plus Protein Kaleidoscope Prestained Protein Standard (Cat.: 1610375, Lot.: 64313981, Bio-Rad, USA) were loaded and run on 4–20% Mini-PROTEAN® TGX™ Precast Protein Gels (Cat.: 4561094, Lot.: 64360183, Bio-Rad, USA) at a constant voltage of 120V for 65 min in a Mini-PROTEAN Tetra Cell (Cat.: 1658001, Bio-Rad, USA) filled with diluted Tris-Glycine SDS Buffer (Cat.: 1610732, Lot.: 64359578, Bio-Rad, USA), and then transferred onto a polyvinylidene fluoride (PVDF) membrane at constant voltage of 25V for 3 min using Trans-Blot TurboTransfer Packs (Cat.: 1704156, Lot.: 64340580, Bio-Rad, USA) and Trans-Blot Turbo system (Cat.: 1704155, Bio-Rad, USA). The membrane was washed in diluted 20X modified Dulbecco's PBS Tween 20 Buffer (Cat.: 28346, Lot.: VL315361, Thermo Fisher Scientific, USA) for 5 min and then blocked with Blotting-Grade Blocker (Cat.: 1706404, Lot.: 64329693, Bio-Rad, USA) in PBS-Tween buffer at room temperature for 60 min. The blots were probed with primary antibodies at 4°C overnight: CD63 (1:2000; Cat.: ab59479, Lot.: GR3288353-7, Abcam, UK), CD81 (1:2000; Cat.: ab79559, Lot.: GR3314758-5, Abcam, UK), calnexin (1:1000; Cat.: 2679S, Lot.: 6, Cell Signaling Technology, USA) and GM130 (1:500; Cat.: 610822, Lot.: 9140853, BD Biosciences, USA), followed by horseradish peroxidase conjugated secondary anti-mouse (1:1000; Cat.: 7076P2, Lot.: 34, Cell Signaling Technology, USA) or anti-rabbit antibody (1:1000; Cat.: 7074P2, Lot.: 28, Cell Signaling Technology, USA) incubation at room temperature for 60 min. The PVDF membranes were then exposed to Clarity Western ECL Substrate (Cat.: 170-5060, Bio-Rad, USA) for 10 min at room

temperature and then exposed to Bio-Rad Chemidoc XRS system (Cat.: 1708265, Bio-Rad, USA) for imaging.

3.3.8 Transmission Electron Microscopy (TEM)

sEV morphology was visualized by transmission electron microscopy. Briefly, 5 µl of solution was applied to freshly glow discharged on 300 mesh copper grids coated with a thin carbon film (Cat.: BZ10023b, ZJKY, China) for 2 min, blotted with filter paper and stained with 2% uranyl acetate (Cat.: GZ02625, ZJKY, China) for 15 s, then blotted and air dried. Grids were imaged in a Tecnai G2 F20 S-TWIN transmission electron microscope (FEI, USA) at 200 KV.

3.3.9 Preparation of Different Secretome Treatments for Functional Assay

The sEVs (MSC-sEV and HDF-sEV) were diluted in fresh DMEM to concentrations of 30 µg/mL, 1 µg/mL, 0.1 µg/mL, 0.01 µg/mL, respectively. The CMs (MSC-CM and HDF-CM) and NsEVs (MSC-NsEV and HDF-NsEV) were diluted in fresh DMEM to concentrations of 1500 µg/mL, 750 µg/mL, 30 µg/mL, 1 µg/mL, respectively. As sEV pellets were suspended in PBS, an equal volume of PBS vehicle was added to fresh DMEM as DMEM control (0 µg/mL).

3.3.10 sEV-uptake Assay

NHDFs at passage 8 were seeded at 4000 cell/cm^2 with 500 uL of NHDF growth medium, making around 8000 cells per well in a Costar 24-well plate (Cat.: 3524, Corning, USA). After 24 hours of attachment, cells were gently washed once with PBS.

The sEVs (MSC-sEV and HDF-sEV) were freshly labelled with PKH67 green fluorescent dye (Cat.:P7333-1ML, Lot.: MKCK0731, Sigma-Aldrich, USA) according to the manufacturer's protocol, with some modifications. Briefly, 8 μL PKH67 was dissolved in 2 mL Diluent C (Cat.:CGLDIL-10ML, Lot.: MKCK8658, Sigma-Aldrich, USA) to prepare a 2x stain solution (4×10^{-6} M). Separately, sEV pellet was resuspended in 1 mL Diluent C. The same volume of PBS was mixed with 1 mL of Diluent C parallelly as a control group. The sEV suspension was mixed with an equal volume of 2x stain solution and incubated for 10 min. The labelling reaction was stopped by adding an equal volume of 1% BSA (Cat.:A1933-25G, Lot.: WXBD2613V, Sigma-Aldrich, USA) in PBS to bind excess dye. The labelled sEVs were washed once with PBS by ultracentrifugation at 100,000 ×g for 90 min. Fresh DMEM supplemented with PKH67 labelled sEVs (30 μg/mL) was used to incubate the NHDFs. The PBS control group was treated following the same protocol. After 6-hour coculture, the NHDFs were washed once with PBS, fixed with 4% paraformaldehyde (Cat.: 43368, Lot.: M21H030, Alfa Aesar, China) for 15 min, and then treated with 0.5% Triton® X-100 (Cat.: T9284-100ML, Lot.: SLBF2001V, Sigma-Aldrich, USA) for 15 min for cell membrane permeation, washed 3 times with PBS for 5 min each time between and after each step. The nuclei was stained by adding 1 μg/mL DAPI stain solution (Cat.: 62248, Lot.: VC2962251, Thermo Fisher Scientific, USA) for 2 min following the manufacturer's protocol, washed 3 times with PBS for 5 min each time between and after each staining step. 500 μl PBS was added to each well to keep the cells hydrated

while imaging. The cells were imaged by FV3000 confocal microscope (OLYMPUS, Japan).

3.3.11 Proliferation Assay

NHDFs at passage 8 were seeded at 15000 cells/cm^2 with 100 uL of NHDF growth medium, making 5000 cells per well in a Costar 96-well plates (Cat.: 3599, Corning, USA). After 24 hours of attachment, cells were gently washed once with PBS. Different secretome treatments (CMs, sEVs, NsEVs from hBM-MSCs and NHDFs) at different concentrations were used to incubate the NHDFs for 3 days, respectively. The day when the original NHDF growth medium replaced with different secretome treatments was deemed as Day 0. HDF proliferation assay was performed using the Cell Counting Kit-8 (Cat.: CK04, Lot.: PF724, Dojindo, Japan). CCK-8 reagent and DMEM was mixed at volume ratio of 1:10. On Day 0, cells were washed once with PBS and replaced with 110 uL CCK-8 and DMEM mixture in each cell testing wells and blank wells (110 uL CCK-8 and DMEM mixture without cells). Absorbance expressed as Optical Density (OD) was assessed at 450 nm (OD 450) using a Tecan Spark microplate reader (Tecan, Switzerland) after 2 hours of incubation at 37 ºC. OD values were determined on Day 0, Day 1, Day 3 at the same time-point of the day using the same protocol. Triplets were performed for each secretome treatment group on each day. All the OD450 values were normalised as ratios of OD450 at Day 0 by dividing OD450 values of Day 0.

3.3.12 Migration Assay

NHDFs at passage 8 were seeded at 50000 cell/cm^2 with 1.5 mL of NHDF growth medium, making 100000 cells per well in a 24-well plate with a 2-well culture-insert (ibidi, Germany). After 24 hours of attachment, a confluent cell layer was resulted in each well and then 2-well culture inserts were gently removed by using sterile tweezers, leaving a cell-free gap of 500 µm in the middle of each well of the plate. Cells were gently washed once with PBS and different secretome treatments (CMs, sEVs, NsEVs from hBM-MSCs and NHDFs) at different concentrations were used to incubate the NHDFs in triplets for 60 hours. The time point when the original NHDF growth medium replaced with different secretome treatments was deemed as 0 h. Cell performance was recorded as bright field images by optical microscope using a 4x objective at 0 h, 6 h, 12 h, 18 h, 24 h, 30 h, 36 h, 42 h, 48 h, 60 h. The images were analysed by ImageJ and the cell covered area of the gap was quantified in µm^2 using Matlab.

3.3.13 Statistical Analysis

Statistical analysis of the data were performed using IBM SPSS Statistics, version 28 and GraphPad Prism, version 8. Data were expressed as mean ± standard deviations (SD). Each experiment was repeated at least three times. Data were analysed by General Linear Model (GLM) ANOVA and Tukey method was chosen for post-hoc multiple comparisons to assess statistical significance. Probability value below 0.05 was considered statistically significant. * means $P < 0.05$, ** means $P < 0.01$, *** means P

< 0.001, **** means P < 0.0001, ns means not significant. Graphs were delineated by GraphPad Prism, version 8.

3.4 Results

3.4.1 Characterisation of MSC-sEV and HDF-sEV

sEV samples were characterised in terms of size, surface marker expressions, morphology and yield. Both MSC-sEV and HDF-sEV displayed a bell-shaped curve with a peak at 118.87 nm and 117.60 nm, and mean particle diameters at 143.60 nm and 144.07 nm, respectively, consistent with characteristic size range of sEVs (Figure 3.2a-c). No significant difference was found in size distribution or mean particle size between MSC-sEV and HDF-sEV. Both MSC-sEV and HDF-sEV were positive for typical EV markers such as CD63 and CD81, and negative for intracellular compartment markers, like Calnexin and GM130, which confirmed the purity of the sEV samples (Figure 3.2d). Classic cup-shaped sEV particles were found in TEM images (Figure 3.2e). The yield of sEVs was quantified as EV-associated protein amount by BCA method, showing that 45.27 μg for MSC-sEV and 40.68 μg for HDF-sEV can be obtained from 100 mL corresponding conditioned medium, respectively (Figure 3.2c).

3.4.2 Internalisation of sEVs by NHDFs

To determine whether the recipient cell NHDFs can internalise sEVs, PKH67-labelled sEVs were incubated with NHDFs for 6 hours. The cellular uptake of sEVs by NHDFs was confirmed by the confocal image. (Figure 3.2f).

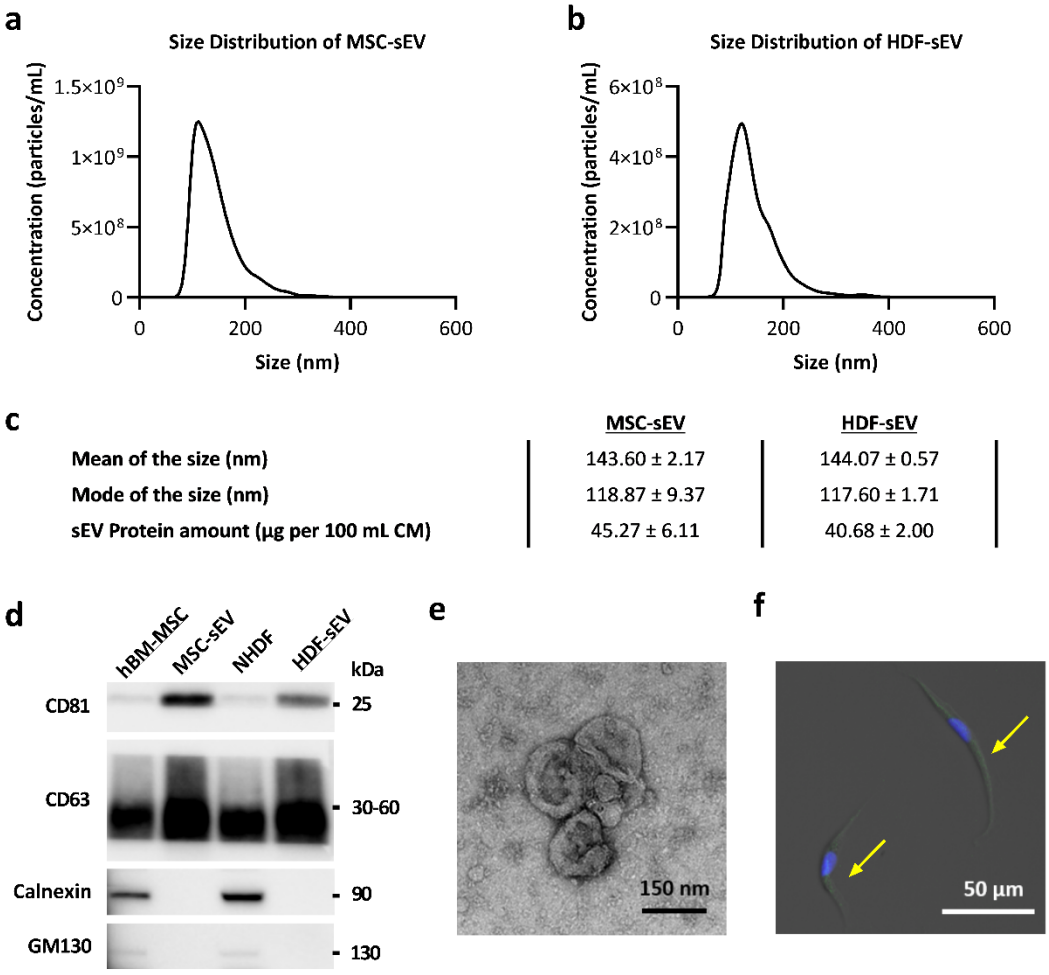


Figure 3.2 Characterisation of MSC-sEV and HDF-sEV. (a) Average size distribution of MSC-sEV samples determined by NTA (n=15). (b) Average size distribution of HDF-sEV samples determined by NTA (n=15). (c) Size (n=3) and yield (n=3) of MSC-sEV and HDF-sEV. (d) Western blot analysis of MSC-sEV, HDF-sEV and their parental cell lysates. Original blots/gels are presented in Supplementary Figure 3.1. (e) TEM image of sEVs. (f) Fluorescence images of sEVs taken by NHDFs. Cell nucleus of NHDFs were stained by DAPI. sEVs were stained by PKH67 (green signal was pointed out by arrows).

3.4.3 The Effect of Cellular Secretome on Migration of NHDFs

To determine the effects of different secretome treatments on migration of NHDFs, the migration assay was performed on NHDFs treated with MSC-CM, MSC-sEV, MSC-NsEV at different concentrations (0 µg/mL, 1 µg/mL, 30 µg/mL) for 60 hours. Blank (DMEM) control group was represented as 0 µg/mL. Representative bright field

images of NHDFs migration were shown in Supplementary Figure 3.2. To compare the difference in a quantitative way, all the bright field images were processed by ImageJ and the cell covered area of the gap changed with time course was quantified by Matlab. General Linear Model (GLM) ANOVA was used to analyse factors of migration time, secretome fraction type and concentration of secretome. As expected, a typical growth curve of migration consist of a linear growth phase and a saturation phase was showed in Figure 3.3a, indicating the migration velocity was nearly constant when cell migration started and then slowed down to zero when the NHDFs reached confluency at 42 h probably due to lack of space. Migration of NHDFs was significantly affected by the secretome fraction type (Treatment) [$F(2, 756) = 29.77$, $P < 0.001$] and concentration of secretome (Concentration) [$F(2, 756) = 11.48$, $P < 0.001$], and significant interaction was observed between these two variables [$F(4, 756) = 11.38$, $P < 0.001$], showing different functional dynamics of the components in MSC-CM, MSC-sEV and MSC-NsEV (see Supplementary Table 3.1). Tukey's post-hoc multiple comparisons were therefore performed between different secretome fractions of MSCs at different concentrations for their effects on migration behaviour of NHDFs (see Supplementary Table 3.2) and an interaction plot (Figure 3.3b) was showed based on the results of Tukey's post-hoc multiple comparisons (the growth curve of migration of each group was expressed by its mean on the interaction plot). Generally, both MSC-CM and MSC-sEV mediated an overall positive effect on migration of NHDFs when compared to blank control group (0 μg/mL), and it was interesting to observe that the

promotion performance of MSC-sEV was consistently above that of the MSC-CM at the same concentration (Figure 3.3b). Specifically, MSC-sEV started to show promotive effect on NHDF migration at lower dose (1 μg/mL) than MSC-CM (30 μg/mL), although no significance difference was found between them at higher dose (30 μg/mL). There was no significant difference found between MSC-NsEV treatments at dose ≤30 μg/mL and blank control group.

To further investigate the difference of the performance between MSC-CM and MSC-NsEV on NHDF migration, NHDFs were treated with MSC-CM and MSC-NsEV at high concentrations (750 μg/mL, 1500 μg/mL). Again, all the images were processed and quantified by ImageJ and Matlab to compare the difference in a quantitative way. GLM ANOVA and Tukey's post-hoc multiple comparisons were performed (see Supplementary Table 3.3 and Supplementary Table 3.4) and the interaction plot (Figure 3.3c) showed that both two types of secretome enhanced the NHDF migration ability at high concentration treatment, compared to the blank control group. Particularly, MSC-CM started to show a significance promotive effect on NHDF migration at 30 μg/mL, and the level of enhancement firstly increased and then showed a reduction with increased dose level, suggesting that there might be both synergic and antagonistic components in the CM, and there might be a critical value as optimal dose for NHDF migration in the range of 30 – 1500 μg/mL, although no significant difference was found between 30 μg/mL, 750 μg/mL and 1500 μg/mL. A similar trend was demonstrated with increased dose of MSC-NsEV treatments, while significance

improvement on NHDF migration was only observed at 750 μg/mL among different concentration treatments, compared with blank control group.

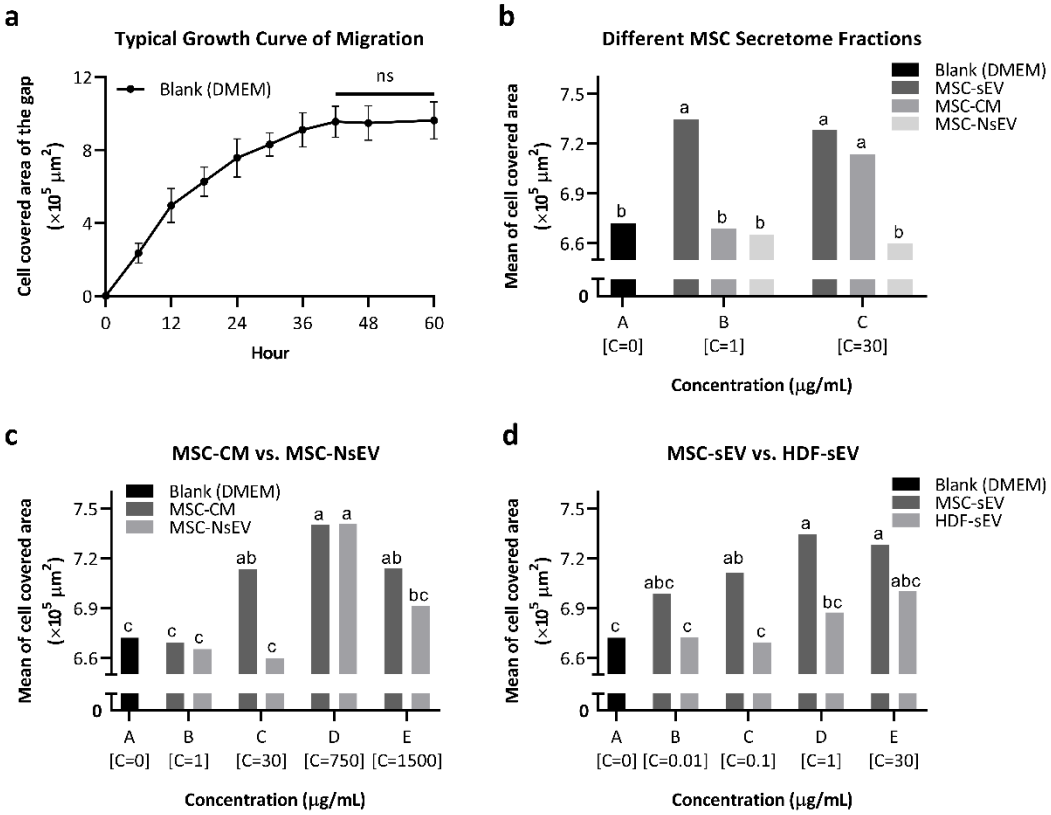


Figure 3.3 The effect of cellular secretome at different concentration (represented as C) on migration of NHDFs. (a) A typical growth curve of migration. NHDFs in all treatment groups showed growth curves in a similar trend. The migration curve of NHDFs treated with blank (DMEM) was chosen (n=9). (b) Interaction plot for migration behaviour of NHDFs in response to factors of secretome fraction type from MSCs (MSC-sEV, MSC-CM and MSC-NsEV) and concentration of secretome based on the results of Tukey's post-hoc multiple comparisons (n=9). (c) Interaction plot for migration behaviour of NHDFs in response to factors of secretome fraction type from MSCs (MSC-CM and MSC-NsEV) and concentration of secretome (including high concentrations) based on the results of Tukey's post-hoc multiple comparisons (n=9). (d) Interaction plot for migration behaviour of NHDFs in response to factors of sEV types (MSC-sEV and HDF-sEV) and concentration of sEVs based on the results of Tukey's post-hoc multiple comparisons (n=9). $P < 0.05$ was deemed as a statistically significant difference. ns means not significant in (a). Means that do not share a letter are significantly different in (b), (c) and (d).

Based on the previous results, clear evidence suggested that sEV fraction might display superior ability than NsEV fraction for NHDF migration. Therefore, to further investigate the effect of sEV fraction, NHDFs were treated with sEVs from different cell sources (MSC-sEV and HDF-sEV) at several concentrations (0 μg/mL, 0.01 μg/mL, 0.1 μg/mL, 1 μg/mL, 30 μg/mL) and the migration performance was recorded for 60 hours. GLM analysis was performed (see Supplementary Table 3.5), indicating that cell source of sEVs (sEV type) [$F(1, 836) = 30.40$, $P < 0.001$] was a variable that affected NHDF migration ability, and it significantly interacted with concentration of sEVs (Concentration) [$F(4, 836) = 2.49$, $P = 0.042$], showing different functional dynamics of the MSC-sEV and HDF-sEV. Tukey's post-hoc multiple comparisons were performed (see Supplementary Table 3.6) and an interaction plot (Figure 3.3d) was showed. The migration performance of MSC-sEV treated NHDFs was consistently above that of HDF-sEV in Figure 3.3d, showing that MSC-sEV mediated an overall promotive effect on NHDF migration when compared to the sEVs produced by NHDFs itself (HDF-sEV). Especially, a dose-dependent trend of MSC-sEV was observed for NHDF migration as the level of enhancement firstly increased and then reached a plateau with increased dose level. MSC-sEV started to show a significance promotive effect on NHDF migration when the dose level ≥ 0.1 μg/mL, although no significant difference of enhancement level was found between the concentration treatments ≥ 0.1 μg/mL. However, HDF-sEV at dose range 0 – 30 μg/mL didn't show any significant

positive effect on the migration of NHDFs compared to blank control group, although a similar dose-dependent trend probably existed.

3.4.4 The Effect of Cellular Secretome on Proliferation of NHDFs

To investigate the effects of different cellular secretome treatments on proliferation of NHDFs, Cell Counting Kit-8 assay was performed on NHDFs and absorbance expressed as Optical Density (OD) was assessed at 450 nm (OD 450). All the OD450 values were normalised as folds of OD450 at Day 0. To compare the cell proliferation behaviour of NHDFs under treatments of CMs, sEVs and NsEVs from both hBM-MSCs and NHDFs at different doses (concentration of treatments ≤ 30 μg/mL were considered as low doses, 750 μg/mL and 1500 μg/mL were considered as high doses), factors of treatment time, cell source of secretome and secretome fraction type were evaluated by GLM (see Supplementary Table 3.7). As expected, a typical growth curve of proliferation was showed in Figure 3.4a, indicating that the NHDF proliferation behaviour increased from Day0 to Day3 in all treatments. Out of surprise, compared to blank (DMEM) control group, all the treatments at low doses did not make any significant difference on the proliferation of NHDFs, and there was no significant difference between either different secretome fractions from the same cell source or corresponding secretome fraction from different cell sources at low doses (Figure 3.4b). However, with the increase of concentration, both MSC-CM and MSC-NsEV at high doses displayed significant promotive ability on the proliferation of NHDFs, indicating that there were beneficial factors for proliferation in both MSC-CM and MSC-NsEV.

As it mentioned before, the NHDF proliferation behaviour represented by the folds of OD450 at Day 0 was significantly affected by treatment time, showing a clear increase trend from Day0 to Day3 in all treatments, however, the exact effective acting time for the secretome treatments was unknown. Therefore, the daily growth rate of OD450 during different time periods of MSC-CM treatment was calculated by equation (3.1) and equation (3.2):

$$\text{Daily growth rate of OD450 from Day 0 to Day 1} = \frac{OD450\ at\ Day\ 1}{OD450\ at\ Day\ 0} \quad (3.1)$$

$$\text{Daily growth rate of OD450 from Day 1 to Day 3} = \sqrt{\frac{OD450\ at\ Day\ 3}{OD450\ at\ Day\ 1}} \quad (3.2)$$

It was interesting to observe that the daily growth rate of Day 0 – Day 1 were consistently above that of Day 1 – Day 3 (Figure 3.4c), indicating that the exact effective acting time is highly likely to be the first 24 hours after secretome treatments. Moreover, the daily growth rate of Day 1 – Day 3 remained constant, while a dose-dependent trend was found for the daily growth rate of first 24 hours, which also supports the previous result that there might be beneficial factors for proliferation in MSC-CM.

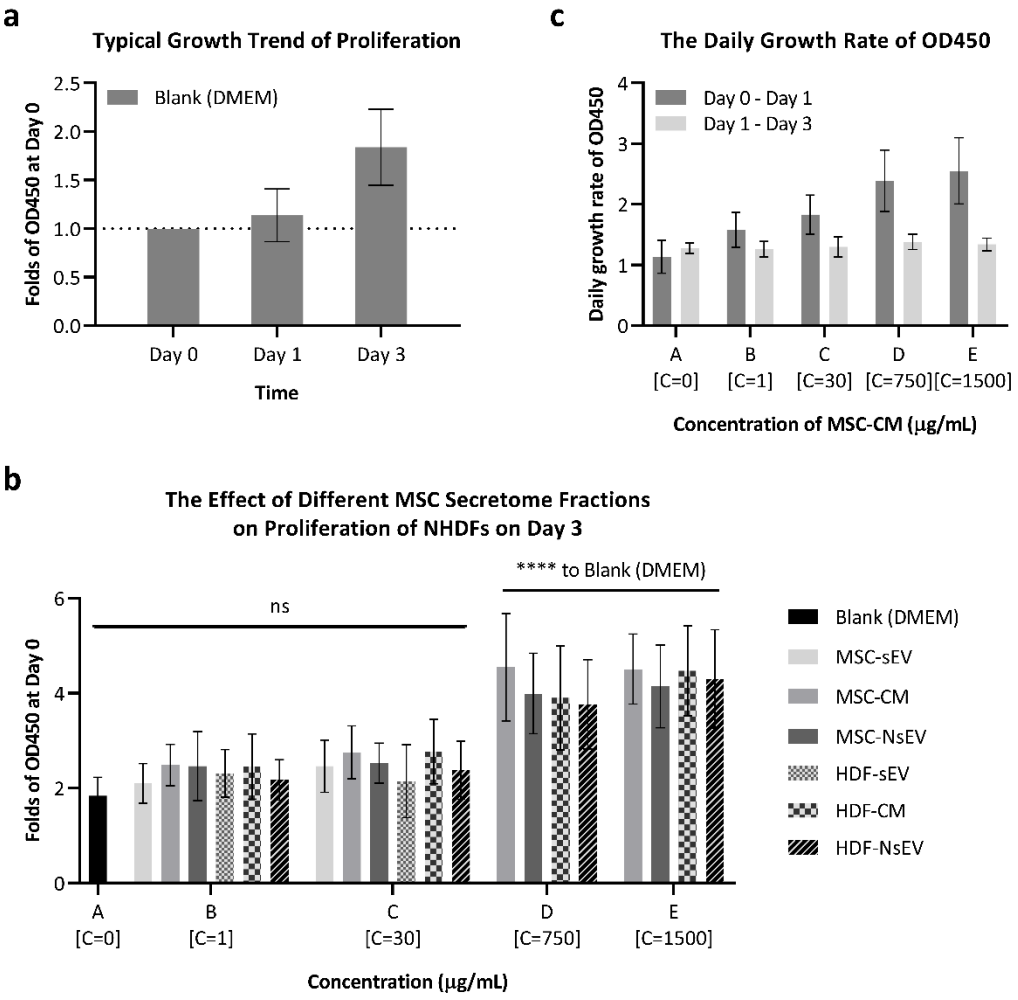


Figure 3.4 The effect of cellular secretome at different concentration (represented as C) on proliferation of NHDFs. (a) A typical growth curve of proliferation. NHDFs in all treatment groups showed growth curves in a similar trend. The proliferation curve of NHDFs treated with blank (DMEM) was chosen (n=9). (b) Plot for proliferation (Folds of OD450 at Day 0) of NHDFs at Day 3 in response to different secretome fraction types from both hBM-MSCs and NHDFs at different concentrations. Blank (DMEM) control group was represented by 0 μg/mL (n=9). $P < 0.05$ was considered statistically significant to Blank (DMEM) control group (see statistical analysis results in Supplementary Table 3.8). * means $P < 0.05$, ** means $P < 0.01$, *** means $P < 0.001$, **** means $P < 0.0001$, ns means not significant. (c) The daily growth rate of OD450 during different time periods of MSC-CM treatment at different concentrations (n=9).

3.5 Discussion

Evidence is mounting that MSCs play various therapeutic effects through secretion and regulation of a variety of paracrine factors [4,57]. Cellular secretome is actually a combination of membrane-bound extracellular vesicles such as sEVs, secreted soluble proteins including cytokines, chemokines, growth factors, proteases and probably some metabolism waste inside the conditioned medium. It has been verified that different components of the secretome derived from MSCs (in the MSC conditioned medium), especially MSC derived sEVs, displayed promising regenerative effects on wound healing, skin regeneration and anti-aging [18,24,35]. However, few researchers conducted a comprehensive and rigorous comparison of the functions between different fractions (MSC-sEV and MSC-NsEV) of MSC conditioned medium and the whole conditioned medium itself on skin wound healing in a quantitative way, with the parallel control of corresponding secretome fractions from recipient cells. To fill the knowledge gap, in this study, we produced conditioned medium by incubating hBM-MSCs in DMEM with EV-depleted serum for 48 hours. MSC-sEV was isolated from MSC-CM by differential ultracentrifugation and the discards were collected as MSC-NsEV. CM and corresponding fractions derived from the recipient cells (NHDFs) produced under the same conditions were served as control. Different concentrations of CMs, sEVs and NsEVs from hBM-MSCs and NHDFs were prepared by serial dilution in fresh DMEM without additives and tested in NHDF migration assay for 60 hours and NHDF

proliferation assay for 3 days, respectively. Fresh DMEM without additives was served as blank control.

According to our results, both MSC-sEV and MSC-NsEV fractions as well as MSC-CM itself showed an overall promotive effect on migration behaviour of NHDFs (Figure 3.3b&c), it is therefore reasonable to conclude that both sEV fraction and non-sEV fraction of the conditioned medium from MSCs have beneficial factors and there might be multiple, rather than a single, active components in the MSC derived conditioned medium that enhance the NHDF migration. This result is in line with previous reports that the whole conditioned medium derived from BM-MSCs significantly enhanced wound closure by accelerating the migration of keratinocytes, fibroblasts, endothelial cells, with identified wound healing mediators from MSC-CM, including TGF-β1, the chemokines IL-6, IL-8, collagen type I, fibronectin [206–208]. Shabbir et al. and Hoang et al. claimed that sEVs alone derived from BM-MSCs could also display promotive effects on the migration of dermal fibroblasts by activating important signalling pathways (Akt, ERK, and STAT3) in wound healing [94]. However, on this basis, our study further suggests that the role of the non-sEV part of the secretome should also be valued during the functional investigation. This might be due to the fact that the non-sEV fraction was actually the left-over of conditioned medium after isolation of sEVs, which contains those non-sEV beneficial factors of the conditioned medium, mainly secreted soluble proteins including cytokines, chemokines, growth factors.

Also, although both two fractions and CM itself showed their bioactivity in promoting migration, the difference between their potency cannot be ignored. Significant interaction was observed between the secretome fraction type and concentration of secretome, showing non-unified functional dynamics of the components in different fractions. MSC-sEV, MSC-CM and MSC-NsEV started to show their significance promotive effect on NHDF migration at 0.1 μg/mL, 30 μg/mL and 750 μg/mL, respectively, and the performance line of MSC-sEV was consistently above that of MSC-CM while the line of MSC-NsEV was at the bottom among three treatments (Figure 3.3b-d), suggesting that solely MSC-sEV fraction might display superior ability of accelerating NHDF migration than those non-sEV beneficial factors in MSC-NsEV fraction, and as a mixture of MSC-sEV and MSC-NsEV, MSC-CM displays a moderate effects between the two. A similar superior therapeutic ability of sEV derived from BM-MSCs were also reported by Takeuchi et al. but in promoting bone regeneration and angiogenesis, showing that MSC-sEV enhanced cellular migration, osteogenesis and angiogenesis-related gene expression, compared to MSC-CM group [209].

MSC-sEV also mediated a significant beneficial effect on migration over sEVs produced by recipient NHDFs itself (HDF-sEV, Figure 3.3d). This result might be explained by the superior potential of its parental cells (BM-MSCs) to accelerate wound healing, which is supported by previous studies that BM-MSCs showed greater activity than dermal fibroblasts in terms of granulation tissue formation, collagen synthesis,

epithelialization and angiogenesis in vivo [210–213]. Chen et al. also demonstrated that conditioned medium of BM-MSCs significantly enhanced migration and proliferation of keratinocytes and endothelial cells compared to HDF-CM [59]. sEVs are shown to carry cell-specific cargoes such as proteins, lipids and genetic materials [214], served as cell-to-cell communication mediators to regulate the properties of target cells. Therefore, it is reasonable to infer that MSC-sEV may carry biological information from BM-MSCs and regulate the wound healing behaviour of the recipient NHDFs. Indeed, Hu et al. showed that MSC-sEV promoted a faster rate of wound recovery by significantly enhancing the proliferation and migration of NHDFs, and also displayed a potential of ameliorating skin photoaging, compared with HDF-sEV [215]. To investigate the similarities and the differences between the two, further research with omics technique should be conducted to study the biomolecules and molecular mechanisms that contribute to the composition and function of MSC-sEV and HDF-sEV.

However, different to those reported MSC-sEV can accelerate wound closure in a dose-dependent manner [94,216–218], our results displayed a dose-dependent trend firstly and then the enhancement level reached a plateau with rising dose (Figure 3.3d). It would be likely that the dose at the turning point had already reach to the maximum stimulation potential under this condition. Due to the limitation of productivity, higher concentration of sEVs were not applied to NHDFs, it is therefore unclear whether the plateau status would be maintained for MSC-sEV or whether higher dose of HDF-sEV

would display any significant change on NHDF migration; further study is therefore required when the productivity limitation was overcome.

Nevertheless, the level of enhancement on NHDF migration firstly increased and followed by a reduction with rising dose for both MSC-CM and MSC-NsEV group (Figure 3.3c). It might because there are probably both beneficial soluble proteins and defective components such as some metabolism waste in the non-sEV fraction of the conditioned medium, and their functional kinetics were not unified. It is possible that the positive effect of the beneficial components might be dominant at low concentration, but with the rising dose, the defective components start to display negative influence. The level of enhancement would likely reach to a maximum threshold when the balance is reached between the two, and with the further increased concentration, the effect of the deleterious components might become more significant. More concentration sets between 30 – 1500 μg/mL are needed to find the critical value as the optimal dose for NHDF migration. For future applications of the MSC secretome, further fractionation steps are required to remove deleterious components.

The existence of beneficial factors in CMs and NsEVs had also been supported by the results of NHDF proliferation assay in a dose-dependent manner (Figure 3.4b&c). Again, due to the limitation of productivity ability, the proliferation behaviour of NHDFs with treatments of higher doses of sEVs is unclear, further study is therefore required. However, it is an interesting finding that these treatments might mainly play their functional roles on proliferation in the first 24 hours after treatments (Figure 3.4c).

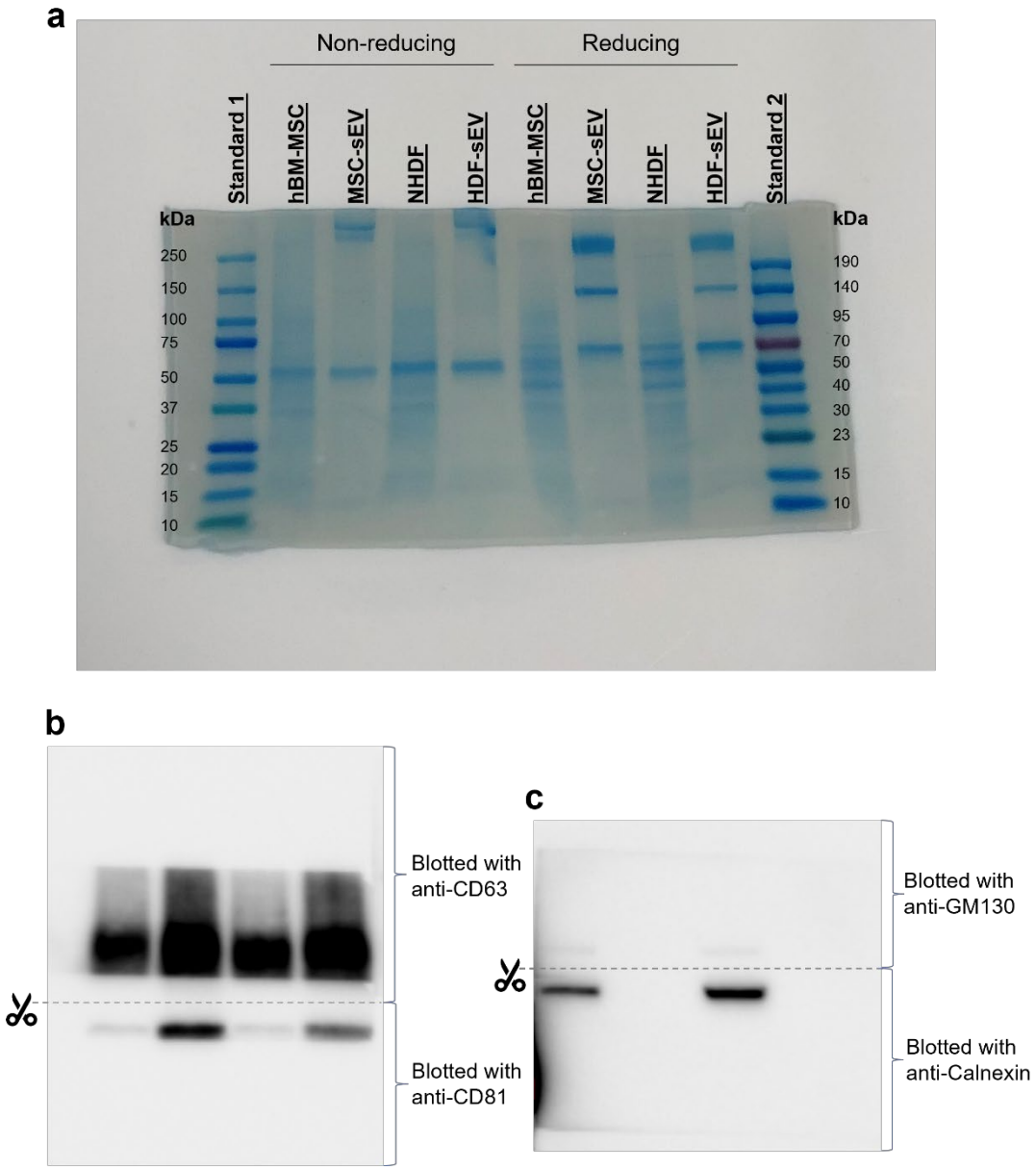
This might because that no other supplements except these secretome fractions were added in the DMEM medium and therefore the beneficial factors inside started to show their promotive effect in the first instance of treatment and then were ran out of quickly under these nutrition starvation background. It also indicates that to investigate the function of cellular secretome, the simplest approach is to culture the testing/recipient cells in DMEM-only medium throughout the testing period, and our experiment setting provides a sensible environment without interference from additives for evaluating the beneficial activities of cellular secretome.

Our study provides a NHDF-based model of wound healing for comprehensive functional comparison of cellular secretome and its fractions from both the parent MSCs and the recipient NHDFs under a sensible environment without interference from additives. To improve this model, more cells such as keratinocytes and endothelial cells, which play non-negligible roles in skin wound healing, should also be taken into account as the recipient cells. In addition, a limitation of this model was that it only shows cellular response to the stimuli of the secretome, therefore, complementary to this cell-based model, further research about molecular level characterisation such as the transcriptome of the recipient cells after different secretome treatments is ongoing, aiming at creating a more rigorous detection platform for functional identification using functional biomarker, which would strongly support precise medical research and application. It should also be noted that the research of sEV fractions in this study was limited by the productivity of sEVs to some extent, which is a common but serious

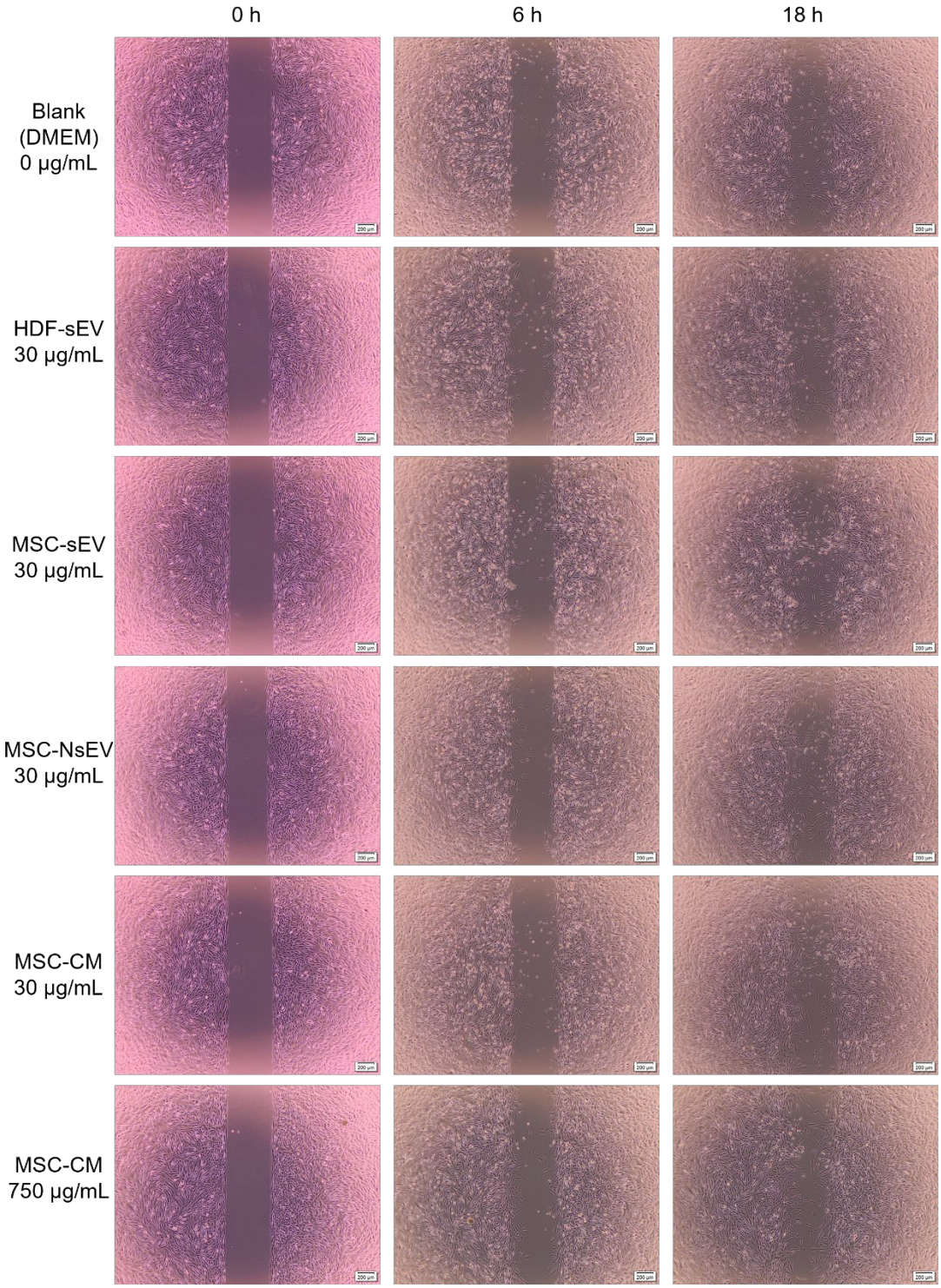
challenge in the field of extracellular vesicles. To break the bottleneck, our team is conducting research in an automated bioreactor for the large-scale production of sEVs for the purpose of extensive research, clinical trial and application in the future.

In conclusion, there might be multiple active components but also defective components in the MSC derived conditioned medium for wound healing. sEV fraction from MSCs seems to be more potent for NHDF migration among different secretome fractions from MSCs and also superior in effect to the corresponding sEVs produced by the recipient NHDFs. Non-sEV fraction from MSCs also showed its promotive effect in skin cell migration and proliferation and therefore should be valued during the functional evaluation, but the defective components inside should be treated with caution. Our findings provide referential significance for the choice of cellular secretome fractions to be used as skin regeneration strategies. The secretome fractionation method and the cell-based functional comparison strategy designed by us would be a useful tool for comprehensive functional evaluation of cellular secretome and its fractions from the parental cells and the recipient cells under a sensible environment without interference from additives.

3.6 Supplementary Information



Supplementary Figure 3.1 Original images from the western blot data shown in Figure 3.2d. (a) Proteins in the gel visualised by Coomassie Blue. Anti-CD63 antibody and anti-CD81 antibody should be used under non-reducing condition (reducing agent was not added to the sample). Anti-GM130 antibody and anti-Calnexin antibody should be used under reducing condition. (b) Western blot for CD63 and CD81. (C) Western blot for GM130 and Calnexin.



Supplementary Figure 3.2 Bright field images of NHDFs treated with different secretome fractions at 0 h, 6 h and 18 h.

Supplementary Table 3.1 GLM ANOVA results for migration (cell covered area of the gap in μm2) of NHDFs in response to factors of migration time (Hour), three secretome fraction types from MSC (Treatment) and concentration of secretome (Concentration). DF is the abbreviation for Degree of Freedom.

Variable	DF	F Value	P Value
Hour	9	2032.78	<0.001
Treatment	2	29.77	<0.001
Concentration	2	11.48	<0.001
Hour*Treatment	18	0.62	0.889
Hour*Concentration	18	2.10	0.005
Treatment*Concentration	4	11.38	<0.001

Supplementary Table 3.2 Results of Tukey's post-hoc multiple comparisons between different secretome fractions of MSC at different concentrations (e.g. MSC-sEV-1 means the group treated with MSC-sEV at 1 μg/mL) for their effects on migration behaviour of NHDFs. Mean Diff. is the abbreviation for Mean Difference.

Tukey's multiple comparisons test	Mean 1	Mean2	Mean Diff.	Significance	P Value
Blank (DMEM) vs. MSC-sEV-1	672165	734542	-62376	****	<0.0001
Blank (DMEM) vs. MSC-sEV-30	672165	728205	-56040	****	<0.0001
Blank (DMEM) vs. MSC-CM-1	672165	668993	3172	ns	>0.9999
Blank (DMEM) vs. MSC-CM-30	672165	713417	-41251	***	0.0007
Blank (DMEM) vs. MSC-NsEV-1	672165	665273	6893	ns	0.9927
Blank (DMEM) vs. MSC-NsEV-30	672165	659940	12225	ns	0.8787
MSC-sEV-1 vs. MSC-sEV-30	734542	728205	6336	ns	0.9954
MSC-sEV-1 vs. MSC-CM-1	734542	668993	65548	****	<0.0001
MSC-sEV-1 vs. MSC-CM-30	734542	713417	21125	ns	0.3304
MSC-sEV-1 vs. MSC-NsEV-1	734542	665273	69269	****	<0.0001
MSC-sEV-1 vs. MSC-NsEV-30	734542	659940	74602	****	<0.0001
MSC-sEV-30 vs. MSC-CM-1	728205	668993	59212	****	<0.0001
MSC-sEV-30 vs. MSC-CM-30	728205	713417	14789	ns	0.7458
MSC-sEV-30 vs. MSC-NsEV-1	728205	665273	62933	****	<0.0001
MSC-sEV-30 vs. MSC-NsEV-30	728205	659940	68265	****	<0.0001
MSC-CM-1 vs. MSC-CM-30	668993	713417	-44423	***	0.0002
MSC-CM-1 vs. MSC-NsEV-1	668993	665273	3720	ns	0.9998
MSC-CM-1 vs. MSC-NsEV-30	668993	659940	9053	ns	0.9698
MSC-CM-30 vs. MSC-NsEV-1	713417	665273	48144	****	<0.0001
MSC-CM-30 vs. MSC-NsEV-30	713417	659940	53477	****	<0.0001
MSC-NsEV-1 vs. MSC-NsEV-30	665273	659940	5333	ns	0.9982

Supplementary Table 3.3 GLM ANOVA results for migration (cell covered area of the gap in μm2) of NHDFs in response to factors of migration time (Hour), two secretome fraction types from MSC (Treatment) and concentration of secretome (Concentration). DF is the abbreviation for Degree of Freedom.

Variable	DF	F Value	P Value
Hour	9	2143.94	<0.001
Treatment	1	11.20	0.001
Concentration	4	31.06	<0.001
Hour*Treatment	9	0.43	0.919
Hour*Concentration	36	2.20	<0.001
Treatment*Concentration	4	4.75	0.001

Supplementary Table 3.4 Results of Tukey's post-hoc multiple comparisons between two secretome fractions of MSC at different concentrations (e.g. MSC-CM-1 means the group treated with MSC-CM at 1 μg/mL) for their effects on migration behaviour of NHDFs. Mean Diff. is the abbreviation for Mean Difference.

Tukey's multiple comparisons test	Mean 1	Mean2	Mean Diff.	Significance	P Value
Blank (DMEM) vs. MSC-CM-1	672165	668993	3172	ns	>0.9999
Blank (DMEM) vs. MSC-CM-30	672165	713417	-41251	**	0.0035
Blank (DMEM) vs. MSC-CM-750	672165	740091	-67926	****	<0.0001
Blank (DMEM) vs. MSC-CM-1500	672165	714119	-41953	**	0.0027
Blank (DMEM) vs. MSC-NsEV-1	672165	665273	6893	ns	0.9993
Blank (DMEM) vs. MSC-NsEV-30	672165	659940	12225	ns	0.9656
Blank (DMEM) vs. MSC-NsEV-750	672165	740701	-68535	****	<0.0001
Blank (DMEM) vs. MSC-NsEV-1500	672165	691481	-19315	ns	0.6674
MSC-CM-1 vs. MSC-CM-30	668993	713417	-44423	**	0.0010
MSC-CM-1 vs. MSC-CM-750	668993	740091	-71098	****	<0.0001
MSC-CM-1 vs. MSC-CM-1500	668993	714119	-45125	***	0.0008
MSC-CM-1 vs. MSC-NsEV-1	668993	665273	3720	ns	>0.9999
MSC-CM-1 vs. MSC-NsEV-30	668993	659940	9053	ns	0.9951
MSC-CM-1 vs. MSC-NsEV-750	668993	740701	-71707	****	<0.0001
MSC-CM-1 vs. MSC-NsEV-1500	668993	691481	-22487	ns	0.4593
MSC-CM-30 vs. MSC-CM-750	713417	740091	-26674	ns	0.2257
MSC-CM-30 vs. MSC-CM-1500	713417	714119	-702	ns	>0.9999
MSC-CM-30 vs. MSC-NsEV-1	713417	665273	48144	***	0.0002
MSC-CM-30 vs. MSC-NsEV-30	713417	659940	53477	****	<0.0001
MSC-CM-30 vs. MSC-NsEV-750	713417	740701	-27284	ns	0.1994
MSC-CM-30 vs. MSC-NsEV-1500	713417	691481	21936	ns	0.4952
MSC-CM-750 vs. MSC-CM-1500	740091	714119	25972	ns	0.2586
MSC-CM-750 vs. MSC-NsEV-1	740091	665273	74818	****	<0.0001
MSC-CM-750 vs. MSC-NsEV-30	740091	659940	80151	****	<0.0001
MSC-CM-750 vs. MSC-NsEV-750	740091	740701	-609.5	ns	>0.9999
MSC-CM-750 vs. MSC-NsEV-1500	740091	691481	48610	***	0.0002
MSC-CM-1500 vs. MSC-NsEV-1	714119	665273	48846	***	0.0002
MSC-CM-1500 vs. MSC-NsEV-30	714119	659940	54179	****	<0.0001
MSC-CM-1500 vs. MSC-NsEV-750	714119	740701	-26582	ns	0.2298
MSC-CM-1500 vs. MSC-NsEV-1500	714119	691481	22638	ns	0.4497
MSC-NsEV-1 vs. MSC-NsEV-30	665273	659940	5333	ns	0.9999
MSC-NsEV-1 vs. MSC-NsEV-750	665273	740701	-75428	****	<0.0001
MSC-NsEV-1 vs. MSC-NsEV-1500	665273	691481	-26208	ns	0.2472
MSC-NsEV-30 vs. MSC-NsEV-750	659940	740701	-80761	****	<0.0001
MSC-NsEV-30 vs. MSC-NsEV-1500	659940	691481	-31541	ns	0.0736
MSC-NsEV-750 vs. MSC-NsEV-1500	740701	691481	49220	***	0.0001

Supplementary Table 3.5 GLM ANOVA results for migration (cell covered area of the gap in μm2) of NHDFs in response to factors of migration time (Hour), cell source of sEVs (sEV type) and concentration of sEVs (Concentration). DF is the abbreviation for Degree of Freedom.

Variable	DF	F Value	P Value
Hour	9	1844.09	<0.001
sEV type	1	30.40	<0.001
Concentration	4	9.28	<0.001
Hour*sEV type	9	0.53	0.850
Hour*Concentration	36	1.70	0.007
sEV type*Concentration	4	2.49	0.042

Supplementary Table 3.6 Results of Tukey's post-hoc multiple comparisons between different sEV types at different concentrations (e.g. MSC-sEV-0.01 means the group treated with MSC-sEV at 0.01 μg/mL) for their effects on migration behaviour of NHDFs. Mean Diff. is the abbreviation for Mean Difference.

Tukey's multiple comparisons test	Mean 1	Mean2	Mean Diff.	Significance	P Value
Blank (DMEM) vs. MSC-sEV-0.01	672165	698860	-26695	ns	0.3469
Blank (DMEM) vs. MSC-sEV-0.1	672165	711355	-39189	*	0.0225
Blank (DMEM) vs. MSC-sEV-1	672165	734542	-62376	****	<0.0001
Blank (DMEM) vs. MSC-sEV-30	672165	728205	-56040	****	<0.0001
Blank (DMEM) vs. HDF-sEV-0.01	672165	672552	-386.9	ns	>0.9999
Blank (DMEM) vs. HDF-sEV-0.1	672165	669409	2756	ns	>0.9999
Blank (DMEM) vs. HDF-sEV-1	672165	687378	-15212	ns	0.9291
Blank (DMEM) vs. HDF-sEV-30	672165	700293	-28127	ns	0.2759
MSC-sEV-0.01 vs. MSC-sEV-0.1	698860	711355	-12494	ns	0.9778
MSC-sEV-0.01 vs. MSC-sEV-1	698860	734542	-35681	ns	0.0569
MSC-sEV-0.01 vs. MSC-sEV-30	698860	728205	-29345	ns	0.2230
MSC-sEV-0.01 vs. HDF-sEV-0.01	698860	672552	26308	ns	0.3675
MSC-sEV-0.01 vs. HDF-sEV-0.1	698860	669409	29451	ns	0.2187
MSC-sEV-0.01 vs. HDF-sEV-1	698860	687378	11483	ns	0.9870
MSC-sEV-0.01 vs. HDF-sEV-30	698860	700293	-1432	ns	>0.9999
MSC-sEV-0.1 vs. MSC-sEV-1	711355	734542	-23187	ns	0.5489
MSC-sEV-0.1 vs. MSC-sEV-30	711355	728205	-16851	ns	0.8785
MSC-sEV-0.1 vs. HDF-sEV-0.01	711355	672552	38802	*	0.0251
MSC-sEV-0.1 vs. HDF-sEV-0.1	711355	669409	41945	*	0.0100
MSC-sEV-0.1 vs. HDF-sEV-1	711355	687378	23977	ns	0.5013
MSC-sEV-0.1 vs. HDF-sEV-30	711355	700293	11062	ns	0.9898
MSC-sEV-1 vs. MSC-sEV-30	734542	728205	6336	ns	0.9998
MSC-sEV-1 vs. HDF-sEV-0.01	734542	672552	61989	****	<0.0001
MSC-sEV-1 vs. HDF-sEV-0.1	734542	669409	65132	****	<0.0001
MSC-sEV-1 vs. HDF-sEV-1	734542	687378	47164	**	0.0018
MSC-sEV-1 vs. HDF-sEV-30	734542	700293	34249	ns	0.0804
MSC-sEV-30 vs. HDF-sEV-0.01	728205	672552	55653	****	<0.0001
MSC-sEV-30 vs. HDF-sEV-0.1	728205	669409	58796	****	<0.0001
MSC-sEV-30 vs. HDF-sEV-1	728205	687378	40828	*	0.0140
MSC-sEV-30 vs. HDF-sEV-30	728205	700293	27913	ns	0.2860
HDF-sEV-0.01 vs. HDF-sEV-0.1	672552	669409	3143	ns	>0.9999
HDF-sEV-0.01 vs. HDF-sEV-1	672552	687378	-14826	ns	0.9386
HDF-sEV-0.01 vs. HDF-sEV-30	672552	700293	-27740	ns	0.2942
HDF-sEV-0.1 vs. HDF-sEV-1	669409	687378	-17969	ns	0.8341
HDF-sEV-0.1 vs. HDF-sEV-30	669409	700293	-30883	ns	0.1665
HDF-sEV-1 vs. HDF-sEV-30	687378	700293	-12915	ns	0.9727

Supplementary Table 3.7 GLM ANOVA results for proliferation (Folds of OD450 at Day 0) of NHDFs in response to factors of treatment time (Day), cell source of secretome (Cell Source) and secretome fraction type (Treatment) at concentration ≤ 30 μg/mL. DF is the abbreviation for Degree of Freedom.

Variable	DF	F Value	P Value
Day	2	407.25	<0.001
Cell source	1	0.82	0.364
Treatment	2	3.10	0.046
Day*Cell source	2	0.23	0.796
Day*Treatment	4	1.29	0.273
Cell source*Treatment	2	0.34	0.709

Supplementary Table 3.8 Results of Tukey's post-hoc multiple comparisons between different secretome fraction types at different concentrations (e.g. MSC-sEV-1 means the group treated with MSC-sEV at 1 μg/mL) for their effects on proliferation behaviour of NHDFs. Mean Diff. is the abbreviation for Mean Difference.

Tukey's multiple comparisons test	Mean 1	Mean2	Mean Diff.	Significance	P Value
Blank (DMEM) vs. MSC-sEV-1	1.838	2.101	-0.263	ns	0.9957
Blank (DMEM) vs. MSC-sEV-30	1.838	2.461	-0.624	ns	0.4988
Blank (DMEM) vs. MSC-CM-1	1.838	2.486	-0.648	ns	0.4419
Blank (DMEM) vs. MSC-CM-30	1.838	2.754	-0.917	ns	0.0750
Blank (DMEM) vs. MSC-CM-750	1.838	4.547	-2.710	****	<0.0001
Blank (DMEM) vs. MSC-CM-1500	1.838	4.510	-2.672	****	<0.0001
Blank (DMEM) vs. MSC-NsEV-1	1.838	2.465	-0.627	ns	0.4907
Blank (DMEM) vs. MSC-NsEV-30	1.838	2.527	-0.689	ns	0.3565
Blank (DMEM) vs. MSC-NsEV-750	1.838	3.993	-2.156	****	<0.0001
Blank (DMEM) vs. MSC-NsEV-1500	1.838	4.142	-2.304	****	<0.0001
Blank (DMEM) vs. HDF-sEV-1	1.838	2.310	-0.472	ns	0.8516
Blank (DMEM) vs. HDF-sEV-30	1.838	2.145	-0.307	ns	0.9942
Blank (DMEM) vs. HDF-CM-1	1.838	2.455	-0.617	ns	0.5144
Blank (DMEM) vs. HDF-CM-30	1.838	2.771	-0.933	ns	0.0655
Blank (DMEM) vs. HDF-CM-750	1.838	3.901	-2.063	****	<0.0001
Blank (DMEM) vs. HDF-CM-1500	1.838	4.473	-2.636	****	<0.0001
Blank (DMEM) vs. HDF-NsEV-1	1.838	2.173	-0.335	ns	0.9878
Blank (DMEM) vs. HDF-NsEV-30	1.838	2.382	-0.545	ns	0.6916
Blank (DMEM) vs. HDF-NsEV-750	1.838	3.767	-1.930	****	<0.0001
Blank (DMEM) vs. HDF-NsEV-1500	1.838	4.302	-2.464	****	<0.0001

Chapter 4 An Automated, High-throughput, Hollow Fibre Bioreactor System for Production of Mesenchymal Stromal Cells Derived Small Extracellular Vesicles

This chapter presents the following article:

Lei, R., Zeng, Y., Cui, Z., Ye, H. An Automated, High-throughput, Hollow Fibre Bioreactor System for Production of Mesenchymal Stromal Cells Derived Small Extracellular Vesicles. To be submitted.

Author contributions:

Z.C. and H.Y. defined the project scope and provided research funding and supervised the research. R.L. designed the experiments. R.L. and Y.Z. performed the experiments. R.L. analysed data and drafted the manuscript. Z.C. and H.Y. reviewed the manuscript.

4.1 Abstract

Small extracellular vesicles derived from mesenchymal stromal cells (MSC-sEVs) have been identified as a promising cell-free alternative to mesenchymal stromal cell (MSC) based therapy in the field of regenerative medicine, as it has been confirmed by numerous studies that MSC-sEVs are the key roles to mediate the curative action of the MSCs. However, the low sEV yield is currently the major hurdle for the realization of MSCs-sEV in further therapeutic applications. To address this problem, here we developed an automated, scalable and bio-safe method relied on hollow fibre bioreactor (HFBR) based cell expansion system (CES) from Oxford MEStar, which would be feasible for large scale production of high quality sEVs. The growth of MSCs in the HFBR based CES was closely monitored, and the produced MSC-sEVs were characterised and compared to the traditional flask produced MSC-sEVs in terms of their physiochemical properties and functional potency. Our finding demonstrated that the developed CES method successfully achieve a 13-day continuous MSC cultivation and a 250-fold higher yield of MSC-sEVs with comparable properties and bioactivities but higher purity, compared to the traditional flask method. This HFBR based CES method also allows simplification of previous manually procedures, increases the reproducibility and biosafety of the sEV production, and largely reduces the associated capital and operational costs. Overall, our study is the first one that demonstrates the feasibility of the Oxford MEStar Cell Expansion System for sEV production, and provides a promising, industrial-applicable methods for mass production of MSC-sEVs

with satisfied quality, which could make considerable contribution to the clinical applications of MSC-sEV based therapeutics.

4.2 Introduction

Extracellular vesicles (EVs) are non-replicable, lipid bilayer membrane-bound nanoparticles naturally secreted by most cells [10], with a diameter mainly ranging from 30 nm to 1000 nm. Small extracellular vesicle (sEV), which refer to the EVs < 200 nm in diameter [11], is the major and the most popular EV type that has been widely reported for their role as significant cell-cell communication mediators [12]. By delivering preassembled complex biological information (including nucleic acids, proteins and lipids) from parent cells to the recipient cells, sEVs can play their function role in numerous physiological and pathological processes [13–15]. Due to their intrinsic nature, sEVs can serve as a promising diagnostic and therapeutic strategy and have huge potential in the application of circulating markers for disease diagnostics [16], drug delivery vehicles [17], immunomodulation [19], and tissue regeneration [18]. sEVs, especially released by mesenchymal stromal/stem cells (MSCs), are attracting increasing interest, as extensive studies have demonstrated that MSC derived sEVs (MSC-sEVs) are responsible for the regenerative effect of MSCs through paracrine secretion [21,65]. Thus, MSC-sEVs can be regarded as a powerful cell-free therapeutic substitute for MSC-based therapy to overcome the risk factors that accompanied with MSC treatment in regenerative medicine, including tumorigenesis occurred by cell dysfunction, immune rejection and other technical issues [3].

The translation of MSC-sEV therapy is based on the mass production of MSC-sEVs with excellent quality to satisfy the requirement of clinical studies and

applications [24]. However, the advancements of MSC-sEV based products is considerably hampered by the extremely low production yield of sEVs [25]. The current approach of sEV production relies on the collection of the conditioned medium (CM) from the classic batch cell cultivation in flasks, where the total yield of sEVs is limited by the restricted growth of the adherent MSCs within the small surface area [26]. Scale up of the platform for cell culture to accommodate the maximal cell number can be the most straightforward approach for large scale production of sEV-based products. For example, by increasing the surface area, multilayer cell culture flasks like Nunc™ Cell Factory™ Systems [28], stirred tank bioreactors with microcarriers [29], and perfusion hollow fibre bioreactors (HFBR) [30,31] have been tested to replace the traditional single layer flask-based cell culture for sEV manufacture.

Hollow fibre bioreactor has been increasingly used in the field, because of its continuous production, pre-concentration ability of the cell secreted products and excellent scalability. Indeed, Watson et al. showed that the sEV yield given by the HFBR was about 40-fold higher than that of the traditional flask-based production [83]. However, most of these studies have been confined to a simple and crude, relatively small lab-scale sEV production with the disadvantages of bad monitoring and controls, and extra GMP facilities requirement, which is far from the automatic production and therefore is not feasible for the commercialisation of the sEV products. As a result, an automated, high-throughput and bio-safe method is still required to meet the needs of a cost-effective, industrial-sized production of sEVs with consistent quality.

In this study, we utilised the Oxford MEStar Cell Expansion System (CES), an enclosed automated and scalable HFBR-based platform that was originally established to produce clinical doses of adherent or suspended cells for cell therapies. The main body of the HFBR is a cartridge cylinder which is divided into two compartments called extracapillary space (ECS) and intracapillary space (ICS) by hollow fibres. Cells can be cultured on the outer layer of the hollow fibre membrane for several weeks or months without passage [24], with continuous feeding of the fresh medium to the cell culture compartment and removal of the waste by the circulated flow in the system. We further modified the process flow and the tubing, and developed the operating protocols specialised for the purpose of mass production of high quality sEVs for 13 days. The conditioned medium would be collected from the ECS every 48 hours since Day 3 for sEV purification. Besides, the preservation of the physiochemical properties and bioactivity of sEVs is of significant importance during the large-scale production by HFBR. Therefore, the assessment of sEV yield, size distribution, morphology, purity, expression of sEV markers were conducted by nanoparticle tracking analysis, protein quantification, transmission electron microscopy and western blot, and the functional potency was evaluated using normal human dermal fibroblast-based proliferation and migration assay for the quality control of sEV production. This is the first study that demonstrates the feasibility of the Oxford MEStar Cell Expansion System for sEV production. It also provides a promising industrial applicable method to address the

obstacle of MSC-sEV production, which may have great implications for the clinical translation and commercialisation of MSC-sEV based therapeutics.

4.3 Materials and Methods

4.3.1 Preparations

4.3.1.1 Cell Expansion in Flasks

Human Bone Marrow derived Mesenchymal Stem Cells (MSCs) (Cat.: C-12974, PromoCell, Germany) were expanded to passage 8 in T175 flasks (Cat.: 10296861, Corning, USA). Complete medium consists of PromoCell MSC growth medium (Cat.: C-28009, PromoCell, Germany), 1% Anti-Anti (Cat.: 15240-062, Gibco, USA) and corresponding supplement (Cat.: C-39809, PromoCell, Germany) was used to culture the cells.

4.3.1.2 Preparation of EV-depleted Medium

The supplement was ultracentrifuged overnight at 120,000 × g, 4°C using Himac CP70NE Ultracentrifuge (Himac, Japan) and P28S Rotor (Himac, Japan) to deplete autologous EVs. The supernatant was regarded as EV-depleted supplement. 0.22 µm vacuum filter apparatus (Cat.: 431097, Corning, USA) was used to sterilise the supernatant from the ultracentrifugation. The EV-depleted medium was made up of PromoCell MSC growth medium (Cat.: C-28009, PromoCell, Germany), 10% sterilised EV-depleted supplement and 1% Anti-Anti (Cat.: 15240-062, Gibco, USA).

4.3.2 Design and Operation of the Hollow Fibre Bioreactor based Cell Expansion System for Production of MSC-sEVs

4.3.2.1 Configuration of the Hollow Fibre Bioreactor based Cell Expansion System

The Oxford MEStar Cell Expansion System consists of an electronic control panel for adjustment of valves, pumps and operating parameters, a customised refrigerator for storage of pre-prepared buffer and medium, and an incubator where the HFBR system is located (Figure 4.1a). The process flow was modified, consisting of an intracapillary space feed line (ICS FEED), an extracapillary space feed line (ECS FEED), an intracapillary space circulation line (ICS CIRC.), an extracapillary space circulation line (ECS CIRCULATION) and a waste line, which were expressed in different colour in Figure 4.1c. The layout and the tubing were changed accordingly in the incubator. Cells were cultured on the outer layer of the hollow fibre in the HFBR and was fed by the ECS loop and the ICS loop as shown in Figure 4.1b. The culture process is computerised, and all the parameters can be shown and adjusted on the touch screen of the control panel. The whole loop is enclosed or under the protection of the sterile 0.2 μm filter during the operation to prevent contamination.

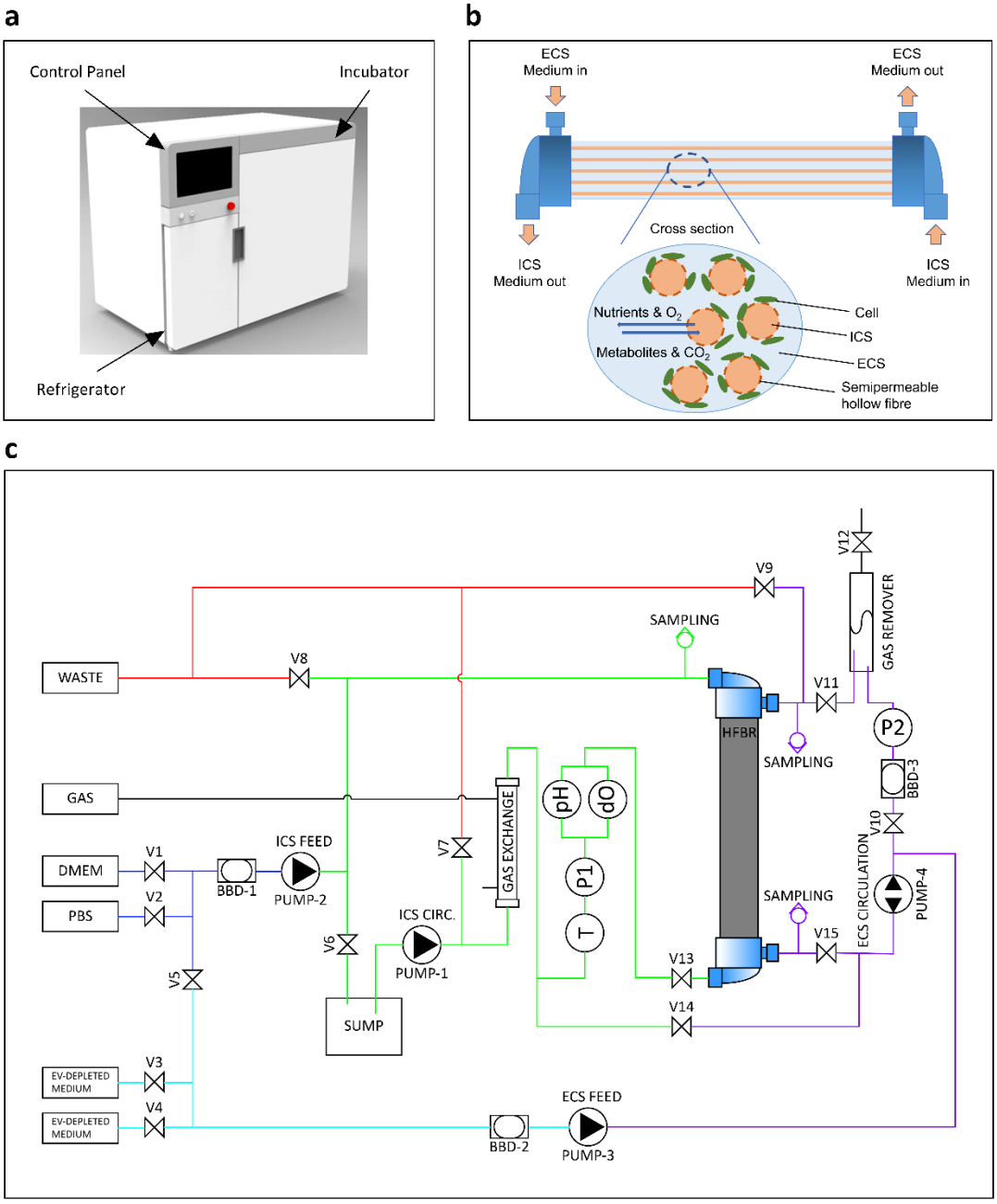


Figure 4.1 Detail information of the modified Oxford MEStar Cell Expansion System. (a) The outside appearance of the CES. (b) Schematic diagram and working principle of the HFBR cartridge. (c) Process flow diagram of the sEV production. BBD – bubble detector, V – valve, T – temperature sensor, P – pressure sensor, pH – pH sensor, dO – oxygen sensor.

4.3.2.2 Pre-coating of the HFBR Cartridge

Phosphate buffered saline (PBS, Cat:10010-031, Gibco, USA) was supplied to the ICS (i.e., culture medium circulation zone) and then ECS (i.e. the growth zone) of the

hollow fibre cartridge FX10 (Fresenius, China) using a 60 mL luer-lock syringe. After emptying the liquid in the ECS as much as possible, the coating solution was prepared with 5 mL of 0.1% Fibronectin human plasma solution (Cat: F0895-5MG, Sigma-Aldrich, USA) and 45 mL of PBS, and then loaded to the ECS through its inlet using a 60 mL luer-lock syringe. The membrane of the growth zone was allowed to be coated with fibronectin overnight before use.

4.3.2.3 Assembly of the HFBR Loop and Setting of the CES

The coated hollow fibre cartridge, gas exchange cartridge, reservoir bottle, sensor sets, pumps, tubing, medium bags with PBS and corresponding medium, as well as other consumables (all the items were purchased as a consumable package from MeStar, UK) were sterile and then assembled according to the manufacturer's inductions and the modified process flow in the biosafety cabinet. The medium bags were fitted into the customised refrigerator of the CES and the rest of the loop were fitted into the incubator of the CES. The temperature of the CES incubator was set to 37℃ and gas with 5% CO_2 was connected to the gas exchange cartridge.

4.3.2.4 Priming of the HFBR Loop

The whole loop was thoroughly flushed with PBS, followed by DMEM (Cat:11885-084, Gibco, USA) and finally EV-depleted medium for 24 hours. Afterwards, the medium in the loop was discarded and replaced with fresh EV-depleted medium. The fresh medium was circulated in the ICS circulation line (green) and ECS circulation line (purple) by setting Pump 1 and Pump 4 to 100 mL/min, with V1, V2, V3, V4, V7, V8, V9, V14 closed and Pump 2, Pump 3 set at 0 mL/min.

4.3.2.5 Cell Seeding for the CES

MSCs were digested from T175 flasks, and about 9.2 x 10^7 cells were resuspend in 40 mL EV-depleted medium. Specifically, the hollow fibre cartridge was placed horizontally. The circulation of the culture medium was stopped by setting Pump 1 and Pump 4 to 0 mL/min, and V15 was closed. The tubes at the inlet and outlet of both the ECS and ICS were clamped. The prepared cell suspension was seeded into the growth zone by a syringe via the inlet sampling port of the ECS. At the same time, the culture medium of the ECS was replaced by the cell suspension and collected by another syringe at the outlet sampling port of the ECS. The collected culture medium from the outlet sampling port was then injected through the inlet sampling port, and the replaced cell-containing medium was again withdrawn from the outlet sampling port with a syringe. The cell suspension was then pumped back and forth by these two syringes at the inlet and outlet sampling ports for about 5 to 6 times until the turbidity of the cell suspension inside both syringes was almost the same to ensure a uniform cell distribution. The inlet and outlet of the ICS was unclamped and all the cell suspension inside the syringes was injected into the ECS. The hollow fibre cartridge was then rotated every 30 minutes for 8 times in the CES incubator at 37°C and 5% CO_2, allowing uniform attachment of cells to the hollow fibre membrane. At the same time, the circulation of the culture medium in ICS was turned on to provide required gas by setting the flow rate of Pump 1 to 100 mL/min. After 4.5 hours of attachment, the inlet and outlet of the ECS were unclamped, and fresh EV-depleted culture medium was supplied to the ECS by opening V3 and V4 and setting the flow rate of Pump 3 to 0.1

mL/min. The automatic mode was then achieved that the whole system was automatically replenished, culture medium and oxygen was applied to the growth zone while waste was removed with the ICS cycle. The day of cell seeding was regarded as Day 0. The cells were allowed to adapt to the culture environment for overnight and Day 1 was regarded as the first day of sEV production. The conditioned medium was collected every 48 hours since then.

4.3.2.6 Monitoring of the Cell Culture in the CES

The ECS medium was collected on Day 0, 3, 5, 7, 9, 11 and 13 of the cell culture, and the glucose and lactate level were measured by High Sensitivity Glucose Assay Kit (Cat: MAK181-1KT, Sigma-Aldrich, USA) and Lactate Assay Kit (Cat: MAK064-1KT, Sigma-Aldrich, USA) according to the manufacturer's instructions, respectively. The flow rate of the fresh culture medium supply would be doubled when either the glucose level was below 3.8 mM or the lactate level was higher than 4 mM. Other parameters including temperature, pressure, pH, CO2 and oxygen level were closely monitored by the CES system.

4.3.2.7 Collection of the Conditioned Medium from the CES

The real volume of the conditioned medium per harvest is actually equal to the volume of the ECS (about 55 mL). However, to maximise the number of sEV collected, an extra volume of medium (about 45 mL) was drawn from the ICS to the ECS to allow back and forth flushing by syringe to collect the sEVs as much as possible, making the final CM volume equal to 100 mL per harvest. Specifically, the fresh medium feeding and circulation were stopped by setting the flow rate of Pump 1 and Pump 3 to 0

mL/min. V11 and V13 was closed, and about 45 mL conditioned medium in ECS was drawn by a syringe from the ECS sampling port close to V11, after which the sampling point of ICS was clamped, and another syringe was connected to the ECS sampling port close to V15. The conditioned medium was pumped back and forth by these two syringes at the inlet and outlet of the ECS for about 6 times and then the 45 mL conditioned medium was collected. After the first collection, the ECS sampling port close to V11 was connected with a 0.22 μm vacuum filter apparatus and then a luer-lock syringe with 55 mL air. The 55 mL conditioned medium in the ECS space and the connected tubes was then replaced with the air, collected by the syringe from the ECS sampling port close to V15, and then pooled together with the conditioned medium of the first collection. Therefore, 100 mL of the conditioned medium was harvested from the CES. The air in the CES was then replaced with fresh EV-depleted medium and the CES was set back to the automatic mode for cell culture. Conditioned medium was collected on Day 3, and then every 2 days until Day 13.

4.3.3 Traditional Flask Method for Production of MSC-sEVs

MSCs were digested from T175 flasks, and 2.5 x 10^6 cells were seeded per T175 flask and cultured in 25 mL of complete medium at 37℃, 5% CO_2 on Day 0. After overnight attachment, the complete medium was replaced with 25 mL EV-depleted medium on Day 1, with 2 times of wash with PBS in between. The conditioned medium was harvested after 48 hours on Day 3.

4.3.4 sEV Isolation, Characterisation and Analysis

4.3.4.1 Isolation of sEVs by Ultracentrifugation

sEVs were isolated from conditioned medium by differential centrifugation, included 300 × g for 15 min, 2000 × g for 30 min, and 10,000 × g for 40 min by Eppendorf 5810R Centrifuge (Eppendorf, Germany), followed by 100,000 × g ultracentrifugation (90 min) by Himac CP70NE Ultracentrifuge (Himac, Japan) and P70AT Rotor (Himac, Japan). The crude sEV pellets obtained were then resuspended in PBS and again centrifuged at 100,000 × g for 45 min by Optima™ MAX-TL Ultracentrifuge (Beckman Coulter, USA) and TLA-120.2 Rotor (Beckman Coulter, USA). The final pellets obtained from the second-round ultracentrifugation were resuspended in PBS. sEVs of the conditioned medium from flasks and the CES were termed as Flask-sEV and CES-sEV, respectively.

4.3.4.2 Nanoparticle Tracking Analysis (NTA)

NanoSight NS300 (Malvern Panalytical Ltd, UK) was used to measure the size distribution and concentrations of sEVs by recording the particle movement for 60 seconds and 5 repeats at camera level 13 for each sample. NTA 3.2 software (Malvern Panalytical Ltd, UK) was used to analyse the results at detect threshold 7.

4.3.4.3 Protein Extraction and Quantification

At the end of cell culture, MSCs were digested by 0.05% trypsin-EDTA solution (Cat.: 25300-054, Gibco, USA) from T175 flasks (Flask-MSC) and the CES (CES-MSC), respectively. The pellets of Flask-MSC and CES-MSC after 5-minute centrifugation at 300 × g were lysed on ice by the mixture of RIPA buffer (Cat.: 89901,

Thermo Fisher Scientific, USA) and Protease Inhibitor Cocktail (Cat.: 04693159001, Roche, Switzerland) for 30 min, respectively. Afterwards, the supernatant after 20-minute centrifugation at 12000 rpm was taken as the lysate of Flask-MSC and CES-MSC. The sEV preparations from both methods were lysed on ice with the same lysing buffer for 30 min. Protein concentration of the sEV lysates and cell lysates were measured by QuantiPro™ BCA Assay Kit (Cat.: QPBCA-1KT, Sigma-Aldrich, USA).

4.3.4.4 Western Blot

Equivalent proteins quantities of the lysates were mixed with 4x Laemmli buffer (Cat.: 1610747, Bio-Rad, USA) and reducing agent (Cat.: NP0004, Thermo Fisher Scientific, USA), heated to 95℃ for 5 min, and electrophoresed for 65 min on 4–20% Precast Protein Gels (Cat.: 4561094, Bio-Rad, USA) at 120V. Subsequently, proteins were transferred to a polyvinylidene fluoride (PVDF) membrane by Trans-Blot Turbo system (Cat.: 1704155, Bio-Rad, USA). After blocked by Blotting-Grade Blocker (Cat.: 1706404, Bio-Rad, USA) for 60 min and washed by PBS-Tween buffer (Cat.: 28346, Thermo Fisher Scientific, USA) before and after the blocking, the membrane was incubated with primary antibodies including anti-CD63 (1:2000; Cat.: ab59479, Abcam, UK), anti-CD81 (1:2000; Cat.: ab79559, Abcam, UK), anti-calnexin (1:1000; Cat.: 2679S, Cell Signaling Technology, USA) and anti-GM130 (1:500; Cat.: 610822, BD Biosciences, USA) at 4℃ overnight. The membrane was then washed 3 x 5 min with PBST and followed by 60 min secondary antibody incubation at room temperature, using secondary anti-mouse (1:1000; Cat.: 7076P2, Cell Signaling Technology, USA)

and anti-rabbit antibody (1:1000; Cat.: 7074P2, Cell Signaling Technology, USA). The protein bands were then visualised by Bio-Rad Chemidoc XRS system (Cat.: 1708265, Bio-Rad, USA), after treated with ECL Substrate (Cat.: 170-5060, Bio-Rad, USA) for 10 min.

4.3.4.5 Transmission Electron Microscopy (TEM)

The copper grids with a thin carbon coated film (Cat.: BZ10023b, ZJKY, China) was glow discharged and was incubated with 5 µl of sEV samples for 2 min. Filter paper was used to remove excess liquid by blotting. The grids were negatively stained with 10 µl 2% uranyl acetate (Cat.: GZ02625, ZJKY, China) for 15 s, followed by blotting. sEVs were visualised by a Tecnai G2 F20 S-TWIN transmission electron microscope (FEI, USA) under 200 KV.

4.3.4.6 Proliferation Assay

Flask-sEV suspension was diluted to 1, 10, 30 µg/mL and CES-sEV suspension was diluted to 1, 10, 30, 50, 70 µg/mL by fresh DMEM, respectively. An equal volume of PBS was diluted by fresh DMEM, served as blank control (0 µg/mL). NHDFs (5000 cells per well) in 96-well plates (Cat.: 3599, Corning, USA) were treated with 100 µL Flask-sEV and CES-sEV at different concentrations as well as blank control (0 µg/mL) in triplets, respectively. After 72 hours, the medium was removed from each well and cells were washed with 100 µL PBS per well. The cells were then treated with the mixture of 100 µL DMEM and 10 µL CCK-8 reagent (Cat.: CK04, Dojindo, Japan) per well and incubated for 2 hours at 37 ºC. The absorbance results at 450 nm were

expressed as Optical Density (OD 450), and were determined by Spark microplate reader (Tecan, Switzerland). The proliferation assay was repeated for 3 times.

4.3.4.7 Migration Assay

NHDFs were seeded to 24-well plates (10^5 cells per well) with pre-attached 2-well culture-insert (ibidi, Germany) in the middle of each well. A 500 μm gap was created on the confluent cell layer in each well, after overnight cell attachment and removal of the inserts. NHDFs were washed with PBS and then treated with Flask-sEV (30 μg/mL), CES-sEV (30 μg/mL) and blank control (0 μg/mL) in triplets for 48 hours, respectively. Bright field images of cell migration were taken at 0 h, 4 h, 8 h, 12 h, 16 h, 20 h, 24 h, 30 h, 36 h, 48 h. ImageJ and Matlab were used to analyse the cell covered area of the gap. The migration assay was repeated for 3 times.

4.3.4.8 Statistical Analysis

Experiments were done at least in triplets with data showed in mean ± standard deviations (SD). The statistical significance between the purity of Flask-sEV and CES-sEV was analysed by two tailed t-test. One-way ANOVA or two-way ANOVA followed by Tukey's multiple comparisons were applied to assess the statistical significance of the rest data using GraphPad Prism, version 8. The probability $p \leq 0.05$ was considered statistically significant, *$p \leq 0.05$, **$p \leq 0.01$, ***$p \leq 0.001$.

4.4 Results

4.4.1 Cell Culture in the CES

Due to the about 100-fold larger surface area, 90 million of cells could be seeded in the HFBR of the CES, which was 36-fold higher than that of the flask method. With lower seeding density, the MSCs was successfully cultured in the ECS of the HFBR cartridge for 13 days without passage (Table 4.1). The consumption of glucose and the production of lactate has been adopted as surrogate markers to monitor the metabolism and expansion status of the MSCs in the CES. During the whole period of cell culture, the seeded MSCs continuously consumed the glucose in the culture medium, leading to a consistent drop in the glucose level, although with the perfusion of the fresh medium at 0.1 mL/min from day 0. A doubled perfusion rate was applied since day 11 when the glucose concentration was below 3.8 mM, for the purpose of providing sufficient nutrients but also out of the cost-effective consideration. A subsequent rapid increase in lactate concentration was also observed (Figure 4.2).

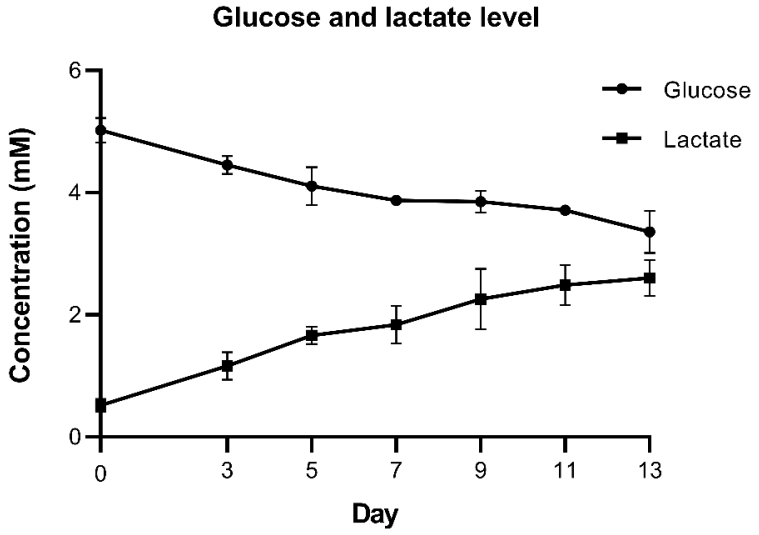


Figure 4.2 Glucose and lactate level in the CES during the 13-day cell culture (n=3).

4.4.2 Comparison of the Characterisation Results between Flask-sEV and CES-sEV

For the traditional flask method, 2.5 x 10^6 MSCs were seeded per T175 flask and after overnight attachment, cells were gently washed twice with PBS and replaced with 25 mL sEV collection medium per flask. The conditioned medium was harvested after incubation for further 48 hours. In contrast, for the CES method, 90 millions MSCs were seeded to the CES system on day 0. After 4.5 hours attachment, fresh sEV collection medium started to be pumped to the system. 100 mL conditioned medium were harvested on day 3 and then every 48 hours until day 13. The sEVs were isolated from the conditioned medium of flask method (Flask-sEV) and CES method (CES-sEV) by ultracentrifugation method, respectively. The sEVs isolated from the flasks or CES at different period showed a consistent size distribution and was corresponding to the characteristic profiles of sEVs (Figure 4.3a&b), peaking at modes between 115 and 125 nm, with about 83% of the particles being 30 to 200 nm in size and no significant difference in the mean size (Figure 4.3c&d). The existence and the purity of the sEVs was confirmed by that both sEV preparations were positive for typical sEV markers such as CD63 and CD81, and negative for intracellular compartment markers, like Calnexin and GM130 (Figure 4.3e). Classic cup-shaped sEV particles were found in TEM images from both as well (Figure 4.3f&g).

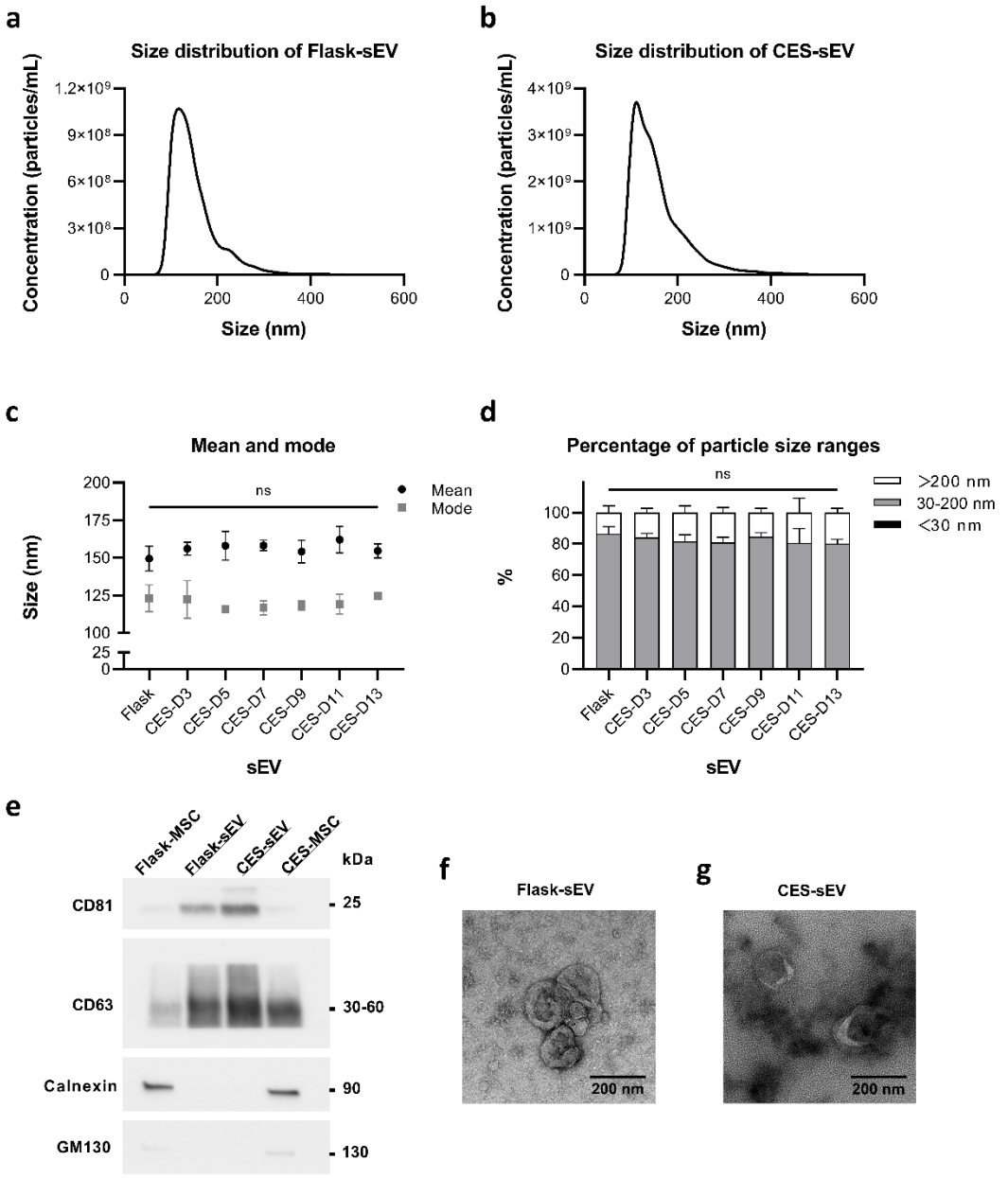


Figure 4.3 Characterisation of Flask-sEV and CES-sEV. (a) Average size distribution of Flask-sEV (n=5). (b) Average size distribution of CES-sEV (n=5). (c) Mean and mode of Flask-sEV and CES-sEV isolated on day 3 (D3), day 5 (D5), day 7 (D7), day 9 (D9), day 11 (D11) and day 13 (D13) (n=5). (d) Percentage of sEV particles of different size ranges (n=5). (e) Western blot results of Flask-sEV, CES-sEV and their parent cells. (f) TEM image of Flask-sEV. (g) TEM image of CES-sEV.

4.4.3 Comparison of the sEV Production Capacity between Traditional Flask Method and CES Method

The yield of sEVs was quantified by nanoparticle tracking analysis in particle number and BCA method in protein amount, respectively. Compared to the traditional flask method, CES method demonstrated a remarkable production capacity as shown in Table 4.1. sEVs could be produced and concentrated continuously for 13 days in the ECS of HFBR, and CM could be harvested regularly (6 times during the whole process) from the CES in contrast to the batch production of the flask method. More than 600 billion particles in total were produced by CES, which is equal to the yield (in particle number) of 250 T175 flasks. And when quantify the yield in protein amount, the CES method was able to produce more than 2 mg sEVs during the whole process, which is 170-fold higher than that of the traditional flask method.

Table 4.1 Comparison of traditional flask method and CES method for sEV production.

	Flask	CES
Number of cells seeded (million)	2.5	90
Surface area of cell culture (cm^2)	175	18000
Seeding density (cells / cm^2)	14285	5000
Culture period without passage (day)	3	13
Culture medium required in total (mL)	25	4150
Number of harvestings	1	6
CM collected every harvesting (mL)	25	55 (CM) + 45 (extra medium)
Total yield - particle number	$2.51\times10^{9} \pm 5.63\times10^{8}$	$6.24\times10^{11} \pm 8.00\times10^{10}$
Total yield - protein amount (μg)	12.67 ± 2.02	2157.94 ± 261.18

Specifically, the amount of sEV produced per million cells on Day 3 of CES process was slightly lower than that of the T175 flask, no matter quantified in particle number or protein amount. However, from Day 5 onwards, there was no significant

difference in sEV yield per million cells between the CES method and the flask method. This indicates that cells can grow and produce sEVs normally in the CES (Figure 4.4a). However, the amount of sEVs produced per 48 hours from the CES was significantly higher (about 30 to 40-fold) than that of a single T175 flask, mainly due to that the HFBR-based CES provides more growing surface and can accommodate more cells to grow (Figure 4.4b). In addition, from the same volume of the conditioned medium, the amount of sEVs produced by the CES was about 20-fold higher than that of the flask, indicating that the membrane bioreactor could have a function in pre-concentration of the conditioned medium (Figure 4.4c). Moreover, it can also be deduced that the sEVs produced by the CES method was about 1.4-fold purer than that of the flask method, as the particle-to-protein ratio, which is a parameter to evaluate the purity of sEV preparations, was calculated as 2.958×10^8 particles/μg protein and 2.126×10^8 particles/μg protein for the CES-sEV and Flask-sEV, respectively. (Figure 4.4d).

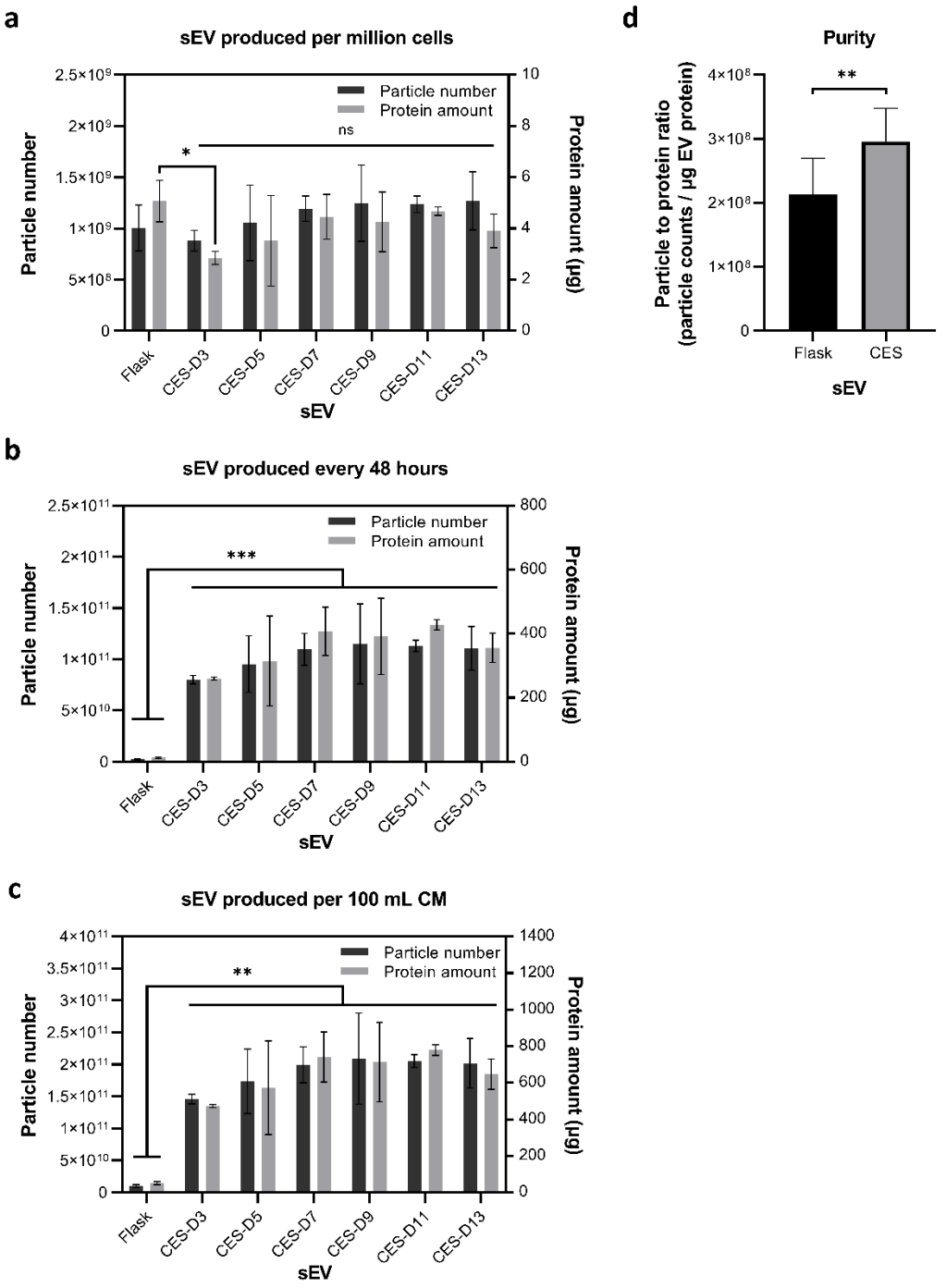


Figure 4.4 The yield and purity of sEVs produced by traditional flask method and CES method. (a) Yield per million seeded cells (n=3). (b) Yield every 48 hours (n=3). (c) Yield per 100 mL CM (n=3). (d) The purity of CES-sEV and Flask-sEV was assessed by the ratio of particles per μg protein (n=5).

4.4.4 Functional Characterisation of Flask-sEV and CES-sEV

sEVs produced by both methods were co-cultured with normal human dermal fibroblasts, respectively. Due to the limited productivity of the traditional flask method, normal human dermal fibroblasts were only able to be co-cultured with the flask derived sEVs at a maximum concentration of 30 μg/ml (Figure 4.5a), while the CES method allow a higher concentration treatment up to 70 μg/ml because of its powerful sEV production capacity (Figure 4.5b). Particularly, a promotion of the cell proliferation was shown with the treatment of 70 μg/ml CES-derived sEVs, while the rest treatment groups with lower concentrations no matter produced by the flask method or CES method, didn't show a significant effect on the cell proliferation, although a dose dependent trend was found. In addition, sEVs produced by both methods exhibited promotion of migration of normal human dermal fibroblasts, and there was no significant difference in the promotion effect between the two (Figure 4.5c).

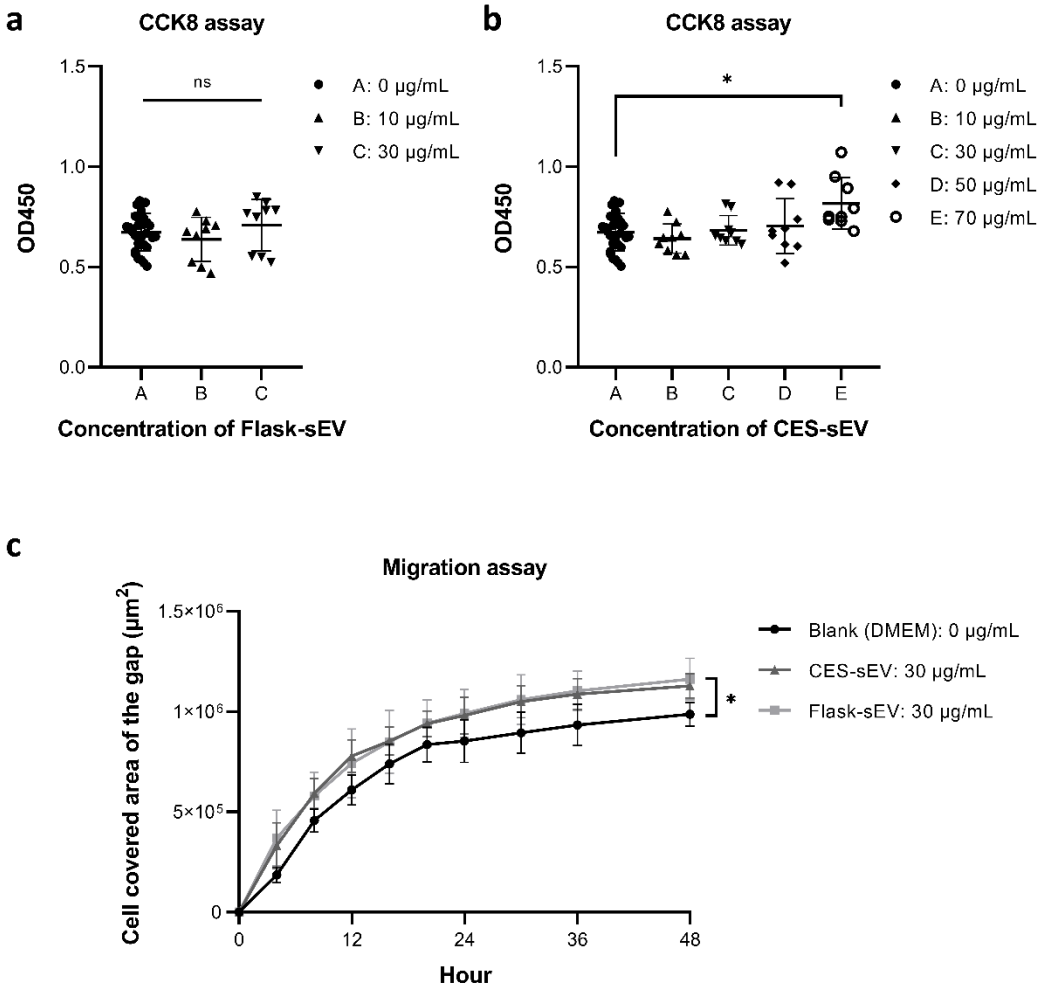


Figure 4.5 Functional potency of sEVs. (a) The effect of different concentrations of Flask-sEVs on the proliferation of NHDFs (n=9). (b) The effect of different concentrations of CES-sEVs on the proliferation of NHDFs (n=9). (c) The effect of 30 μg/mL sEVs on the migration of NHDFs. Blank (DMEM) at 0 μg/mL served as control group (n=12).

4.5 Discussion

The clinical translation of MSC-sEVs to therapeutic products largely depends on the development of a robust, large scale, minimum human intervened and cost-effective method to achieve an industrial-sized production of high quality sEVs with consistent physiochemical properties and biopotency. Therefore, in this study, we established an efficient method for sEV mass production using a hollow fibre bioreactor-based cell expansion system. As this equipment was originally designed for cell therapy, the tubing design and operating parameter setting of the CES were modified, and protocols for seeding and MSC cultivation as well as CM collection were developed for the purpose of high yield production of bioactive sEVs. We proved that the hollow fibre bioreactor based CES provides the necessary culture environment to maintain the viability of MSCs during the 13-day cell culture period, and in turn allows for a continuous production of large quantities of sEVs with high purity and expected bioactivity, which could make considerable contributions to downstream clinical studies and future therapeutic applications.

As sEVs are secreted products of cells, the total yield of sEV manufacture is partially dependent on the number of the producer cells [125]. However, the cell growth can be largely limited by the small surface area in routine flask culture [40]. Hollow fibre bioreactors with the advantage of maximising surface area are reported to be a promising method to achieve a higher yield of MSCs within a small 3D space [130]. A bundle of hollow fibres is sealed in a cartridge cylinder, where cells are cultured outside

of the tube-like, semi-permeable hollow fibres, and fresh medium was continuously introduced to the system by the perfusion pump. Gas, nutrients and metabolite wastes are exchanged between ECS and ICS through the porous structure of the fibres.

sEVs can be regarded as a fingerprint of the their parent cells, thus, a healthy status of the MSCs in the HFBR is the premise of successful production of high quality sEVs with satisfied properties and potency, and close monitoring of the cell condition is a vital step of EV manufacture [24]. Glucose is the primary energy source for cell metabolism, and glycolytic metabolism would lead to an accumulation of lactate in continuous incubation of mammalian cells [219], while lactate at high level could play a negative role in growth and metabolism of the cells [220]. As a result, the glucose and lactate levels were analysed as an indicator of expansion and metabolic activities of cells in the closed bioreactor system [221–223], and the perfusion rate of the fresh medium would be doubled to maintain a good cell culture environment when either the glucose level was below 3.8 mM or the lactate level was higher than 4 mM. According to the results in Figure 4.2, the consumption of glucose and the production of lactate was continuously increased with the time course, indicating active metabolism and possible expansion of MSCs during the 13-day cell cultivation period. This might because of the consistent fresh medium perfusion and efficient mass transfer inside the bioreactor, key nutrients were continuously replenished to support cell proliferation, and the level of metabolic wastes (e.g. lactate) was controlled via diffusion through the porous membrane to minimise their negative impact on cell growth [224]. Similar results were

also reported by Haack-Sørensen et al., Mizukami et al. and Li et al., showing successful long term culture of human MSCs using hollow fibre bioreactor system [223–225].

Our results further confirmed an exceptionally remarkable sEV productivity of the developed HFBR-based CES, showing a continuous production of considerable amount of sEVs with comparable biophysical properties and biological activities to those of traditional flask derived sEVs. It seems that the MSCs cultured in the HFBR-based CES can still preserve an overall similar sEV production ability per cell to that of flask-cultured MSCs, although a relative lower sEV yield per million seeded cells was found at the early stage of cell culture in CES (Figure 4.4a). A possible explanation could be that not all the cells injected to the CES were successfully attached to the surface of hollow fibres, leading to an overestimation of the seeded cell number and thus an underestimated sEV yield per million seeded cells. Indeed, obvious cell and debris pellets were observed during the 300 × g and 2000 × g centrifugation steps for the conditioned medium harvested from the CES on day 3 (the first collection). Another possible reason could be that a longer period of environmental adaption may be required by the seeded cells at the beginning of cell culture in the CES, as a result, sEV secretion may be affected by the initial status of their parent cells. It was not surprising that a rising trend of the sEV yield per million seeded cells was then observed at later stage (Figure 4.4a), which could be corresponding to the cell expansion within the CES, based on the previous cell monitoring results. Besides, although the average sEV

production ability per million seeded cells in the CES was on par to that of flask-based process, a 30 to 40-fold higher sEV yield can be achieved per harvest by the CES method (Figure 4.4b). This mainly due to the key feature of the HFBR that an extremely large surface area was provided by a bundle of hollow fibres. Actually, an effective surface area of 1.8 m^2 is reported by the supplier of the hollow fibre cartridge, which is equal to the total surface area of 103 T175 flasks, allowing the cultivation of a significant number of MSCs and thus promoting the sEV production. Our self-developed CM collection protocol also maximise the number of sEV collected per harvest. The real volume of the conditioned medium per harvest is actually equal to the volume of the ECS (about 55 mL). However, as some of the sEVs might attached on the internal surface of the cartridge or tubes or be trapped by the hollow fibre membrane, an extra volume of medium (about 45 mL) was drawn from the ICS to the ECS to allow this syringe-based back and forth flushing protocol to collect the sEVs as much as possible, making the final CM volume equal to 100 mL per harvest. And with the practical advantage of continuous cell culture and multiple CM harvest, HFBR-based CES was eventually able to achieve a 250-fold total sEV yield (in particle number) from a single batch of cell cultivation in contrast to that of a traditional flask method (Table 4.1). In addition, the biological activities of sEVs, especially on promoting proliferation and migration of the human dermal fibroblasts, were confirmed to be preserved by the CES method. Yan et al. has also reported that umbilical cord MSC derived sEVs produced by 3D HFBR can even have a stronger ability in anti-apoptosis

and accelerating proliferation and migration of chondrocytes, compared to conventional 2D flask derived sEVs [226]. Meanwhile, the results in terms of the CCK8 assay again supported that the productivity of the HFBR-based CES method can meet the need of higher dose for effective treatment, which is very promising to tackle the current bottleneck of sEV translation (Figure 4.5).

Retention and pre-concentration of the sEVs is another vital strength of HFBR-based CES. An average hollow fibre membrane pore size of 1.8 nm (reported by the supplier) allows removal of those metabolic wastes and non-EV contaminants that are smaller than the membrane pore size, and meanwhile MSC-sEVs can be continuous produced and accumulated within the small volume of ECS to produce sEV-concentrated conditioned medium (Figure 4.4c), due to their larger size than the membrane pore size, which largely facilitates the downstream isolation process with easier liquid handling, less operational costs and labour costs [26]. Similar to our findings, a 7.5-fold higher yield per mL conditioned medium was reported by Yan et al. for umbilical cord MSCs cultured in HFBR against the conventional flask cultured cells [226]. Watson et al. also demonstrated that HFBR could allow for a yield of sEVs 40-fold higher from the same volume of conditioned medium than that of the classic method, although using a cell type different from our studies [83]. Also, a better purity of sEV preparations post-separation might be very likely to be achieved by the CES method (Table 4.1), which is consistent to the findings reported by Grangier rt al. that suggests a higher particle-to-protein ratio of sEVs from hollow fibre bioreactor than that of

classic flask method [33]. Further scalability is also available by modification of the tubing sets and parallel connection of numerous HFBR cartridge to enable multi-HFBR production at the same time.

Other benefits provided by this HFBR-based CES should also be taken into account. With the characteristic of automated process, our HFBR-based CES method can considerably simplifies the previous labour-intensive procedure for cell cultivation and CM collection, reduces labour costs and the potential human error, minimise the process variability from batch to batch, and therefore would contributes to a reproducible production of high quality sEVs. Moreover, this closed HFBR-based CES with a good manufacturing practice (GMP) setting can largely reduce the risk of contamination, which is a common problem of traditional cell culture in open design flasks, and thus ensure the biosafety of sEV production. As a result, cell cultivation and CM collection can be conducted in local undesirable conditions, such as hospitals, without high-end GMP facilities, which significantly reduce the capital costs and widen the range of applications. On the other hand, the consumable and operational costs can also be saved, given the fact that the total yield of the CES method was about 250-fold higher than that of traditional flask method, hence, to achieve the same yield, about 6250 mL of the culture medium is required to culture 250 T175 flasks of cells, in contrast to the 4150 mL needed by the CES method.

However, the possible phenotypic changes of cells and thus the alteration of secreted sEVs could be a potential risk for long-term sEV production by the HFBR

method [24,40]. Hence, further studies should be conducted for immunophenotyping analysis and trilineage mesoderm differentiation potential analysis of the MSCs before and after the cultivation in the CES. Besides, complementary to the cellular functional tests, research about immunotyping of the sEV products as well as the molecular level characterisation of the sEV cargoes is warranted for further characterisation and the quality control of the CES-based sEV production.

Overall, the establishment of this automated, high-throughput and bio-safe HFBR-based method would allow for a continuous and cost-effective production of MSC-sEVs with satisfied quality. The considerable sEV production capacity of this method can meet the high demand of the sEV product for either downstream studies or further applications, and subsequently accelerate the progress of the MSC-sEV products in clinical translation. Future optimisation of this method would be continued, in terms of various operation parameters and development of specialised hollow fibre cartridge for sEV production. It is encouraged as well to make parallel comparisons between the CES technique and other commercially accessible bioreactors/platforms in terms of cell cultivation and sEV production capability. Study with more focus on its universal applicability is also recommended, with the means of evaluating the sEV production ability using different cell types.

Chapter 5 Purification of Mesenchymal Stromal Cell derived Small Extracellular Vesicles Using Ultrafiltration

This chapter presents the following article:

Lei, R., Ren, S., Ye, H., Cui, Z. Purification of Mesenchymal Stromal Cells Derived Small Extracellular Vesicles Using Ultrafiltration. To be submitted.

Author contributions:

Z.C. and H.Y. provided research funding and supervised the research. R.L. designed and performed the experiments. R.L. analysed the data and drafted the manuscript. S.R. completed the computational fluid dynamics simulation part. Z.C., H.Y. reviewed the manuscript.

5.1 Abstract

Mesenchymal stromal cell derived small extracellular vesicles (MSC-sEVs) have been reported to play a vital role in exerting curative effects of mesenchymal stromal cells (MSCs), while the translation of MSC-sEVs into clinical products is hindered by the technical challenges associated with scaled production and isolation / purification of sEVs. Among various feasible separation technologies, ultrafiltration is identified as an efficient, scalable and cost-effective method that has the potential to be adopted for scaled sEV isolation or purification. However, there has been no study so far that evaluates the potential application of ultrafiltration for sEV purification and comprehensively investigates the effects of different ultrafiltration design and operational parameters on the isolation of sEVs. Hence, in this study, the impacts of membranes and operational parameters including stirring speed, operational pressure, feed concentration and diafiltration on the yield, purity and productivity of MSC-sEVs were investigated using a stirred cell ultrafiltration system. The results indicated that 500 kDa molecular weight cut-off (MWCO) membrane is more suitable for the MSC-sEV purification, giving a higher purity and productivity of sEVs, compared to 100 kDa and 300 kDa membranes. Shear rate (stirring speed) also affects the purification performance and so does the transmembrane pressure, as expected. The MSC-sEV productivity and purity can be improved by applying a moderate stirring speed and lower operational pressure, respectively. Isovolumetric diafiltration process could further enhance the purity of MSC-sEVs, which was able to remove about 99% of the

protein contaminants by 6 diafiltration volumes. Based on the experimental results, a fed-batch ultra-diafiltration process with optimised filtration parameters was then developed and its performance was compared with the currently most used ultracentrifugation method for the isolation of MSC-sEVs. The developed fed-batch ultra-diafiltration protocol shows an exceptional ability and performance in the isolation of MSC-sEVs: the yield of MSC-sEV preparation (recovery of particles) was increased from 20.59% to 60.88% (about 3 folds increase), and the purity (particle to protein ratio) was increased from 6.93×10^{8} to 1.33×10^{9} (nearly doubled), compared to that of the commonly used ultracentrifugation method. The outcome of this study concluded that ultrafiltration could be a promising method for both lab-scale preparation and industrial scale manufacture of MSC-sEVs with advantages of high recovery, scalable, fast, and cost effective.

5.2 Introduction

Small extracellular vesicles (sEVs) are nano-sized bilipid membranous particles released by cells, ranging from 30 to 200 nm and usually with spherical shape [10,62]. Due to their immunomodulating potency [70], regenerative activity, systematically distribution and specific targeting ability [17], sEVs have been broadly reported to have a huge potential as a therapeutic strategy for various disease and tissue regeneration, for example in skin [84,85], adipose [227], kidney [87], liver [88], heart [86], bone [228], cartilage [89]. Particularly, sEVs derived from mesenchymal stromal/stem cells (MSC-sEVs) have emerged as key paracrine mediators that induce the curative functions of MSCs, and therefore can serve as critical cell-free therapeutic tool in regenerative medicine, without introducing safety issues associated with live cell-based treatment.

Robust isolation and purification of MSC-sEVs from MSC conditioned medium (CM), which is a complex mixture of cell secretome with high heterogeneity [32], is a key technical requirement to ensure the application of high quality MSC-sEVs with a consistent properties, purity and yield for the downstream therapy [27,33]. In addition, to meet the high demand of MSC-sEVs in their clinical translation and commercialisation, scalability is an essential characteristic of any practical separation and purification methods. Ultracentrifugation (UC) is currently the most commonly used approach for laboratory scale sEV separation, which allows the isolation process from about several hundred mL conditioned medium [34]. However, UC suffers the obvious drawbacks of co-isolation of the contaminants, mechanical damage of sEVs due to high shear force

[35], poor accessibility of the ultracentrifuges and rotors owing to their high cost, and labour intensive [36]. The commercial rotor-dependant working capacity and the batch process also largely limit the scalability of the UC method [31,158]. Other separation methods including precipitation [38], affinity-based capture [37], and size exclusion chromatography [39], have also been studied in the previous sEV research, while limitations regarding the introduction of undesirable precipitating reagents, high expenses, and the small working volume hamper the application of above methods in large scale isolation of sEVs for clinical purpose, respectively [40].

Recently, ultrafiltration has been proposed as a preferred sEV isolation method due to its high scalability and affordable costs, which makes it applicable for the industrial scale sEV manufacture [27]. Indeed, a 7-fold yield of MSC-sEVs was demonstrated by Haraszti et al. using tangential flow filtration with 500 kDa MWCO hollow fibre filter, compared to the UC method [29]. Heinemann et al. also reported that sEVs with satisfied purity and size distribution could be obtained by their self-developed sequential filtration protocol consisting of dead-end filtration with 0.1 μm polyethersulfone membrane, tangential flow filtration by 500 kDa MWCO hollow fibre filter , and final filtration with 100 nm track etch filter [229]. Increasing applications of membrane filtration method in the field has been reported. However, little is known about sEV-membrane interaction and the influence of various ultrafiltration parameters on the recovery, purity and productivity of sEVs, which are important to the development and optimisation of ultrafiltration-based sEV isolation protocol.

In this study, the effects of different ultrafiltration parameters including membrane pore size, stirring speed, operational pressure, feed concentration and diafiltration on the isolation of sEVs were systematically studied, with the aim of retaining most of the sEV particles (yield), maximising the removal the non-sEV protein contaminants (purity). and meanwhile achieving higher sEV productivity. In the experiments, 20 mL conditioned medium (also termed as feed) was concentrated to 2 mL through the ultrafiltration membrane within a stirred cell membrane filtration system, and the permeate flowrate was recorded at the meantime. The feed, the permeate and the retentate were collected and analysed in terms of particle number, particle size distribution and protein amount. The recovery of the particle, the transmission of the protein contaminants, the purity and the productivity of the sEVs were subsequently calculated to evaluate the purification of sEVs. Based on the test results, a fed-batch ultra-diafiltration protocol with optimised filtration parameters was established for the isolation and purification of MSC-sEVs. The sEV isolated by this method was compared with that of the traditional ultracentrifugation method, regarding the processing time, sEV size distribution, yield, purity, biomarker expression and morphology. Our research is the first study that comprehensively explore the influence of different ultrafiltration parameters on the purification of sEVs. And such a fed-batch ultra-diafiltration process showed outstanding advantages for both lab-scale preparation and industrial scale purification of MSC-sEVs.

5.3 Materials and Methods

5.3.1 Preparations

5.3.1.1 Preparation of EV-depleted Medium

The Fetal Bovine Serum (FBS, Cat.: 10270106, Gibco, USA) was ultracentrifuged for 18 hours at 120,000 × g, 4℃ using Optima™ XPN-80 Ultracentrifuge (Beckman Coulter, USA) with SW 32 Ti Rotor (Beckman Coulter, USA) to deplete autologous EVs. The supernatant, regarded as EV-depleted FBS, was collected and sterilised by filtering through 0.22 μm vacuum filter apparatus (Cat.: 431097, Corning, USA). The EV-depleted medium was made up of Dulbecco's Modified Eagle Medium (DMEM, Cat.: 31885049, Gibco, USA), 10% sterilised EV-depleted FBS and 1% Penicillin-streptomycin (Cat.: 15140122, Gibco, USA).

5.3.1.2 Cell Cultivation

The human telomerase reverse transcriptase-immortalized bone marrow mesenchymal stromal cells (hTERT-MSCs) at passage 22 were cultured at a seeding density of 2.5×10^6 cells in 25 mL complete medium (DMEM with 10% FBS and 1% Penicillin-streptomycin) per T175 flask (Cat.: 10296861, Corning, USA) at 37℃, 5% CO_2. After overnight cell attachment, the medium was discarded and replaced with 25 mL fresh EV-depleted medium in each T175 flask. The crude conditioned medium was collected after 48 hours.

5.3.1.3 Preparation of Conditioned Medium

The crude conditioned medium was centrifuged at 2000 × g for 15 min by Labofuge™ 400R Centrifuge (Heraeus, Germany) to remove the dead cells and cell debris, and then centrifuged at 10,000 × g for 40 min by Eppendorf centrifuge 5804R (Eppendorf, Germany), of which the supernatant was collected for later sEV isolation experiments.

5.3.2 Ultrafiltration Method for sEV Isolation

5.3.2.1 Ultrafiltration System

The HP4750 stirred cell (Sterlitech, USA) was utilized to conduct ultrafiltration for sEV isolation (Figure 5.1). The membrane disc, with the diameter of 4.7 cm and surface area of 17.35 cm^2, was mounted at the bottom of this stirred cell. The operational pressure was provided by the compressed air (BOC, UK) and controlled by the pressure regulator and the valve. Stirring speed was applied by the stir bar using the IKA RCT basic magnetic stirrers (IKA, Germany). The permeate would go through the permeate tube and be collected in the permeate collection vessel on the Kern KB 2000-2N precision balance (Kern, Germany), and the mass of the permeate was constantly recorded by the software RsWeight Ver.5.40 during the whole ultrafiltration process and can then be converted to the volume of the permeate.

5.3.2.2 Membrane Ultrafiltration Test for sEV Isolation

The membrane disc was firstly flushed with 250 mL UltraPure™ Distilled Water (Cat.: 10977035, Thermo Fisher Scientific, USA). The stirred cell was then filled with 20mL conditioned medium, and the ultrafiltration was conducted under pre-set pressure

and stirring speed. The ultrafiltration process was completed when 18 mL permeate was collected, i.e. 2 mL retentate was obtained (10-fold concentration by volume). The feed, retentate and permeate were collected and analysed after the filtration experiment. The influence of membrane pore size, stirring speed, applied pressure, feed concentration (direct dilution) and diafiltration process on sEV separation were examined. Membrane discs with 100 kDa, 300 kDa and 500 kDa (Merck Millipore, USA) MWCO were used to study the effects of the membrane pore size. Stirring speeds ranged in 100 – 400 rpm and operational pressures from 5 psi to 25 psi were also tested. For the study of feed concentrations, 1x means no dilution process applied, 0.5x means that the feed is 20mL conditioned medium diluted by 20mL Phosphate Buffered Saline (PBS), 0.25x means that the feed is 20mL conditioned medium diluted by 60mL PBS. For the study of diafiltration process, 20 mL conditioned medium was firstly concentrated to 10 mL, followed by diafiltration including a dilution step with equal amount (10 mL) of PBS and a concentration step to the half volume (10 mL), which is recorded as one diafiltration volume (DV). DV0 means no diafiltration process applied, DV2 means 2 times of such diafiltration step applied, DV6 means 6 times of such diafiltration step applied.

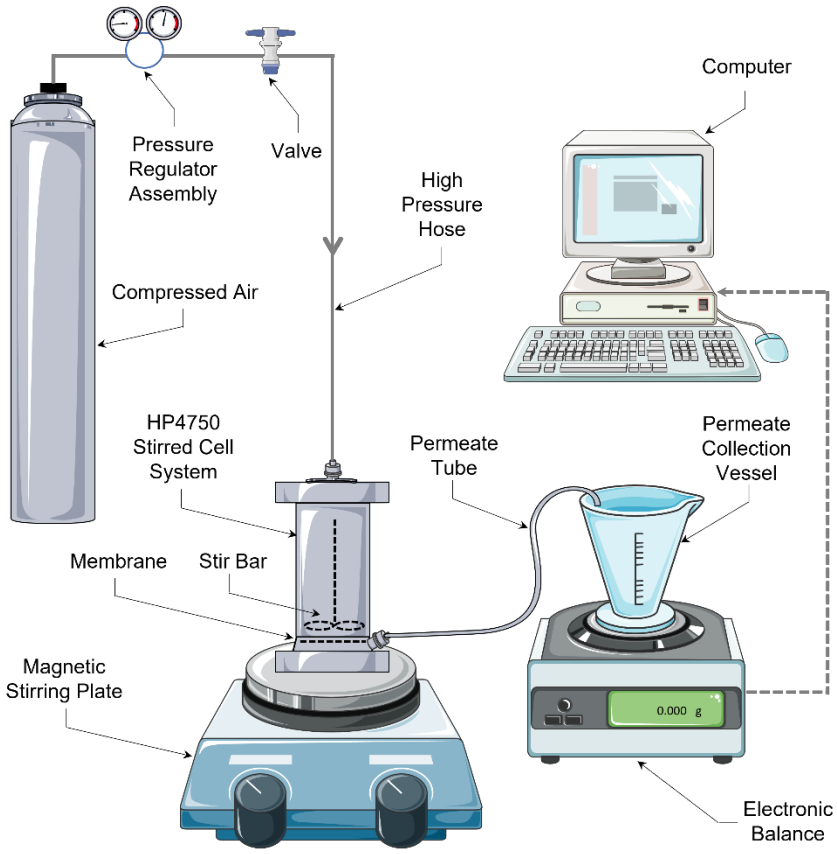


Figure 5.1 Experimental set-up for stirred cell ultrafiltration system.

5.3.2.3 Fed-batch Ultra-diafiltration (UF/DF) Protocol for sEV Isolation

This method was developed based on the setting shown in Figure 5.1. Totally 100 mL conditioned medium was fed to the system in several batches, with a concentration and diafiltration step in between. Specifically, 20 mL conditioned medium was firstly concentrated to 10 mL by 500 kDa MWCO membrane, followed by one diafiltration step (described in previous section), a feed step of adding 10 mL conditioned medium and another concentration step to half volume, of which the last three steps together were regarded as one fed-batch. After 8 times of fed-batch, the 100 mL conditioned medium was concentrated to 10 ml. 7 times of isovolumetric diafiltration were then applied to the concentrated condition medium, and the retentate was concentrated to

700 µl at the end of the process, which was the sEV preparation obtained by the fed-batch UF/DF method (please find Figure 5.6 for details).

5.3.3 Ultracentrifugation Method for sEV Isolation

100 mL conditioned medium was centrifuged at 100,000 × g for 90 min using Optima™ XPN-80 Ultracentrifuge with 70 Ti rotor (Beckman Coulter, USA). The crude pellets were collected and then washed with PBS (Cat.: 10010015, Gibco, USA) using Optima™ MAX-XP Ultracentrifuge (Beckman Coulter, USA) and TLA-55 rotor (Beckman Coulter, USA) at 100,000 × g and 4 °C for 75 min. The pellets obtained were resuspended in 100 µl PBS.

5.3.4 Characterisation and Analysis

5.3.4.1 Nanoparticle Tracking Analysis (NTA)

Particle movements were recorded for 60 seconds and repeated for 5 times for each sample by NanoSight NS300 (Malvern Panalytical Ltd, UK) at camera level 13. sEV concentrations and size distributions were then analysed using NanoSight NTA 3.3 software (Malvern Panalytical Ltd, UK) at detect threshold 5.

5.3.4.2 Protein Extraction and Quantification

The hTERT-MSCs (passage 22) were trypsinised with 0.05% trypsin-EDTA solution (Cat.: 25300062, Gibco, USA) and the cell pellet was obtained after 300 × g centrifugation for 5 min. Pierce™ RIPA buffer (Cat.: 89901, Thermo Fisher Scientific, USA) with cOmplete™, Mini, EDTA-free Protease Inhibitor (Cat.: 04693159001, Roche, Switzerland) were mixed with the MSC pellet. The mixture was incubated on

ice for 30 min, followed by 20-min centrifugation at 12000 rpm, 4℃ using Eppendorf 5424R Centrifuge (Eppendorf, Germany). The supernatant was taken as MSC-lysate. Feed (conditioned medium), retentate, permeate from membrane ultrafiltration tests as well as sEV preparations from both UC method and fed-batch UF/DF method were lysed by adding RIPA buffer with freshly added protease inhibitor and incubating on ice for 30 min. QuantiPro™ BCA Assay Kit (Cat.: QPBCA-1KT, Sigma-Aldrich, USA) and SpectraMax® i3x Microplate Reader (Molecular Devices, USA) were used to quantify the protein concentration.

5.3.4.3 Western Blot

Based on the previous protein quantification results, the protein concentration of cell lysate and sEV lysates were normalised to the same value by PBS. 4x Laemmli sample buffer (Cat.: 1610747, Bio-Rad, USA) was added to all the samples, and NuPAGE sample reducing agent (Cat.: NP0004, Thermo Fisher Scientific, USA) was also added to the samples except those for CD63 detection. The mixture was boiled for 5 min at 95℃. Precision Plus Protein Kaleidoscope Prestained Protein Standard (Cat.: 1610375, Bio-Rad, USA) and all the samples were electrophoresed on 4–20% Mini-PROTEAN® TGX™ Precast Protein Gels (Cat.: 4561094, Bio-Rad, USA) for 95 min in Pierce™ Tris-Glycine SDS Buffer (Cat.: 28362, Thermo Fisher Scientific, USA) at 120V using Thermo EC135-90 Electrophoresis Power Supply (Thermo Electron Corporation, USA). The proteins were transferred to Immun-Blot PVDF Membrane (Cat.: 1620177, Bio-Rad, USA) in Pierce™ Tris-Glycine Buffer (Cat.: 28363, Thermo

Fisher Scientific, USA) at 100V for 90 min. After 5-min wash in Pierce™ Modified Dulbecco's PBS Tween 20 Buffer (Cat.: 28346, Thermo Fisher Scientific, USA), the membranes were blocked with EveryBlot Blocking Buffer (Cat.: 12010020, Bio-Rad, USA) for 30 min at room temperature. The membranes were probed with anti-CD63 (1:1000; Cat.: ab134045, Abcam, UK), anti-TSG101 (1:1000, ab125011, Abcam, UK) and anti-GM130 (1:1000; Cat.: 610822, BD Biosciences, USA) at 4℃ overnight, and then incubated with secondary HRP-linked Anti-mouse IgG Antibody (1:1000; Cat.: 7076P2, Lot.: 34, Cell Signaling Technology, USA) or HRP-linked Anti-rabbit IgG Antibody (1:1000; Cat.: 7074P2, Lot.: 28, Cell Signaling Technology, USA) for 60 min at room temperature. Clarity Western ECL Substrate (Cat.: 170-5060, Bio-Rad, USA) was applied to the membranes for 5 min at room temperature. The results were then imaged by Bio-Rad Chemidoc MP System (Bio-Rad, USA).

5.3.4.4 Transmission Electron Microscopy (TEM)

Transmission electron microscopy was used to visualize the morphology of sEVs. 10 µl sEV sample was added to freshly glow-discharged 300 mesh carbon-coated copper grids, followed by 10-second negative staining using 2% uranyl acetate. Grids were air-dried and imaged in a FEI Tecnai 12 transmission electron microscope at 120 kV using a Gatan OneView CMOS camera.

5.3.4.5 Statistical Analysis

Each experiment was repeated at least three times. Data were expressed as mean ± standard deviation (SD). Statistical analyses were performed by GraphPad Prism, version 8. Differences between two groups were analysed by two tailed t-test.

Differences between three or more groups were analysed using one-way ANOVA or two-way ANOVA, followed by Tukey method for multiple comparisons. The probability value lower than 0.05 was considered significant: *$p \leq 0.05$, **$p \leq 0.01$, ***$p \leq 0.001$. Graphs were created by GraphPad Prism, version 8.

5.4 Results

5.4.1 Effects of Membrane Pore Size

As membrane filtration is a size-based separation method, it is of great importance to choose the membrane with a suitable pore size for sEV separation. Membranes with different molecular weight cut-off (MWCO) values of 100, 300 and 500 kDa were tested, and their performances on particle recovery, removal of protein contaminants, the purity of sEV preparations, permeate flux, and productivity were evaluated.

The size distribution of the nanoparticles retained by three different membrane filters was similar and corresponding to that of the feed and also the characteristic profiles of EV preparations, with the majority falls within the size range of 30 to 200 nm (Figure 5.2a). The recovery of particles was defined as the ratio of total particle number of the retentate to that of the feed. As expected, the 100 kDa membrane showed the highest recovery of particles as it has the smallest pore size among the three. A significant larger number of particles, nearly 100% of the particles from the feed, was recovered by the 100 kDa membrane, while both 300 and 500 kDa filter showed about 40% loss of the nanoparticles, with no significant difference between the two (Figure 5.2b&c). Surprisingly, the number of particles in the permeates of these two membranes only occupied less than 4% of the total particles in the feed (data not shown), which means that over 30% of the total particles are very likely to be trapped by the membranes.

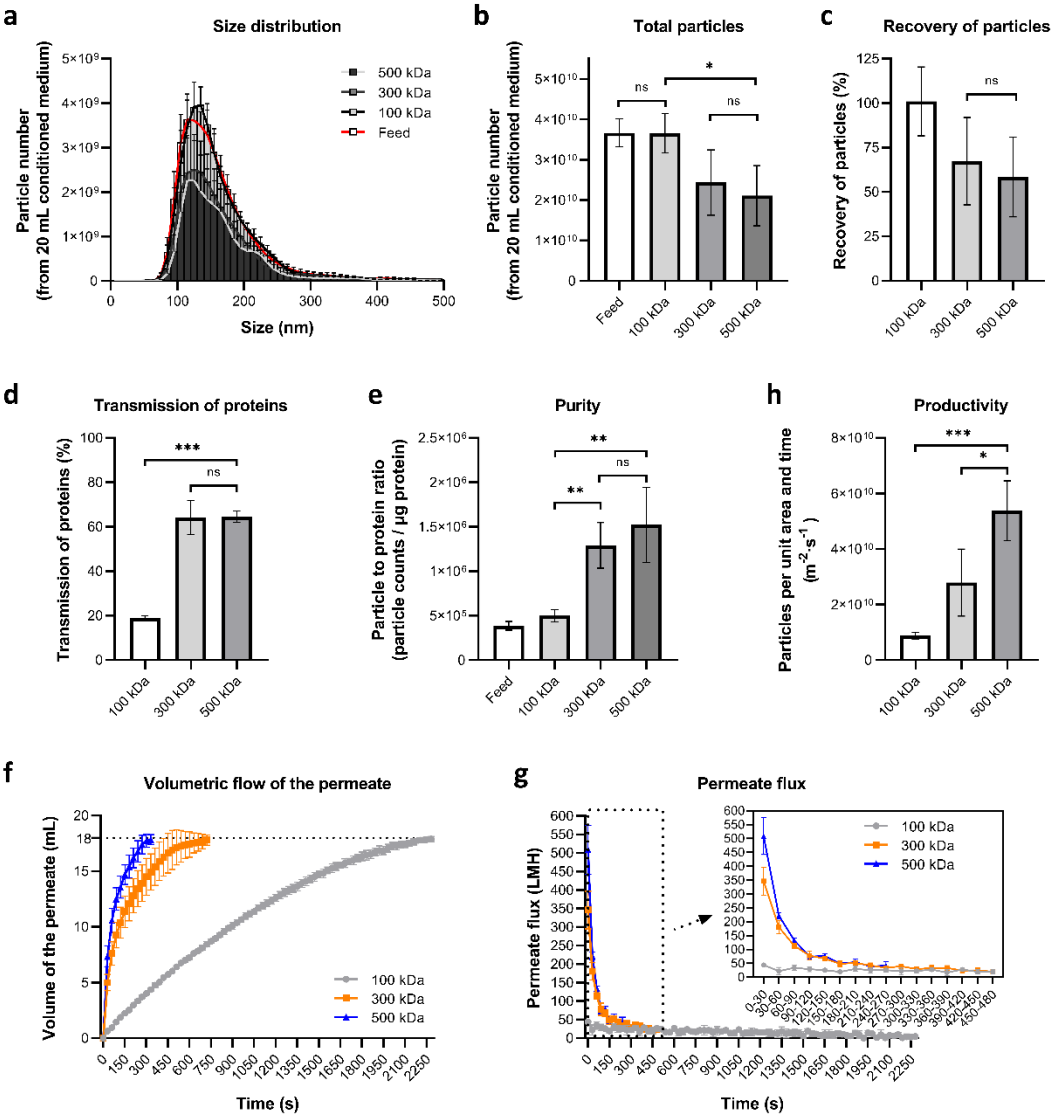


Figure 5.2.The effects of membrane pore size on sEV isolation (n=4). (a) Particle size distributions of the feed solution (CM) and the sEV preparations isolated by different MWCO membranes. (b) Total particle numbers of CM and the sEV preparations. (c) Recovery of particles from CM by different MWCO membranes. (d) Transmission of contaminated proteins during the ultrafiltration using different MWCO membranes. (e) Purity (particle to protein ratio) of CM and the sEV preparations. (f) Volumetric flow rate of the permeate during the ultrafiltration using different MWCO membranes. (g) Permeate flux during the ultrafiltration using different MWCO membranes. (h) Average productivity of sEVs using different MWCO membranes.

Things are different when it comes to the transmission of the protein contaminants and the purity of sEVs. The transmission of the protein is defined as the ratio of total protein amount of the permeate to that of the feed. A significant stronger ability of

removing protein contaminants was shown by both 300 and 500 kDa filter, with the transmission of protein being more than 60%, about 3-fold higher than that of 100 kDa membrane, indicating that the pore size of 100 kDa might be too small for most of the protein contaminants to pass through (Figure 5.2d). During the sEV separation process, a complex range of non-vesicular materials might be co-isolated. Therefore, a straightforward and quantitative method has been applied to estimate the purity of sEV samples by comparing the ratio of nano-vesicle counts to protein concentration. Although both 300 and 500 kDa were not as excellent as 100 kDa in particle recovery, they showed a much better behaviour on the purification of sEV preparations due to their exceptional ability of removing protein contaminants. Compared to the performance of 100 kDa filter, a 2 to 3-fold higher purity was demonstrated by both 300 and 500 kDa membranes, showing that membranes with these two pore sizes might be promising candidates for sEV separation and purification while 100 kDa MWCO might have a wider use in final step sEV concentration instead of separation (Figure 5.2e).

In addition to the properties of the sEV preparations after filtration, the productivity of the membrane filtration process is also an important parameter that should be taken into considered. In this case, the productivity of the membrane filtration process, expressed as particles produced per unit area of membrane per unit time, would largely depend on the permeate flux along with the sEV recovery, where the permeate flux is the quantity of the permeate flowing through the membrane per unit time and membrane

area at a given pressure. As expected, under the same pressure, shortest time was required for 500 kDa membrane to process the 20 mL feed to 2 mL retentate, while 300 kDa filter required more than twice the time, and even much longer for 100 kDa (Figure 5.2f). Based on the volumetric flow with the time course, the permeate flux of every 30 seconds was calculated and showed in Figure 5.2g, where the permeate flux of all three membrane filters was constantly dropped, which might be due to the concentration polarisation or fouling. The permeate flux of 500 kDa membrane was the highest in the first 90 seconds, after which no significant difference was found between the permeate flux value of 300 and 500 kDa (Figure 5.2g). The average productivity of three filters was calculated based on the final particle recovery and the time of the filtration process. Among the three, 500 kDa membrane showed the best productivity, which was 2-fold and 6-fold higher than that of the 300 and 100 kDa membrane, respectively (Figure 5.2h). Based on above findings, for efficient separation of sEVs, larger pore size, i.e. 500 kDa MWCO in this case, is preferable.

5.4.2 Effects of Stirring Speed

The system hydrodynamics could have a distinct role to play in the membrane filtration process. Therefore, rotary stirring speed was applied to generate different shear rates in the filtration system for the investigation of the shear effects on EV separation. As the shear rate depends on both the geometry of the system and the stirring speed, the average shear rates at different stirring conditions were calculated from the

computational fluid dynamics (CFD) simulation (see Supplementary Information) and shown in Table 5.1.

Table 5.1 Calculation of average shear rate at different stirring speeds

Stirring Speed (rpm)	Shear Rate (s^{-1})
100	43.94
150	67.65
200	87.76
300	139.69
400	164.84

No significant difference was found between the stirring speeds in the range of 100 – 400 rpm in terms of size distribution, recovery of nanoparticles, transmission of protein contaminants, and the purity of sEV preparations post-filtration (Supplementary Figure 5.2). However, as expected, it was found that the processing time required for the 20 mL feed to 2 mL retentate was continuously decreased and in turn the permeate flux rose with the increase of stirring speed in the range of 100 – 200 rpm, although no significant difference was shown between the groups from 200 to 400 rpm (Figure 5.3a&b). As a result, with the increase in stirring speed, the average particle productivity was observed to firstly increase and then reach a plateau at 200 rpm (Figure 5.3c), given that the final recovery of particles was quite similar. Therefore, since no significant difference was found in terms of the particle recovery and sEV purity under different stirring speeds, a stirring speed of 200 rpm seems to be a moderate setting to achieve the best sEV productivity and meanwhile minimise the shear effects so that avoid the mechanical damage to the sEVs as much as possible.

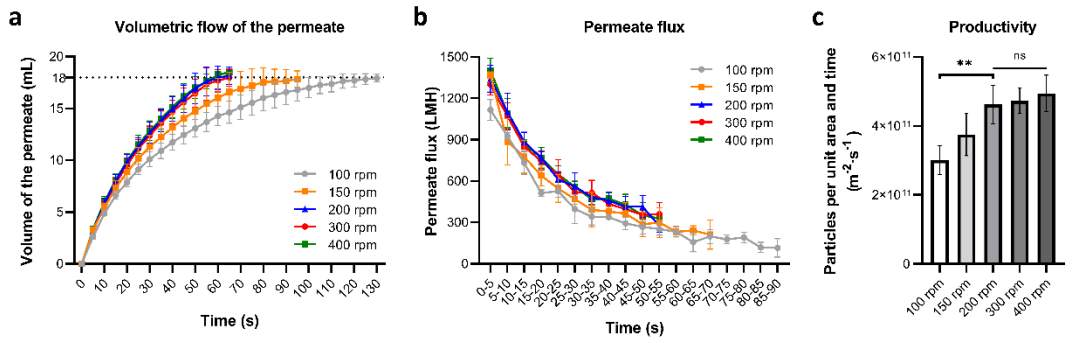


Figure 5.3 The effects of stirring speed on sEV isolation process (n=4). (a) Volumetric flow rate of the permeate during the ultrafiltration under different stirring speeds. (b) Permeate flux during the ultrafiltration under different stirring speeds. (c) Average productivity of sEVs under different stirring speeds.

5.4.3 Effects of Operational Pressure

Pressure is the major driving force of an ultrafiltration process. Different transmembrane pressure (TMP) created by the compressed air was tested to optimize the ultrafiltration-based separation protocol of sEVs. Figure 5.4a demonstrated that the size distribution of the sEV preparations obtained under different pressure was consistent with typical sEV profiles. In the range of 5 - 25 psi, the higher the pressure applied, the less the particles and proteins can be retained, which means a worse particle recovery (Figure 5.4b&c) but a better behaviour in removal protein contaminants (Figure 5.4d) with the increased pressure. Compared to the transmission of protein contaminations, it seems that the particle recovery might be more sensitive to the pressure change as it dropped more than half (from around 63% to 27%) while the removal of the proteins only increased by 9% (from 69% to 78%) when the pressure increased from 5 psi to 25 psi. As a result, the purity of the sEV preparations also dropped when higher pressure was applied (Figure 5.4e). Again, the particle amount in

the permeate occupied less than 4% of the total particles, with no significant difference between that of different pressures, suggesting more particles might be trapped by membranes with higher pressure applied. Nevertheless, as expected, the permeate flux increased with the pressure (Figure 5.4f&g), which in turn leaded to a significant growth of sEV productivity (Figure 5.4h). In view of above findings, 5 psi was chosen as the most appropriate pressure out of a reason that it demonstrated both the best recovery and purity of sEV products, which should not be compromised although higher pressure would give a better productivity of sEVs.

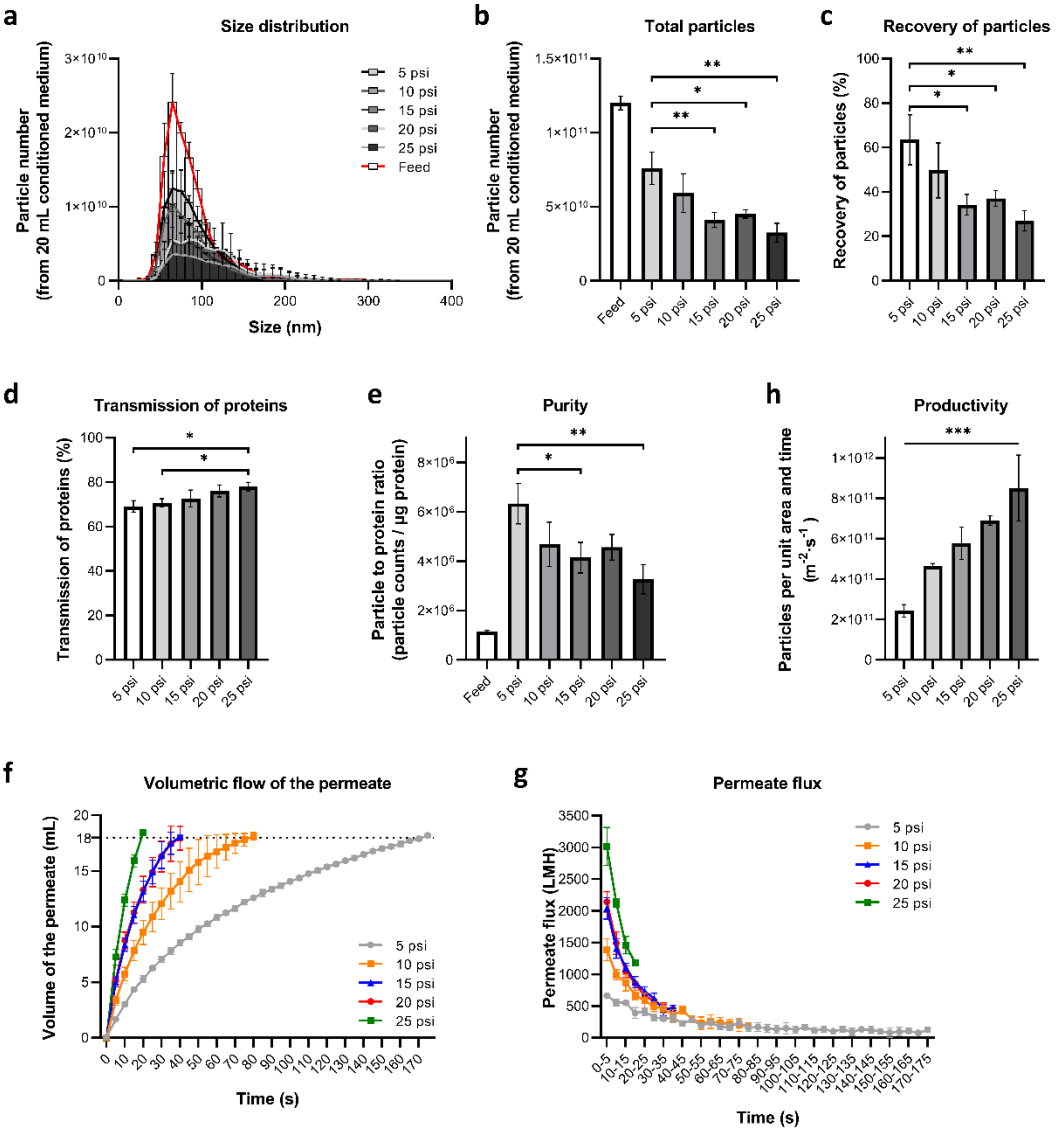


Figure 5.4 The effects of applied pressure on sEV isolation (n=3). (a) Particle size distributions of the feed solution (CM) and the sEV preparations isolated under different pressures. (b) Total particle numbers of CM and the sEV preparations. (c) Recovery of particles from CM under different pressures. (d) Transmission of contaminated proteins during the ultrafiltration under different pressures (e) Purity (particle to protein ratio) of CM and the sEV preparations. (f) Volumetric flow rate of the permeate during the ultrafiltration under different pressures. (g) Permeate flux during the ultrafiltration under different pressures. (h) Average productivity of sEVs under different pressures.

5.4.4 Effects of Feed Concentration (Direct Dilution) and Diafiltration

Introducing washing buffer or fresh solvent to the ultrafiltration system can be a promising solution to further remove or lower the concentration of those contaminants and facilitate the separation to obtain purer sEV preparations. Diafiltration is a commonly used method to wash out the contaminant from the solution, which consists of repeated dilution and concentration steps to achieve buffer exchange. In this case, 20 mL original feed was firstly concentrated to 10 mL by 500 kDa MWCO membrane, followed by adding equal amount (10 mL) of PBS and then diafiltrated to 10 mL again, which is recorded as one diafiltration volume (DV) and was repeated for several times. After the final time of diafiltration, the 10 ml retentate was concentrated to 2 mL as final retentate by the same membrane. The groups that conducted 2 times (2×10 mL PBS in total) and 6 times (6×10 mL PBS in total) diafiltration were termed as group DV2 and group DV6, respectively. A direct dilution process with the addition of the same PBS volume was conducted parallelly for comparison, i.e. 20 mL original feed was diluted with 20 ml PBS (termed as group 0.5x) or 60 ml PBS (termed as group 0.25x) prior to the filtration by 500 kDa MWCO membrane. A control group termed as group 1x (DV0) was also performed, in which 20 mL original feed was directly filtered by a 500 kDa MWCO membrane to 2 mL retentate, without adding any PBS.

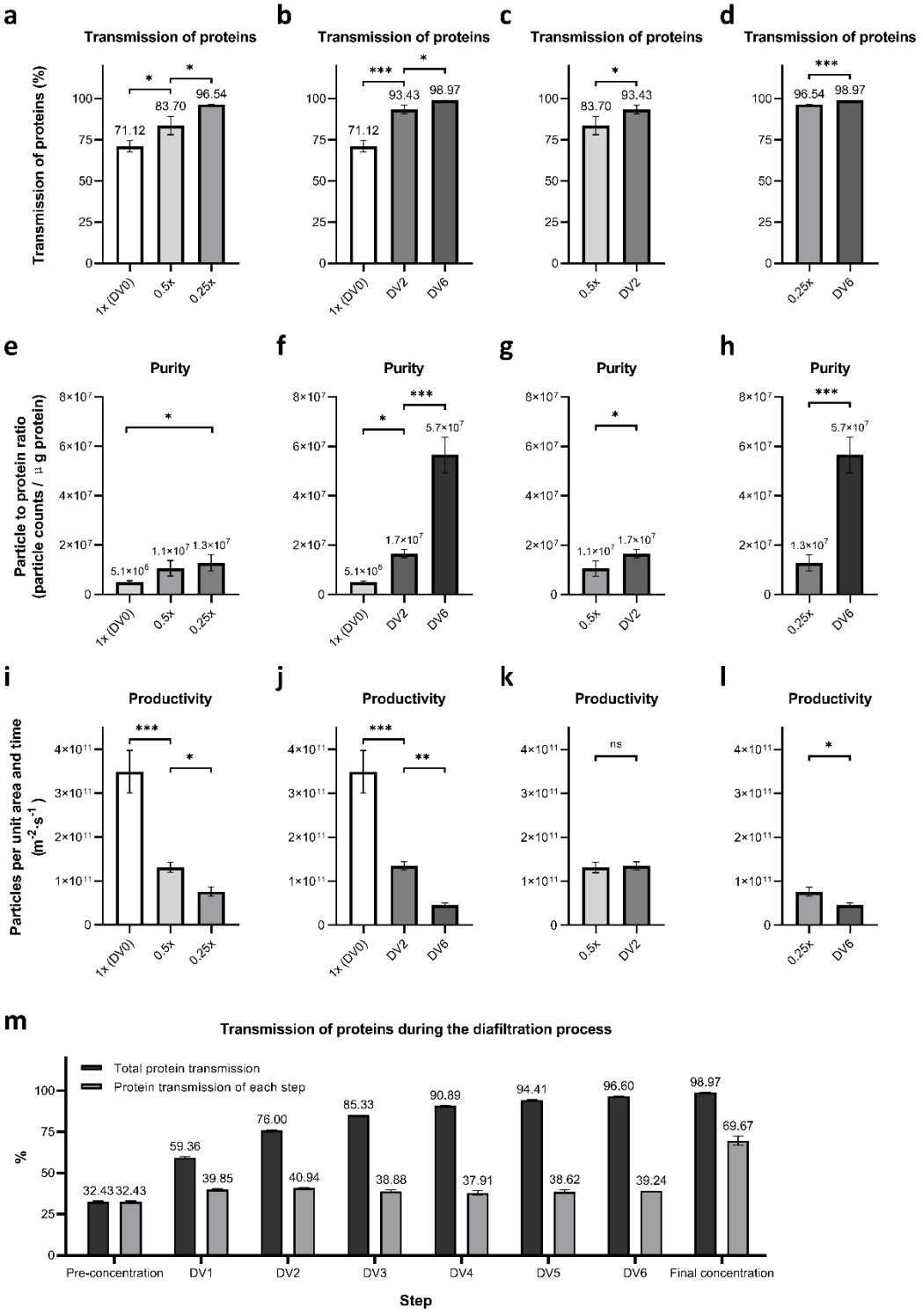


Figure 5.5 The effects of direct dilution and diafiltration on sEV isolation (n=3). (a-d) Transmission of contaminated proteins during the ultrafiltration. (e-h) Purity (particle to protein ratio) of the sEV preparations. (i-l) Average productivity of sEVs. (m) Removal of proteins during each diafiltration step.

The performance of nanoparticle recovery was quite similar among all the groups (Supplementary Figure 5.3a&b), indicating that the dilution and diafiltration process will not lead to further loss of the particle. Both the dilution groups and the diafiltration groups demonstrated an increase in the protein transmission (Figure 5.5a&b) and thus purer sEV preparations (Figure 5.5e&f), with higher dilution folds or more diafiltration volume applied. Particularly, 6 diafiltration volume (DV6) group removed almost 99% of the protein contaminants and demonstrated a remarkable increase in sEV purity, for about 10-fold higher than that of the control group. In addition, with the same volume of the buffer added, the behavior of the diafiltration process was constantly superior to that of the direct dilution process in both removal of protein contaminants (Figure 5.5c&d) and sEV purity (Figure 5.5g&h). Compared to the 4-fold dilution group (0.25x), the DV6 group showed a 4 to 5-fold higher purity. Nevertheless, as expected, although the permeate flux was increased when the feed was more diluted, the processing time was extended (Supplementary Figure 5.3c-e) and the productivity was dropped (Figure 5.5i&j) for the groups with higher dilution folds or more diafiltration repeats, as the total processing volume increased, i.e. 40 mL for the groups of 0.5x and DV2, 80 mL for the groups of 0.25x and DV6. However, the groups of 2-fold dilution and 2 diafiltration volume gave a comparable productivity (Figure 5.5k), and the productivity of DV6 group was only slightly lower than that of 0.25x group (Figure 5.5l). Considering that diafiltration process played an excellent role in sEV purification, it should be adopted to the current membrane-based sEV separation process. To obtain

high quality sEV preparations with required purity, the number of diafiltration volume need to be determined. Therefore, the permeate from each step of the diafiltration process was collected and analysed. As shown in Figure 5.5m, around 40% of the protein contaminants was removed at each DV step, given a protein rejection coefficient of 35% calculated by Equation (5.1), which led to almost 99% of protein transmission in total and gave a satisfied purity after the whole process. As a result, diafiltration volume of 6 is recommended for sEV separation and a safety factor of 1 more diafiltration volume could be added to make the final removal rate over 99%.

$$R_i = 1 - \frac{C_{P,i}}{C_{R,i}} \tag{5.1}$$

where R_i is the rejection coefficient of a component i, $C_{P,i}$ is the concentration of component i in permeate, $C_{R,i}$ is the concentration of component i in retentate.

5.4.5 Development of sEV Purification Process: Fed-batch Ultrafiltration Combined with Diafiltration (UF/DF)

Based on the previous results, the optimal parameters were adopted to our membrane ultrafiltration protocol for sEV separation, i.e. the conditioned medium would go through a pre-concentration step to half of the volume, 7 diafiltration steps and a final concentration step using a 500 kDa MWCO membrane under a condition of 200 rpm stirring speed and 5 psi applied pressure. However, as shown in Figure 5.2g, with a starting volume of 20 mL 1x conditioned medium, the permeate flux was dramatically declined during the process and thus lead to an inefficiency at later stage of ultrafiltration, which reflected a limited processing capacity of a single membrane

disc. To enlarge the processing capacity of a single membrane disc and meanwhile maintain the permeate flux and the productivity at an acceptable level, here we developed a fed-batch ultra-diafiltration protocol (fed-batch UF/DF) as shown in Figure 5.6. 100 mL conditioned medium was divided and fed to the system in batches, and a concentration and diafiltration step was added between each feed.

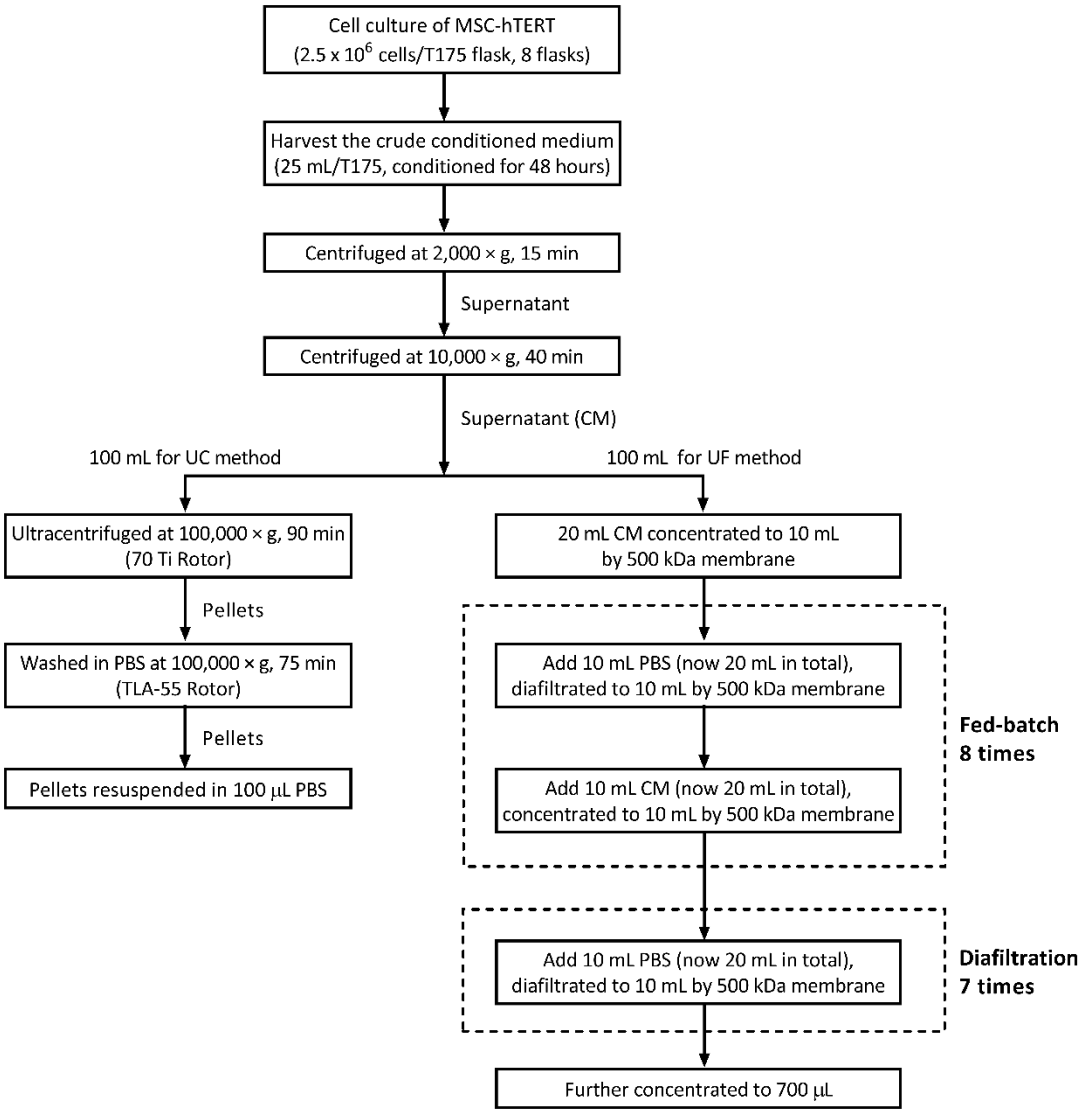


Figure 5.6 Flow chart of the fed-batch UF/DF process and ultracentrifugation process.

The separation result of this fed-batch UF/DF method were compared to that of the ultracentrifugation method, the most used sEV isolation method so far. Compared to

ultracentrifugation, the fed-batch UF/DF reduced the processing time of sEV isolation. It took about 210 min for the fed-batch UF/DF method including the time consumed for manually configuring and taking apart the ultrafiltration system, which can be further shortened after automation, while UC-based method needs at least 4 hours (Table 5.2). In addition, fed-batch UF/DF method showed a remarkable ability in sEV recovery (Figure 5.7c&d), with about 60.88% particles being recovered from the conditioned medium, which was almost 3-fold higher than that of the UC method (20.59%). Moreover, although more PBS buffer was required during the UF-based isolation process (Table 5.2), the purity of sEV preparations (particle to protein ratio) from the fed-batch UF/DF method was about 1300-fold higher than that of the feed solution, and was increased from 6.93×10^{8} to 1.33×10^{9} (nearly doubled), compared to that of the UC method (Figure 5.7e). The size distribution of sEV preparations isolated by both methods was consistent and corresponding to the typical sEV profiles (Figure 5.7a), with about 90% of the particles ranging from 30 to 200 nm (Figure 5.7b). sEV preparations from both methods were positive for typical EV markers such as CD63 and TSG101, and negative for intracellular compartment markers, like GM130, which confirmed the purity of the final sEV samples (Figure 5.7f). Classic cup-shaped EV particles were found in TEM images from both methods, and a higher sEV purity from the fed-batch UF/DF method was further confirmed as less contaminants were found in the background of the image (Figure 5.7g&h).

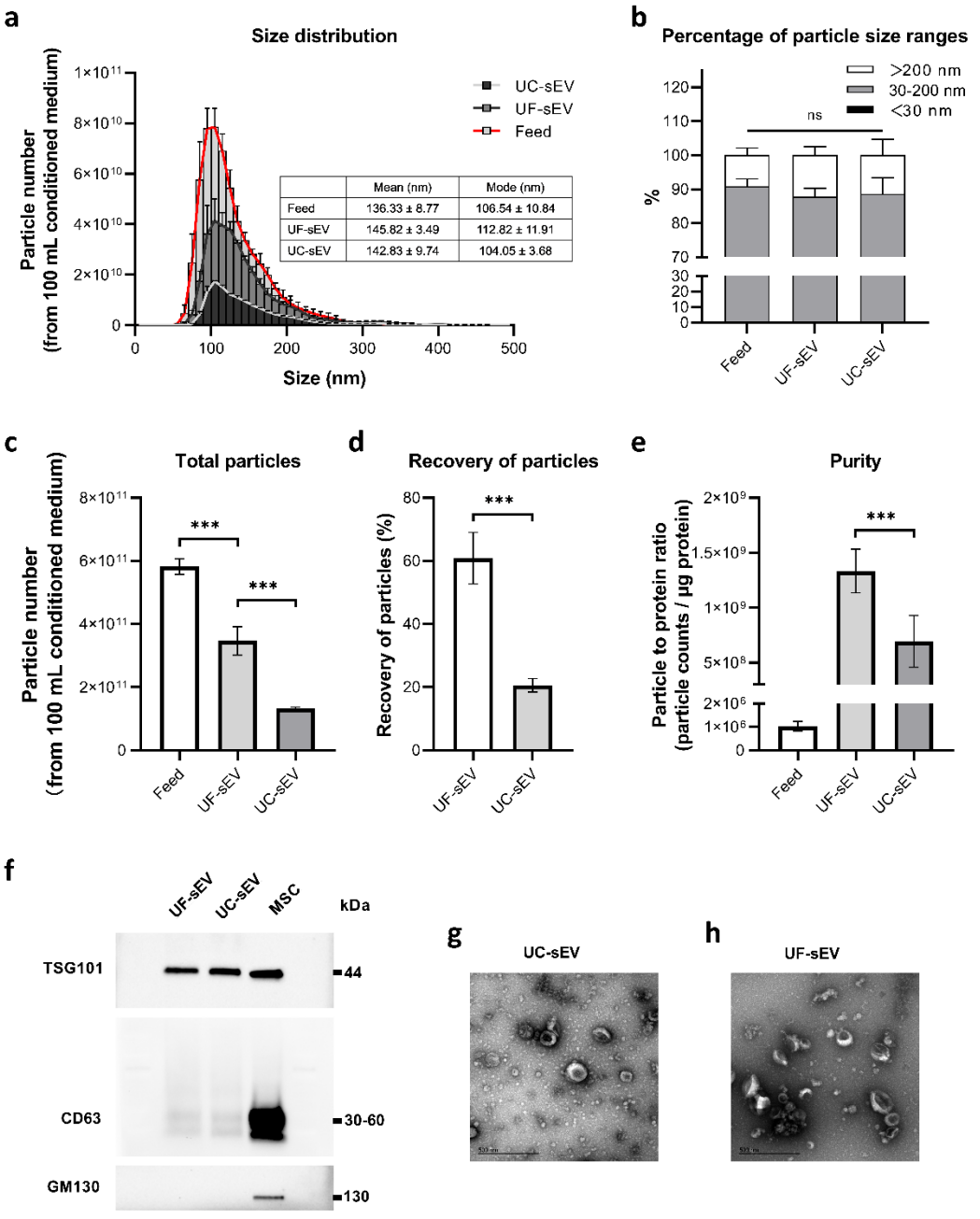


Figure 5.7 Characterisation of sEV preparations from fed-batch UF/DF (UF-sEV) and UC (UC-sEV). (a) Particle size distributions of UF-sEV, UC-sEV and feed solution (CM). (b) Percentage of particles of different size ranges. (c) Total particle numbers of UF-sEV, UC-sEV and CM. (d) Recovery of particles from CM by fed-batch UF/DF and UC. (e) Purity (particle to protein ratio) of UF-sEV, UC-sEV and CM. (f) Western blot results of UF-sEV, UC-sEV and their parent cells. (g) TEM image of UC-sEV (scale bar represents the length of 500 nm). (h) TEM image of UF-sEV (scale bar represents the length of 500 nm).

Table 5.2 Comparison of fed-batch UF/DF method and UC method for sEV isolation.

	Fed-batch UF/DF	UC
Processed conditioned medium (mL)	100	100
PBS required (mL)	150	⩽ 25
Obtained sEV preparation (µL)	700	100
Processing time (min)	210	⩾ 240
Recovery of particles (%)	60.89 ± 8.16	20.59 ± 2.15
Purity (particle counts / µg protein)	$1.33\times10^{9} \pm 1.99\times10^{8}$	$6.93\times10^{8} \pm 2.35\times10^{8}$

5.5 Discussion

5.5.1 Separation Performance with Different Ultrafiltration Design and Operational Parameters

Membrane filtration could be a promising and industrial applicable sEVs isolation method for downstream studies and clinical applications. In this study, we investigated the effects of the different filtration parameters on sEV recovery, purity as well as productivity, then further developed an ultrafiltration-based protocol combined with fed-batch and diafiltration process for sEV separation, which has been approved to achieve a much more excellent recovery of sEVs with higher purity and less processing time, compared with ultracentrifugation, the most used method for sEV isolation in the lab.

The ultimate goal for this separation is to achieve high recovery and excellent purity of the desired sEVs. This needs to retain the sEVs in the desired size range as much as possible and to remove smaller free proteins and other contaminants. A suitable membrane, that provides a barrier to retain sEVs and to transmit protein, would be the first to consider.

It seems that 500 kDa MWCO is the membrane pore size that allows the highest productivity without compromising the purity of EVs among the three. MWCO is defined as the molecular weight that 90% of the molecules cannot pass through the membrane. The pore size of 100 kDa, 300 kDa, and 500 kDa MWCO membrane can

be estimated by Equation (5.2), and the estimated diameters are 6.13 nm, 8.84 nm, and 10.48 nm, respectively [230].

$$R_{min} = 0.066M^{1/3} \quad (5.2)$$

where R_{min} is the radius in nanometer, M is the molecular weight in Dalton.

According to the technical guidance from companies like Pall Corporation and Sterlitech, as a rule of thumb, a MWCO in the range of 3 – 6 times smaller than the molecular weight of the targets is recommended, with an optimum flow rate using 3 times smaller MWCO [231,232]. As a result, knowing that the size of the sEVs is 30 – 200 nm, 500 kDa with a pore size of around 10 nm in diameter could be a suitable choice for sEV separation, which also maximises the transmission of proteins contaminants at the same time and thus improves the purity of sEV preparations.

It is noted the large membrane pores, like 500 kDa, may have higher tendency of pore blocking, compared to membranes with smaller pores, which explains the sharp flux decline observed in Figure 5.2g. Concentration polarisation is caused by the reversible accumulation of components close to the surface of the membrane. It can lead to severe fouling problems of the membrane, including complete/partial/internal pore blocking and filter cake [233]. Both concentration polarisation and fouling can cause higher resistance for transport and flux decline during the pressure-driven filtration, and will further affect the lifetime of the membrane [234,235]. The tendency of flux decline can be closely related to the interaction between the components in the feed and the membrane pores [236]. Particles might be more easily to be immobilized or trapped by

larger membrane pores like 300 kDa and 500 kDa, while tend to roll off the membrane surface with lower MWCO under the same operational condition [237,238]. This problem could be alleviated by changing the hydrodynamic conditions, surface modification and regular cleaning, which should be considered in the process development in the future [239].

The performance of membrane ultrafiltration, including diafiltration, for bioseparation is affected by operational (stirring speed, transmembrane pressure, and temperature) and physiochemical parameters (concentration, solution pH and ionic strength). The former affects concentration polarisation and possible fouling on to the membrane. The latter affects the electrostatic interactions between sEVs, proteins and the membrane surface, and among themselves.

Higher permeate flux and greater productivity can be achieved by the increase of the stirring speed. A possible explanation for this might be that the stirring speed in this system simulate the cross-flow filtration to some extent [237,240]. The higher shear rate generated by the increasing rotary stirring speed could diminish the resistance associated with concentration polarization close to the membrane surface [241], reduce the potential of fouling and enhance the mass transfer coefficient k, leading to the rise of the permeate flux, according to the resistance-in-series model in Equation (5.3) and the concentration polarization model in Equation (5.4) [242].

$$J = \frac{\Delta P - \Delta \pi}{\mu(R_m + R_f)} = \frac{\Delta P - \Delta \pi}{\mu(R_m + R_{ir} + R_r)} \quad (5.3)$$

where J is the permeate flux, ΔP is the TMP, $\Delta\pi$ is the osmotic pressure, μ is the viscosity of the solvent, R_m is the intrinsic resistance of the membrane, R_f is the resistance caused by concentration polarization and fouling (including pore blocking and cake layer), R_{ir} is the irreversible part of R_f, R_r is the reversible part of R_f.

$$J = k \cdot \ln\left(\frac{C_M - C_P}{C_B - C_P}\right) \tag{5.4}$$

where J is the permeate flux, k is the mass transfer coefficient, C_M is the concentration at the membrane surface, C_P is the concentration of the permeate, C_F is the concentration of the feed stream.

However, the permeate flux was not that sensitive to the change of stirring speed over 200 rpm. This is because at a higher shear rate, the concentration polarisation is minimised and no longer a limiting factor. Kang et al. and Yunos et al. suggested that the part of the resistance that can be reduced by stirring may be too low compared to the resistance of membrane and irreversible fouling at this stage, as a result, the flux change was negligible at elevated shear rate [236,237]. On the other hand, as sEVs are not biological inert and might suffer mechanical damage under high shear rate, 200 rpm might be the optimal value so that a balance can be maintained between the sEV productivity and the biophysical integrity. Further study of tangential flow filtration for sEV separation is recommended, which could potentially provide an improved hydrodynamic condition for protocol optimisation.

Lower operational pressure is recommended for sEV separation for higher particle recovery and thus excellent purity of EVs. This might because that more severe fouling

can be caused in dead end filtration mode with higher pressure applied, as more particles might be pushed into the pores of the membrane, which would intensify pore blocking and accelerate cake formation, and eventually lead to poor particle recovery [237]. The increased local concentration of sEVs near the membrane surface would reduce the electrostatic interaction (repulsion) between the sEV particles and hence form denser cake. It must also be pointed out that the high operational pressure and high initial permeate flux increase the local shears the sEV particles experienced, which may lead to breakages of sEVs and hence product loss. This is also a factor to consider when choosing the membrane pore size.

The concentration of sEVs also affect the retention and transmission of sEVs and protein contaminants. Generally, a lower concentration would allow smaller proteins to pass the membrane pores, resulting a higher purity of the retained sEVs. Dilution of the feed solution might help with sEV separation. This result may be explained by the fact that the decrease of the feed concentration might ease the problem of concentration polarisation and fouling, which favours the throughput of the ultrafiltration system and the transmission of protein contaminants to some extent, and thus increases sEV purity. It might also be explained by that higher concentration of the feed could lead to an increase in viscosity and therefore hinders the efficiency of the separation [243].

Diafiltration process shows an exceptional performance in removal of protein contaminants during the sEV separation process. Diafiltration usually involves pre-concentration of feed solution, dilution of feed liquid by adding fresh washing buffer

to replace the volume of the lost permeate, and a volume reduction step by ultrafiltration to wash contaminants away from the retained particles [244]. In this case, concentration to half of the initial feed volume was performed not only to reduce the overall sample volume and the required amount of washing buffer for easier liquid handling and economic purpose, but also to avoid severe polarisation problem which might be caused by further concentration of the feed. In contrast to direct dilution of the feed, with the same volume of the buffer added, the diafiltration process demonstrated an even more remarkable ability in sEV purification. This might be explained by the sequential dilution and buffer exchange process of the diafiltration. The permeable components are sequentially diluted, and half of the feed volume is continuously replaced by the fresh buffer during each diafiltration step, together with the volume reduction during the pre- and final-concentration step, leading to 99.8% (see Supplementary Information) of the original feed volume been replaced by PBS washing buffer after DV6. Compared with the value of 97.5% (see Supplementary Information) of the direct dilution 0.25x group, a larger portion of the original solution was removed or replaced by diafiltration and thus enhanced the removal of contaminants and improved the purity of sEVs post-separation, although with the addition of the same volume of PBS washing buffer. The same reason can also be applied to the DV2 and 0.5x groups.

5.5.2 Process Development

The ultrafiltration design and parameters of the sEV separation protocol were optimised based on the previous results, i.e. the conditioned medium would be pre-

concentrated to half of the volume, diafiltered with PBS for 7 times and then concentrated again with a 500 kDa MWCO membrane at 200 rpm stirring speed and 5 psi. In addition, fed-batch concentration is adopted to our sEV separation protocol prior to the diafiltration separation step. Compared to one time direct feed concentration to half volume (e.g. from 100 mL to 50 mL), greater volume reduction and thus easier liquid handling as well as higher processing capacity can be achieved by fed-batch concentration process, i.e. 100 mL feed solution was divided into several fractions, fed to the system in batches and concentrated to half volume sequentially, making the final volume of the retentate to 10 mL. However, higher concentrations in the retentate can be caused as the feed solution is continuously added and concentrated, which would lead to serious polarisation and fouling problems, and thus poor throughput of the membrane. Therefore, a diafiltration step was designed between each batch of feed concentration to preliminarily dilute and wash away part of the contaminants in order to maintain an acceptable permeate flux of the membrane [245]. The downstream diafiltration process can be operated once all the feed solution has been accommodated and concentrated.

It is important to reserve the characteristics of the sEVs, no matter what separation method is used. Here, we isolated sEVs from the fed-batch UF/DF method and compare with those from conventional UC method. In this study, sEVs with characteristic size distributions, classic morphology and typical expression of EV markers were successfully isolated by our fed-batch UF/DF method, showing comparable

characteristics to those from the UC method. In addition, this method also exhibited its superior ability in sEV separation, in contrast to the UC method.

Co-isolation of non-vesicular contaminants is the major problem that needs to be addressed, which may influence subsequent studies including biomarker exploration, functional studies, clinical trials as well as further applications [160,246,247], therefore, the purity of the EV preparation is of critical importance [10]. Although the purity of the sEV preparations from both fed-batch UF/DF and ultracentrifugation were confirmed by the western blot results, the further difference between the two was unable to be identified due to the lack of sensitivity. A method based on measuring the particle to protein ratio was proposed by Webber et al., allowing quantitative comparison of purity between different sEV preparations [160]. By this mean, a stronger capability of sEV purification was shown by our self-developed fed-batch UF/DF method, with a significant higher particle to protein ratio than that of the traditional UC method, which was also supported by the TEM images in Figure 5.7. However, it should be noted that although this method provides straightforward comparison of the purity between different sEV preparations, further quantitative biochemical studies about various specific non-EV contaminants should be conducted in the future to provide a deeper insight into the co-isolation problems of different sEV separation method.

The recovery of sEVs is another crucial factor to evaluate an sEV separation method. A 3-fold particle recovery was accomplished by fed-batch UF/DF method compared with UC. This result may be due to that the destroyed particle integrity and

particle aggregation under the high shear forces caused by UC leads to a sharp drop of the total particle number, which was also reported by Cvjetkovic et al and Linares et al [35,248]. In contrast, our fed-batch UF/DF method was designed to operate under a relative gentle condition with low pressure and stirring speed for the purpose of minimising the mechanical damage to the sEV particles. Haraszti et al. and Heinemann et al. also reported similar findings that higher quantities of sEVs were produced by filtration than UC method, although the tangential flow filtration method and the sequential filtration method they applied was slightly different from our fed-batch UF/DF [29,229]. It is also essential to bear in mind that an assumption was made that all the particles detected by the NTA method was counted as vesicles due to the limitation of the detection technique, which might not be strictly true.

An ideal sEV separation method should also be time-efficient, user-friendly, cost-effective, and easy to scale up. For a processing volume of 100 mL, it seems our fed-batch UF/DF method doesn't show straightforward advantage in saving processing time and simplifying the separation step. However, considering that the yield of fed-batch UF/DF method was about 3 folds higher than that of the UC, as a result, 3 folds of consumable costs and processing times were required by UC to obtain an equal amount of sEVs, that is 12 hours for UC versus 3.5 hours for fed-batch UF/DF. In addition, the processing time of the UC method mainly depends on the processing capacity of the ultracentrifuge, and was impossible to shorten for each batch, while automation of our fed-batch UF/DF protocol is highly possible to be accomplished, which in turn would

further decrease the processing time and largely reduce manual intervention, and therefore decrease the labour cost. Moreover, the capital costs of an ultracentrifuge and rotors for UC method are extremely higher than that of filtration devices for ultrafiltration, which means our ultrafiltration-based method would be more affordable and accessible.

To summarise, the main findings in this study are shown below: 500 kDa MWCO might be the most suitable membrane pore size for efficient purification and production of sEVs. Higher sEV productivity can also be achieved by increasing stirring speed to a certain level, and lower operational pressure allows a gentle separation of sEVs for excellent particle recovery and sEV purity. By introducing several diafiltration steps, the purity of the sEV preparations can be further improved, with about 99% of the protein contaminants being removed after 6 times of isovolumetric diafiltration. The fed-batch UF/DF method developed based on these findings was able to achieve 3-fold higher yield and nearly doubled purity of sEVs compared to the traditional ultracentrifugation method, which could be a very promising sEV separation method for downstream studies with extra advantages of efficient production and low costs. And due to its scalable and automatable properties, it also has great potential in industrial level sEV manufacture for clinical applications. Nevertheless, a limitation of this study was that only the biophysical properties of sEV preparations was investigated while the functional integrity of the sEV samples post-separation was unclear. Therefore, the functional capacity of sEVs isolated by both methods should be

evaluated and compared. It should also be noted that immortalised cell line hTERT MSC was used in this study for the process development. In the future, the fed-batch UF/DF protocol should also be evaluated for the separation of sEVs from primary MSC, of which the EV properties and functional integrity should also be compared with the sEVs from immortalised MSC. In addition, the fed-batch UF/DF protocol can be further developed in the future. For example, tangential flow filtration should be considered in order to provide better hydrodynamic conditions, which may largely alleviate the problem with concentration polarisation and improve sEV productivity. Also, it might be a good idea to test the (continuous) constant volume diafiltration (CVD) mode, where the fresh buffer is continuously introduced to the filtration system at the same rate of withdrawing the permeate, leading to a more efficient and gentle buffer exchange compared to the discontinuous diafiltration. To aid in future research for the optimum process, design of experiments (DOE) can also be used to undertake multifactorial research for process parameters. A pilot scale sEV isolation system with automatic separation program could then be developed for the manufacture of high-end MSC-sEV products.

5.6 Supplementary Information

5.6.1 Computational Fluid Dynamics (CFD) Simulation

A computational fluid dynamics (CFD) simulation was conducted in the commercial software ANSYS FLUENT (Version 2020 R2) to explain the fluid environment during the ultrafiltration, especially for the fluid shear rate and velocity magnitude in the stirred cell device under different rotary stirring speeds. The whole filtering process was illustrated in Supplementary Figure 5.1 (a). Under a constant air pressure (10 psi), 20 mL sample solution was mixed by the adjustable rotated impeller and filtered by the chosen membrane (500 kDa MWCO), which was mounted at the bottom of the stirred cell. The simulation of this part only predicts the impeller's influence under varying rotary stirring speeds on the sample. The filtering process and efficiency were not considered.

Supplementary Figure 5.1 (b) and (c) indicate the engineering drawing of the working space and the impeller, which reflect the critical geometry parameters. The sample solution filled in a reversed circular truncated cone, which has a 43mm top diameter (D_{up}), 20mm height (H_{SC}) and 32mm bottom diameter (D_{down}). The rotated impeller has the below-listed feature: 22mm for $D_{impeller}$, 15mm for $H_{impeller}$, 6mm for W_{inner} and 5.5mm for H_{inner}. All the models were built by the Inventor Professional 2020 (Autodesk, ltd) and exported to STP files for transferring to ANSYS FLUENT. The models were then meshed by the Ansys Mesh to 1mm tetrahedral units. The whole

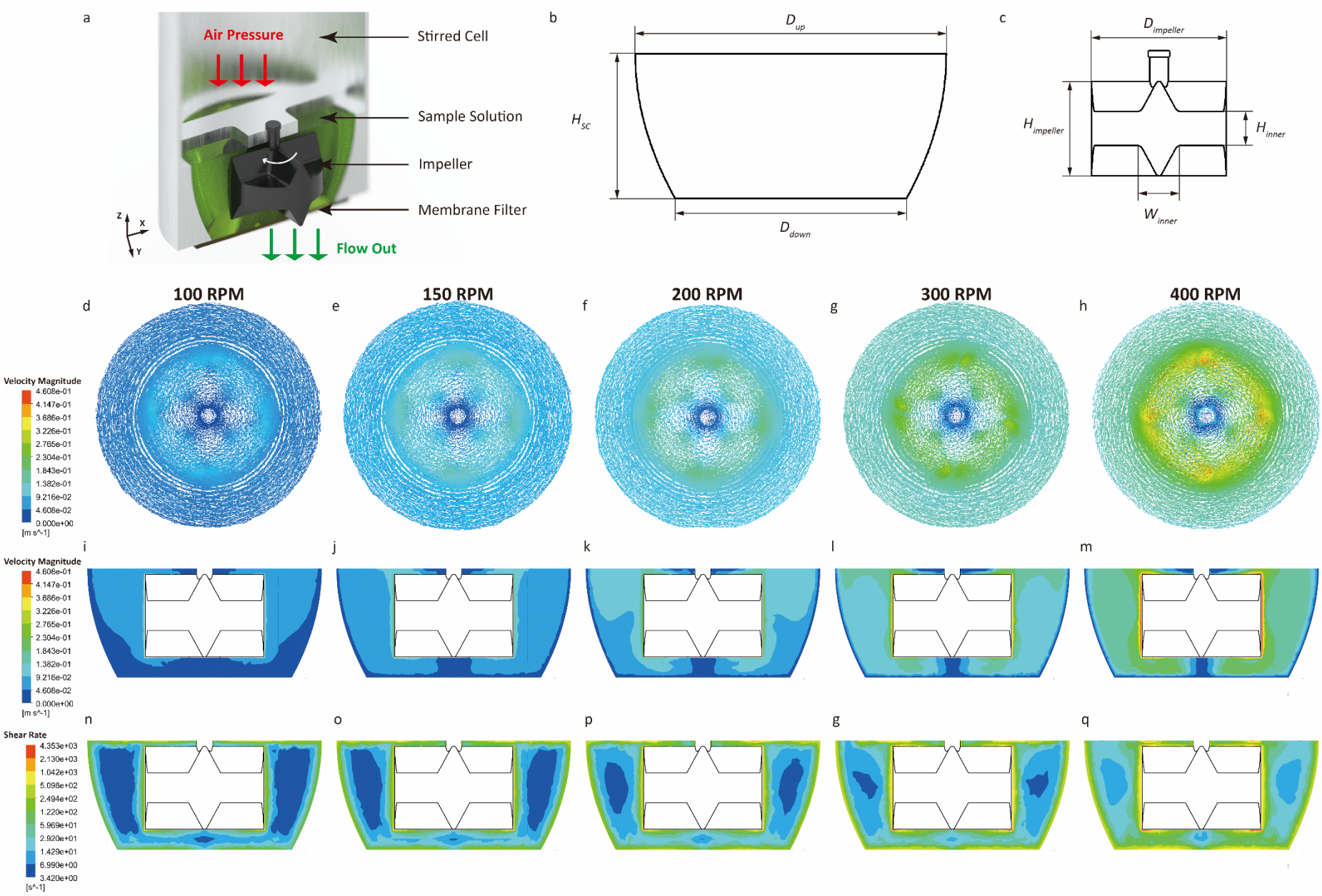
meshed models contain 46900 nodes and 229618 elements. All the other settings were Ansys Mesh default.

This CFD analysis is considered as a transient processing due to the outflow from the stirred cell. The pressure-based type was chosen and 9.81 m/s^2 gravitational acceleration was set. Two phases were set during the simulation: gas (air) and fluid. The property of the fluid was similar to water liquid (turbulent and incompressible) with a measured average viscosity of 1.337×10^{-3} kg/(m·s). The Eulerian multiphase model described the interaction between phases with the grace coefficient and 0.073 surface tension coefficient. The diameter of the air was set as 0.0015mm. The Standard K-epsilon model explained the turbulence. 10 bar pressure was exerted from the top of the filtration chamber. The Sliding Mesh approach was used to simulate the rotation of the central impeller at 100, 150, 200, 300, and 400 rpm.

At the post-simulation step, the fluid shear rate and velocity magnitude were plotted by the CFD-Post (ANSYS, ltd) in Supplementary Figure 5.1 (d) to (q). The velocity magnitude is the absolute value of velocity which refers to the speed or rate at which a liquid unit moves in a particular direction in this project. The vectors show the direction of liquid motion. The fluid shear rate measures the rate at which a fluid is sheared or deformed. Due to there being a 3D CFD simulation, the fluid shear rate was calculated by the Equation below [249]:

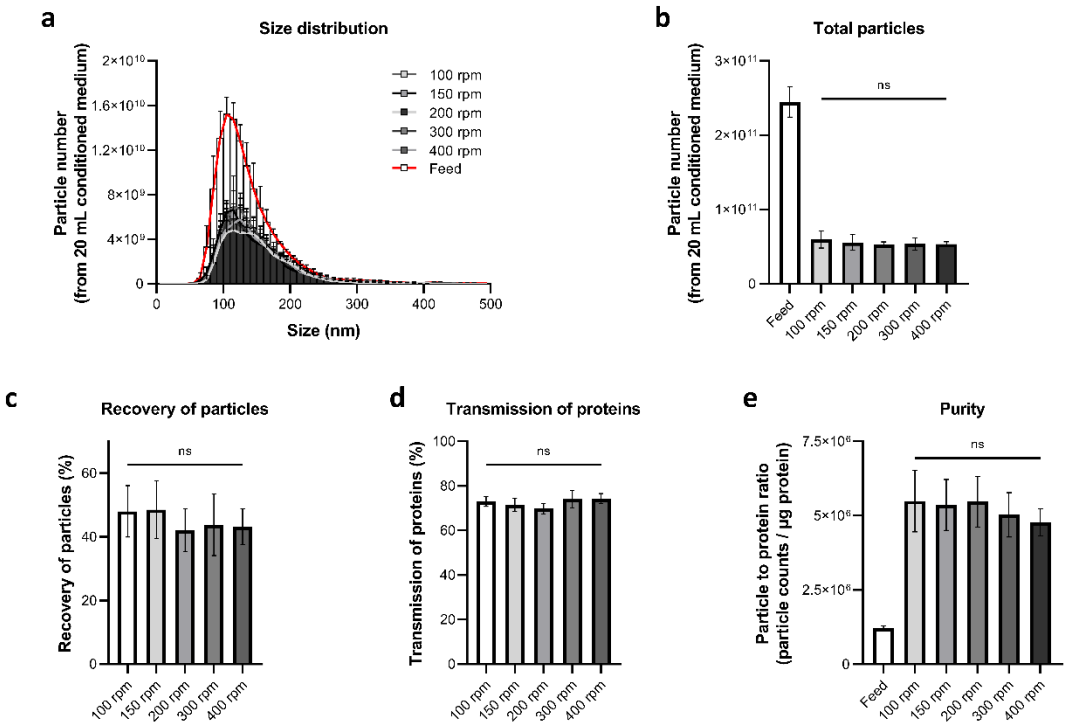
$$\text{Shear Rate} = \left[2\left(\left(\frac{\partial U_x}{\partial x}\right)^2 + \left(\frac{\partial U_y}{\partial y}\right)^2 + \left(\frac{\partial U_z}{\partial z}\right)^2\right) + \left(\frac{\partial U_x}{\partial y} + \frac{\partial U_y}{\partial x}\right)^2 + \left(\frac{\partial U_x}{\partial z} + \frac{\partial U_z}{\partial x}\right)^2 + \left(\frac{\partial U_y}{\partial z} + \frac{\partial U_z}{\partial y}\right)^2\right]^{\frac{1}{2}}$$

where U_x, U_y, and U_z are the velocity components in space.



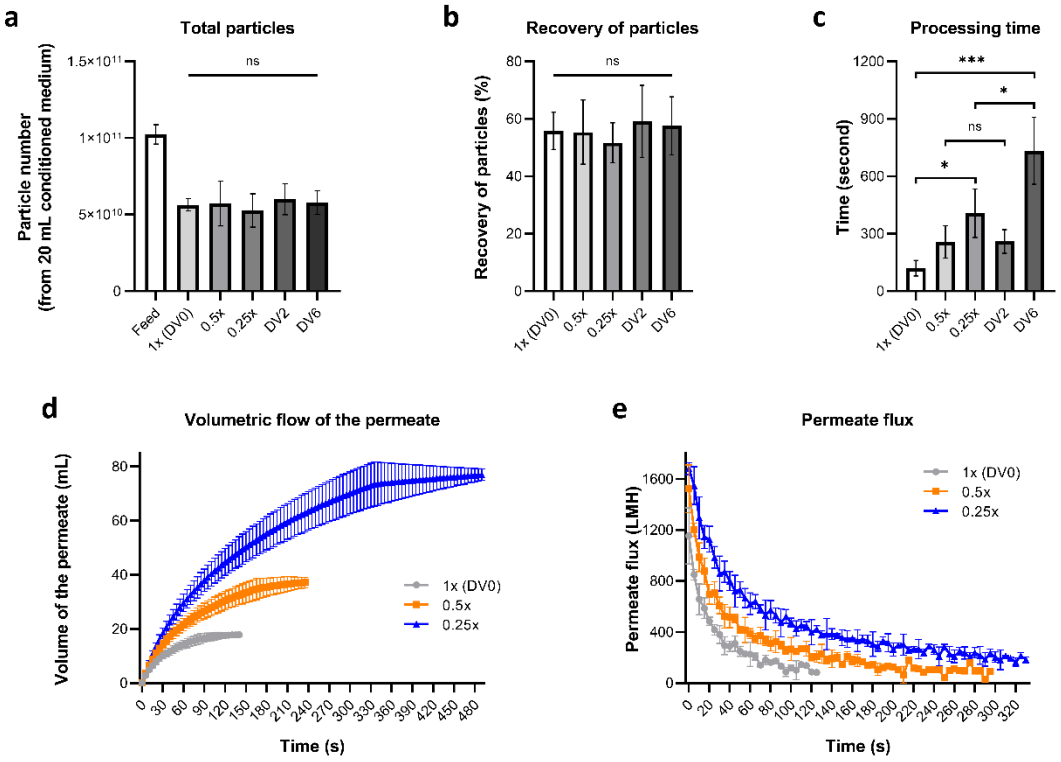
Supplementary Figure 5.1 Computational fluid dynamics simulation. (a) The schematic diagram of the stirred cell working area. (b) and (c) The engineering drawing of the working space and the impeller. Vector figure of the velocity magnitude (d-h) at the top view of the stirred cell under the stirring conditions of 100, 150, 200, 300, 400 rpm, respectively. Contour figure of the velocity magnitude (d-m) and shear rate (n-q) at the cross section of the stirred cell under the stirring conditions of 100, 150, 200, 300, 400 rpm, respectively.

5.6.2 The Effects of Stirring Speed on the Properties of the sEV Preparations



Supplementary Figure 5.2 The effects of stirring speed on the properties of the sEV preparations. (a) Particle size distributions of the feed solution (CM) and the sEV preparations isolated under different stirring speeds. (b) Total particle numbers of CM and the sEV preparations. (c) Recovery of particles from CM under different stirring speeds. (d) Transmission of contaminated proteins during the ultrafiltration under different stirring speeds. (e) Purity (particle to protein ratio) of CM and the sEV preparations.

5.6.3 The Effects of Direct Dilution and Diafiltration on Particle Recovery and Isolation Process



Supplementary Figure 5.3 The effects of direct dilution and diafiltration on particle recovery and isolation process. (a) Total particle numbers of the feed solution (CM) and the sEV preparations. (b) Recovery of particles from CM. (c) Processing time of the isolation process. (d) Volumetric flow rate of the permeate during the ultrafiltration. (e) Permeate flux during the ultrafiltration.

5.6.4 Percentage of the Original Feed Volume being Replaced

0.5x group:

$$X_{total} = \frac{Volume\ reduction}{Original\ volume} = \frac{40 - 2}{40} = 95\%$$

0.25x group:

$$X_{total} = \frac{Volume\ reduction}{Original\ volume} = \frac{80 - 2}{80} = 97.5\%$$

DV2 group:

$$X_{total} = X_{pre-concentration} + X_{diafiltration} + X_{final-concentration}$$

$$X_{total} = \left(\frac{10}{20}\right)^1 + \left[\left(\frac{10}{20}\right)^2 + \left(\frac{10}{20}\right)^3\right] + \left(\frac{10}{20}\right)^3 \times \frac{8}{10} = 97.5\%$$

DV6 group:

$$X_{total} = X_{pre-concentration} + X_{diafiltration} + X_{final-concentration}$$

$$X_{total} = \left(\frac{10}{20}\right)^1 + \left[\left(\frac{10}{20}\right)^2 + \left(\frac{10}{20}\right)^3 + \left(\frac{10}{20}\right)^4 + \left(\frac{10}{20}\right)^5 + \left(\frac{10}{20}\right)^6 + \left(\frac{10}{20}\right)^7\right] + \left(\frac{10}{20}\right)^7 \times \frac{8}{10} = 99.84\%$$

where X_{total} is the total removal of original feed volume in %, $X_{pre-concentration}$ is the removal of original feed volume at pre-concentration step in %, $X_{diafiltration}$ is the removal of original feed volume at diafiltration step in %, $X_{final-concentration}$ is the removal of original feed volume at final concentration step in %.

Chapter 6 Conclusions and Future Work

6.1 Conclusions

6.1.1 Summary

Overall, this thesis aims at addressing the current challenges of functional characterisation and large-scale production of MSC-sEVs to advance the clinical translation of high-end MSC-sEV product. The work of this thesis developed a skin cell-based model for functional identification of MSC secretome, confirmed the potential beneficial effects of MSC-sEVs on skin regeneration, as well as established an automated sEV production method with closed HFBR and an efficient sEV isolation protocol based on fed-batch ultra-diafiltration technique. The detailed findings are outlined in the following sections.

6.1.2 Functional Characterisation of MSC Secretome

The first part of this study provides a comprehensive comparison between different MSC secretome fractions in terms of their wound healing potential. Conditioned medium was harvested from both BM-MSCs and the recipient cells (NHDFs) and then fractionated into sEV fraction and non-sEV (NsEV) fraction, respectively. The functions of the secretome fractions from both cell types were investigated by NHDF-based migration and proliferation assay. The findings can be concluded as followed:

C1. This study provides referential significance for the choice of MSC secretome fractions to be used as skin regeneration strategies. The MSC secretome may contain a variety of advantageous components but also defective components for wound healing. sEV fraction, NsEV fraction and CM from BM-MSCs all showed an overall enhancement of migration behaviour of NHDFs, although MSC-sEV appears to be the more potent of the three and outperforms the corresponding HDF-sEV in promoting NHDF migration. NsEV fraction from MSCs should also be valued due to its beneficial influence in wound healing, while the defective components inside should be handled properly.

C2. The fractionation strategy and the designed NHDF-based wound healing model would be a useful tool for in vitro functional identification of cellular secretome.

6.1.3 Production of MSC-sEVs

The second part of this study developed and modified a HFBR based cell expansion system (CES) and established a specialised operation protocol for MSC-sEV production. The whole production process was closely monitored, and the physiochemical characteristics and functional efficacy of the MSC-sEVs produced by the CES were evaluated and compared to those from the conventional flask method. Conclusions can be derived as below:

C3. The developed HFBR-based CES method enables a large-scale continuous production of high quality MSC-sEVs to meet the great demand of the sEV product for downstream research and applications. In comparison to the

conventional flask approach, the CES method has successfully accomplished continuous MSC cultivation for 13 days, and subsequently achieved a 250-fold higher yield of MSC-sEVs with comparable characteristics and bioactivities but higher purity.

C4. This automated enclosed HFBR-based approach is also a promising method for industrial-scale production of MSC-sEVs, which simplifies the labour-intensive processes, improves the reproducibility and biosafety of the sEV production, and substantially lowers the related capital and operational expenses. The establishment and application of this method could considerably accelerate the development of the MSC-sEV based therapeutics in clinical translation.

6.1.4 Isolation and Purification of MSC-sEVs

The third section of this study investigated how various filtration parameters, such as membrane pore size, stirring speed, operational pressure, feed concentration and diafiltration process, affected sEVs isolation during the dead-end ultrafiltration process. A fed-batch ultra-diafiltration protocol with optimised filtration settings was developed accordingly and was compared with the most commonly used ultracentrifugation method for the isolation of MSC-sEVs. Conclusions can be outlined as followed:

C5. In comparison to the performance of 100 kDa and 300 kDa, 500 kDa MWCO might be the most effective membrane pore size for the isolation of MSC-sEVs, giving the highest purity and productivity of MSC-sEV during the ultrafiltration process.

C6. The stirring speed can also be raised to a specific level to increase sEV productivity. A decrease in operational pressure enables sEVs to be gently separated, leading to excellent particle recovery and purity of MSC-sEVs.

C7. By introducing 6 isovolumetric diafiltration steps, the purification of the MSC-sEVs can be further enhanced by removing about 99% of the protein contaminants.

C8. The developed fed-batch UF/DF protocol can achieve MSC-sEV preparations with a 3-fold higher yield and nearly doubled purity, in comparison to the ultracentrifugation method.

C9. This is the first study to thoroughly examine the impact of various filtration parameters on the isolation of MSC-sEVs, which offers significant insights into the development of ultrafiltration based sEV separation process.

C10. With advantages including high recovery, efficient production, excellent scalability, automatable properties, and cost-effectiveness, the proposed fed-batch ultra-diafiltration protocol could be a very powerful isolation method for both small lab-scale separation and industrial scale manufacture of MSC-sEVs. This would significantly contribute to overcoming the current technical barriers and advancing the clinical translation of MSC-sEVs.

6.2 Limitations and Future Work

The current NHDF-based function identification method has a limitation that it only presents cellular responses after the secretome treatment. Consequently,

functional assays should be further developed. For example, complementary research on molecular level characterisation can be conducted. The generic functional biomarkers assay can be established through comparative transcriptome analysis of the recipient cells, marker screening and quantitative polymerase chain reaction (qPCR) to support accurate function clarification. Additionally, other cell types like endothelial cells and keratinocytes, which also have significant roles in skin regeneration, should be included as recipient cells in order to optimise this wound healing model.

For the developed CES-based sEV production method, the altering of secreted sEVs as a result of MSC phenotypic change could pose a concern to long-term production. Therefore, additional research should be done to examine the immunophenotyping and trilineage mesoderm differentiation capability of the MSCs before and after the production process. In addition, as a complement to the cellular assay, the above-mentioned qPCR-based generic functional biomarkers assay is required for quality control of the MSC-sEV products. Future improvements for the CES-based sEV production method should be continued, including optimisation of the operation parameters, design of customised hollow fibre cartridge for sEV production, and scale-up by connecting numerous HFBR cartridges in parallel to allow multi-HFBR manufacturing simultaneously. It is also recommended to conduct the analysis regarding the universal applicability of this method by assessing the CES sEV production capacity with various cell types. Parallel comparison in terms of the cell

cultivation and sEV production performance between the CES method and other commercially available platforms is also encouraged.

For the established fed-batch ultra-diafiltration isolation protocol, a limitation of this research was that the post-separation functional integrity of the EV samples was unknown, which should be investigated in the future employing both the cellular assay and the qPCR-based functional biomarkers assay mentioned above. Further development can also be applied to the current fed-batch UF/DF technique. For instance, in order to create better hydrodynamic environment, tangential flow filtration should be taken into consideration as an alternative to the present dead-end filtration, which may greatly reduce the issue with concentration polarisation and thereby increase sEV productivity. Additionally, it might be worth testing with the continuous constant volume diafiltration (CVD) mode, which may result in a more effective and gentle buffer exchange than current discontinuous diafiltration since fresh buffer is continuously fed to the filtration system at the same rate as the permeate is being withdrawn. Multifactorial research for process parameters can also be conducted using design of experiments (DOE) to support further investigation for optimum process. An automated ultrafiltration system with programmed separation process is expected for the pilot trial of automatic MSC-sEV isolation and purification.

References

1. Barry, F. P. & Murphy, J. M. Mesenchymal stem cells: Clinical applications and biological characterization. *International Journal of Biochemistry and Cell Biology* **36**, 568–584 (2004).
2. Ding, D. C., Shyu, W. C. & Lin, S. Z. Mesenchymal stem cells. *Cell Transplantation* **20**, 5–14 (2011).
3. Herberts, C. A., Kwa, M. S. & Hermsen, H. P. Risk factors in the development of stem cell therapy. *J. Transl. Med.* **9**, 29 (2011).
4. Gnecchi, M., Danieli, P., Malpasso, G. & Ciuffreda, M. C. Paracrine mechanisms of mesenchymal stem cells in tissue repair. in *Methods in Molecular Biology* **1416**, 123–146 (Humana Press Inc., 2016).
5. Pittenger, M. F. *et al.* Mesenchymal stem cell perspective: cell biology to clinical progress. *npj Regenerative Medicine* **4**, (2019).
6. Makridakis, M., Roubelakis, M. G. & Vlahou, A. Stem cells: Insights into the secretome. *Biochimica et Biophysica Acta - Proteins and Proteomics* **1834**, 2380–2384 (2013).
7. Sagaradze, G. *et al.* Conditioned medium from human mesenchymal stromal cells: Towards the clinical translation. *Int. J. Mol. Sci.* **20**, 1656 (2019).
8. Teixeira, F. G., Carvalho, M. M., Sousa, N. & Salgado, A. J. Mesenchymal stem cells secretome: A new paradigm for central nervous system regeneration? *Cell. Mol. Life Sci.* **70**, 3871–3882 (2013).
9. Madrigal, M., Rao, K. S. & Riordan, N. H. A review of therapeutic effects of mesenchymal stem cell secretions and induction of secretory modification by different culture methods. *Journal of Translational Medicine* **12**, 1–14 (2014).
10. Théry, C. *et al.* Minimal information for studies of extracellular vesicles 2018 (MISEV2018): a position statement of the International Society for Extracellular Vesicles and update of the MISEV2014 guidelines. *J. Extracell. Vesicles* **8**, 1535750 (2019).
11. Möller, A. & Lobb, R. J. The evolving translational potential of small extracellular vesicles in cancer. *Nat. Rev. Cancer* **20**, 697–709 (2020).
12. Yáñez-Mó, M. *et al.* Biological properties of extracellular vesicles and their physiological functions. *J. Extracell. Vesicles* **4**, 1–60 (2015).
13. Yoo, K. W. *et al.* Large-Scale preparation of extracellular vesicles enriched with specific microRNA. *Tissue Eng. - Part C Methods* **24**, 637–644 (2018).
14. El Andaloussi, S., Mäger, I., Breakefield, X. O. & Wood, M. J. A. Extracellular vesicles: Biology and emerging therapeutic opportunities. *Nat. Rev. Drug Discov.* **12**, 347–357 (2013).
15. Valadi, H. *et al.* Exosome-mediated transfer of mRNAs and microRNAs is a novel mechanism of genetic exchange between cells. *Nat. Cell Biol.* **9**, 654–659 (2007).
16. Barile, L. & Vassalli, G. Exosomes: Therapy delivery tools and biomarkers of diseases. *Pharmacol. Ther.* **174**, 63–78 (2017).
17. Vader, P., Mol, E. A., Pasterkamp, G. & Schiffelers, R. M. Extracellular vesicles for drug delivery. *Adv. Drug Deliv. Rev.* **106**, 148–156 (2016).
18. Nagelkerke, A. *et al.* Extracellular vesicles for tissue repair and regeneration: Evidence, challenges and opportunities. *Adv. Drug Deliv. Rev.* **175**, 113775 (2021).
19. Robbins, P. D. & Morelli, A. E. Regulation of immune responses by extracellular vesicles. *Nat. Rev. Immunol.* **14**, 195–208 (2014).
20. M, G., P, D., G, M. & MC, C. Paracrine Mechanisms of Mesenchymal Stem Cells in Tissue Repair. *Methods*

Mol. Biol. **1416**, 123–146 (2016).

21. Rani, S., Ryan, A. E., Griffin, M. D. & Ritter, T. Mesenchymal stem cell-derived extracellular vesicles: Toward cell-free therapeutic applications. *Mol. Ther.* **23**, 812–823 (2015).
22. Ratajczak, M. Z. *et al.* Pivotal role of paracrine effects in stem cell therapies in regenerative medicine: Can we translate stem cell-secreted paracrine factors and microvesicles into better therapeutic strategies. *Leukemia* **26**, 1166–1173 (2012).
23. Tsiapalis, D. & O'Driscoll, L. Mesenchymal Stem Cell Derived Extracellular Vesicles for Tissue Engineering and Regenerative Medicine Applications. *Cells* **9**, (2020).
24. Gobin, J. *et al.* Hollow-fiber bioreactor production of extracellular vesicles from human bone marrow mesenchymal stromal cells yields nanovesicles that mirrors the immuno-modulatory antigenic signature of the producer cell. *Stem Cell Res. Ther.* **12**, 1–20 (2021).
25. Hahm, J., Kim, J. & Park, J. Strategies to Enhance Extracellular Vesicle Production. *Tissue Eng. Regen. Med.* **18**, 513–524 (2021).
26. Paganini, C. *et al.* Scalable Production and Isolation of Extracellular Vesicles: Available Sources and Lessons from Current Industrial Bioprocesses. *Biotechnol. J.* **14**, 1–10 (2019).
27. Syromiatnikova, V., Prokopeva, A. & Gomzikova, M. Methods of the Large-Scale Production of Extracellular Vesicles. *Int. J. Mol. Sci.* **23**, (2022).
28. Ruppert, K. A. *et al.* Human Mesenchymal Stromal Cell-Derived Extracellular Vesicles Modify Microglial Response and Improve Clinical Outcomes in Experimental Spinal Cord Injury. *Sci. Rep.* **8**, 1–12 (2018).
29. Haraszti, R. A. *et al.* Exosomes Produced from 3D Cultures of MSCs by Tangential Flow Filtration Show Higher Yield and Improved Activity. *Mol. Ther.* **26**, 2838–2847 (2018).
30. Patel, D. B., Luthers, C. R., Lerman, M. J., Fisher, J. P. & Jay, S. M. Enhanced extracellular vesicle production and ethanol-mediated vascularization bioactivity via a 3D-printed scaffold-perfusion bioreactor system. *Acta Biomater.* **95**, 236–244 (2019).
31. Watson, D. C. *et al.* Scalable, cGMP-compatible purification of extracellular vesicles carrying bioactive human heterodimeric IL-15/lactadherin complexes. *J. Extracell. Vesicles* **7**, (2018).
32. Dowling, P. & Clynes, M. Conditioned media from cell lines: A complementary model to clinical specimens for the discovery of disease-specific biomarkers. *Proteomics* **11**, 794–804 (2011).
33. Grangier, A. *et al.* Technological advances towards extracellular vesicles mass production. *Adv. Drug Deliv. Rev.* **176**, (2021).
34. Royo, F., Théry, C., Falcón-Pérez, J. M., Nieuwland, R. & Witwer, K. W. Methods for Separation and Characterization of Extracellular Vesicles: Results of a Worldwide Survey Performed by the ISEV Rigor and Standardization Subcommittee. *Cells* **9**, (2020).
35. Linares, R., Tan, S., Gounou, C., Arraud, N. & Brisson, A. R. High-speed centrifugation induces aggregation of extracellular vesicles. *J. Extracell. Vesicles* **4**, 1–7 (2015).
36. Xu, R., Greening, D. W., Zhu, H., Takahashi, N. & Simpson, R. J. Extracellular vesicle isolation and characterization : toward clinical application. *J Clin Invest* **126**, 1152–1162 (2016).
37. Nakai, W. *et al.* A novel affinity-based method for the isolation of highly purified extracellular vesicles. *Sci. Rep.* **6**, 1–11 (2016).
38. Brownlee, Z., Lynn, K. D., Thorpe, P. E. & Schroit, A. J. A novel 'salting-out' procedure for the isolation of tumor-derived exosomes. *J. Immunol. Methods* **407**, 120–126 (2014).
39. Böing, A. N. *et al.* Single-step isolation of extracellular vesicles by size-exclusion chromatography. *J.*

Extracell. Vesicles **3**, (2014).

40. Phan, J. *et al.* Engineering mesenchymal stem cells to improve their exosome efficacy and yield for cell-free therapy. *J. Extracell. Vesicles* **7**, 1522236 (2018).
41. Tonk, C., Witzler, M., Schulze, M. & Tobiasch, E. Mesenchymal Stem Cells. in *Essential Current Concepts in Stem Cell Biology* 21–40 (2020). doi:10.1007/978-3-030-33923-4_4
42. Dominici, M. *et al.* Minimal criteria for defining multipotent mesenchymal stromal cells. The International Society for Cellular Therapy position statement. *Cytotherapy* **8**, 315–317 (2006).
43. Hass, R., Kasper, C., Böhm, S. & Jacobs, R. Different populations and sources of human mesenchymal stem cells (MSC): A comparison of adult and neonatal tissue-derived MSC. *Cell Commun. Signal.* **9**, 12 (2011).
44. Mafi, R., Hindocha, S., Mafi, P., Griffin, M. & Khan, W. S. Sources of Adult Mesenchymal Stem Cells Applicable for Musculoskeletal Applications - A Systematic Review of the Literature. *Open Orthop. J.* **5**, 242–248 (2011).
45. Pittenger, M. F. *et al.* Mesenchymal stem cell perspective: cell biology to clinical progress. *npj Regen. Med.* **4**, (2019).
46. Uccelli, A., Moretta, L. & Pistoia, V. Mesenchymal stem cells in health and disease. *Nature Reviews Immunology* **8**, 726–736 (2008).
47. Chu, D. T. *et al.* An update on the progress of isolation, culture, storage, and clinical application of human bone marrow mesenchymal stem/stromal cells. *International Journal of Molecular Sciences* **21**, (2020).
48. Lin, H., Sohn, J., Shen, H., Langhans, M. T. & Tuan, R. S. Bone marrow mesenchymal stem cells: Aging and tissue engineering applications to enhance bone healing. *Biomaterials* **203**, 96–110 (2019).
49. Le, H. *et al.* Mesenchymal stem cells for cartilage regeneration. *J. Tissue Eng.* **11**, (2020).
50. Hernández, R. *et al.* Differentiation of human mesenchymal stem cells towards neuronal lineage: Clinical trials in nervous system disorders. *Biomol. Ther.* **28**, 34–44 (2020).
51. Gnecchi, M. & Cervio, E. Mesenchymal stem cell therapy for heart disease. in *Stem Cell Biology and Regenerative Medicine* 241 (2013). doi:10.1007/978-1-62703-200-1
52. Volarevic, V., Nurkovic, J., Arsenijevic, N. & Stojkovic, M. Concise review: Therapeutic potential of mesenchymal stem cells for the treatment of acute liver failure and cirrhosis. *Stem Cells* **32**, 2818–2823 (2014).
53. Fu, X. & Li, H. Mesenchymal stem cells and skin wound repair and regeneration: Possibilities and questions. *Cell Tissue Res.* **335**, 317–321 (2009).
54. Liang, X., Ding, Y., Zhang, Y., Tse, H.-F. & Lian, Q. Paracrine Mechanisms of Mesenchymal Stem Cell-Based Therapy: Current Status and Perspectives. *Cell Transplant.* **23**, 1045–1059 (2014).
55. Caplan, A. I. Mesenchymal stem cells: Time to change the name! *Stem Cells Transl. Med.* **6**, 1445–1451 (2017).
56. Vizoso, F. J., Eiro, N., Cid, S., Schneider, J. & Perez-Fernandez, R. Mesenchymal stem cell secretome: Toward cell-free therapeutic strategies in regenerative medicine. *Int. J. Mol. Sci.* **18**, (2017).
57. Shojaei, F., Rahmati, S. & Banitalebi Dehkordi, M. A review on different methods to increase the efficiency of mesenchymal stem cell-based wound therapy. *Wound Repair Regen.* **27**, 661–671 (2019).
58. Wu, Y., Chen, L., Scott, P. G. & Tredget, E. E. Mesenchymal Stem Cells Enhance Wound Healing Through Differentiation and Angiogenesis. *Stem Cells* **25**, 2648–2659 (2007).
59. Chen, L., Tredget, E. E., Wu, P. Y. G., Wu, Y. & Wu, Y. Paracrine factors of mesenchymal stem cells

recruit macrophages and endothelial lineage cells and enhance wound healing. *PLoS One* **3**, 1886 (2008).

60. Yew, T. L. *et al.* Enhancement of wound healing by human multipotent stromal cell conditioned medium: The paracrine factors and p38 MAPK activation. *Cell Transplant.* **20**, 693–706 (2011).
61. Pawitan, J. A. Prospect of stem cell conditioned medium in regenerative medicine. *BioMed Research International* **2014**, (2014).
62. Szatanek, R. *et al.* The methods of choice for extracellular vesicles (EVs) characterization. *Int. J. Mol. Sci.* **18**, (2017).
63. Bjørge, I. M., Kim, S. Y., Mano, J. F., Kalionis, B. & Chrzanowski, W. Extracellular vesicles, exosomes and shedding vesicles in regenerative medicine-a new paradigm for tissue repair. *Biomater. Sci.* **6**, 60–78 (2018).
64. György, B. *et al.* Membrane vesicles, current state-of-the-art: emerging role of extracellular vesicles. *Cell. Mol. Life Sci.* **68**, 2667–2688 (2011).
65. Cataldi, G., Maffei, G. L. & Vaccaro, P. Extracellular vesicles: potential roles in regenerative medicine. *Urban Morphol.* **6**, 3–14 (2002).
66. Alenquer, M. & Amorim, M. J. Exosome biogenesis, regulation, and function in viral infection. *Viruses* **7**, 5066–5083 (2015).
67. Gong, M. *et al.* Mesenchymal stem cells release exosomes that transfer miRNAs to endothelial cells and promote angiogenesis. *Oncotarget* **8**, 45200–45212 (2017).
68. Mathew, S. A., Chandravanshi, B. & Bhonde, R. Hypoxia primed placental mesenchymal stem cells for wound healing. *Life Sci.* **182**, 85–92 (2017).
69. Kholia, S. *et al.* Extracellular vesicles as new players in angiogenesis. *Vascul. Pharmacol.* **86**, 64–70 (2016).
70. Burrello, J. *et al.* Stem Cell-Derived Extracellular Vesicles and Immune-Modulation. *Front. Cell Dev. Biol.* **4**, 83 (2016).
71. Ratajczak, J., Wysoczynski, M., Hayek, F., Janowska-Wieczorek, A. & Ratajczak, M. Z. Membrane-derived microvesicles: Important and underappreciated mediators of cell-to-cell communication. *Leukemia* **20**, 1487–1495 (2006).
72. Rodrigues, M. L., Nimrichter, L., Oliveira, D. L., Nosanchuk, J. D. & Casadevall, A. Exosome-mediated transfer of mRNAs and microRNAs is a novel mechanism of genetic exchange between cells. *Lipid Insights* **2 1**, 27–40 (2008).
73. Rajendran, L. *et al.* Emerging roles of extracellular vesicles in the nervous system. *J. Neurosci.* **34**, 15482–9 (2014).
74. Christianson, H. C., Svensson, K. J. & Belting, M. Exosome and microvesicle mediated phene transfer in mammalian cells. *Semin. Cancer Biol.* **28**, 31–38 (2014).
75. Colombo, M., Raposo, G. & Théry, C. Biogenesis, Secretion, and Intercellular Interactions of Exosomes and Other Extracellular Vesicles. *Annu. Rev. Cell Dev. Biol.* **30**, 255–289 (2014).
76. Tauro, B. J. *et al.* Oncogenic H-ras reprograms Madin-Darby canine kidney (MDCK) cell-derived exosomal proteins following epithelial-mesenchymal transition. *Mol. Cell. Proteomics* **12**, 2148–59 (2013).
77. Rak, J. & Guha, A. Extracellular vesicles - vehicles that spread cancer genes. *BioEssays* **34**, 489–497 (2012).
78. Simpson, R. J., Lim, J. W., Moritz, R. L. & Mathivanan, S. Exosomes: proteomic insights and diagnostic potential. *Expert Rev. Proteomics* **6**, 267–283 (2009).
79. Keshtkar, S., Azarpira, N. & Ghahremani, M. H. Mesenchymal stem cell-derived extracellular vesicles: Novel frontiers in regenerative medicine. *Stem Cell Res. Ther.* **9**, 1–9 (2018).

80. Rak, J. Extracellular Vesicles – Biomarkers and Effectors of the Cellular Interactome in Cancer. *Front. Pharmacol.* **4**, 21 (2013).
81. Beyer, C. & Pisetsky, D. S. The role of microparticles in the pathogenesis of rheumatic diseases. *Nat. Rev. Rheumatol.* **6**, 21–29 (2010).
82. Nawaz, M. *et al.* The emerging role of extracellular vesicles as biomarkers for urogenital cancers. *Nat. Rev. Urol.* **11**, 688–701 (2014).
83. Watson, D. C. *et al.* Efficient production and enhanced tumor delivery of engineered extracellular vesicles. *Biomaterials* **105**, 195–205 (2016).
84. Cabral, J., Ryan, A. E., Griffin, M. D. & Ritter, T. Extracellular vesicles as modulators of wound healing. *Adv. Drug Deliv. Rev.* **129**, 394–406 (2018).
85. Ferreira, A. da F. & Gomes, D. A. Stem cell extracellular vesicles in skin repair. *Bioengineering* **6**, 1–18 (2019).
86. de Abreu, R. C. *et al.* Native and bioengineered extracellular vesicles for cardiovascular therapeutics. *Nat. Rev. Cardiol.* **17**, 685–697 (2020).
87. Grange, C., Iampietro, C. & Bussolati, B. Stem cell extracellular vesicles and kidney injury. *Stem Cell Investig.* **4**, (2017).
88. Psaraki, A., Ntari, L., Karakostas, C., Korrou-Karava, D. & Roubelakis, M. G. Extracellular vesicles derived from mesenchymal stem/stromal cells: The regenerative impact in liver diseases. *Hepatology* **75**, 1590–1603 (2022).
89. Song, H. *et al.* Extracellular Vesicles in chondrogenesis and Cartilage regeneration. *J. Cell. Mol. Med.* **25**, 4883–4892 (2021).
90. Velnar, T., Bailey, T. & Smrkolj, V. The wound healing process: An overview of the cellular and molecular mechanisms. *J. Int. Med. Res.* **37**, 1528–1542 (2009).
91. Wu, P., Zhang, B., Shi, H., Qian, H. & Xu, W. MSC-exosome: A novel cell-free therapy for cutaneous regeneration. *Cytotherapy* **20**, 291–301 (2018).
92. Rani, S. & Ritter, T. The Exosome - A Naturally Secreted Nanoparticle and its Application to Wound Healing. *Adv. Mater.* **28**, 5542–5552 (2016).
93. Zhang, B. *et al.* HucMSc-exosome mediated-Wnt4 signaling is required for cutaneous wound healing. *Stem Cells* **33**, 2158–2168 (2015).
94. Shabbir, A., Cox, A., Rodriguez-Menocal, L., Salgado, M. & Van Badiavas, E. Mesenchymal Stem Cell Exosomes Induce Proliferation and Migration of Normal and Chronic Wound Fibroblasts, and Enhance Angiogenesis in Vitro. *Stem Cells Dev.* **24**, 1635–1647 (2015).
95. Choi, J. S. *et al.* Functional recovery in photo-damaged human dermal fibroblasts by human adipose-derived stem cell extracellular vesicles. *J. Extracell. Vesicles* **8**, (2019).
96. Hu, L. *et al.* Exosomes derived from human adipose mensenchymal stem cells accelerates cutaneous wound healing via optimizing the characteristics of fibroblasts. *Sci. Rep.* **6**, 1–11 (2016).
97. Zhang, B. *et al.* Human Umbilical Cord Mesenchymal Stem Cell Exosomes Enhance Angiogenesis Through the Wnt4/β-Catenin Pathway. *Stem Cells Transl. Med.* **4**, 513–522 (2015).
98. Zhang, B. *et al.* HucMSC Exosome-Delivered 14-3-3ζ Orchestrates Self-Control of the Wnt Response via Modulation of YAP During Cutaneous Regeneration. *Stem Cells* **34**, 2485–2500 (2016).
99. Lai, R. C. *et al.* Exosome secreted by MSC reduces myocardial ischemia/reperfusion injury. *Stem Cell Res.* **4**, 214–222 (2010).

100. Salomon, C. *et al.* Exosomal Signaling during Hypoxia Mediates Microvascular Endothelial Cell Migration and Vasculogenesis. *PLoS One* **8**, 1–24 (2013).
101. Bian, S. *et al.* Extracellular vesicles derived from human bone marrow mesenchymal stem cells promote angiogenesis in a rat myocardial infarction model. *J. Mol. Med.* **92**, 387–397 (2014).
102. Han, C. *et al.* Human umbilical cord mesenchymal stem cell derived exosomes encapsulated in functional peptide hydrogels promote cardiac repair. *Biomater. Sci.* **7**, 2920–2933 (2019).
103. Bruno, S. *et al.* Mesenchymal Stem Cell-Derived Microvesicles Protect Against Acute Tubular Injury. *J. Am. Soc. Nephrol.* **20**, 1053–1067 (2009).
104. Zhao, L., Hu, C., Zhang, P., Jiang, H. & Chen, J. Genetic communication by extracellular vesicles is an important mechanism underlying stem cell-based therapy-mediated protection against acute kidney injury. *Stem Cell Res. Ther.* **10**, 1–9 (2019).
105. Wang, S. Y. *et al.* MiRNAs in stem cell-derived extracellular vesicles for acute kidney injury treatment: Comprehensive review of preclinical studies. *Stem Cell Res. Ther.* **10**, 1–7 (2019).
106. Grange, C. *et al.* Stem cell-derived extracellular vesicles inhibit and revert fibrosis progression in a mouse model of diabetic nephropathy. *Sci. Rep.* **9**, 1–13 (2019).
107. He, J. *et al.* Bone marrow stem cells-derived microvesicles protect against renal injury in the mouse remnant kidney model. *Nephrology* **17**, 493–500 (2012).
108. He, J. *et al.* Micro-vesicles derived from bone marrow stem cells protect the kidney both in vivo and in vitro by microRNA-dependent repairing. *Nephrology* **20**, 591–600 (2015).
109. Tan, C. Y. *et al.* Mesenchymal stem cell-derived exosomes promote hepatic regeneration in drug-induced liver injury models. *Stem Cell Res. Ther.* **5**, 1–14 (2014).
110. Yao, J. *et al.* Extracellular vesicles derived from human umbilical cord mesenchymal stem cells alleviate rat hepatic ischemia-reperfusion injury by suppressing oxidative stress and neutrophil inflammatory response. *FASEB J.* **33**, 1695–1710 (2019).
111. Li, T. *et al.* Exosomes derived from human umbilical cord mesenchymal stem cells alleviate liver fibrosis. *Stem Cells Dev.* **22**, 845–854 (2013).
112. Wu, Y., Deng, W., Klinke II, D. J. & Klinke, D. J. Exosomes: Improved methods to characterize their morphology, RNA content, and surface protein biomarkers. *Analyst* **140**, 6631–6642 (2015).
113. Konala, V. B. R. *et al.* The current landscape of the mesenchymal stromal cell secretome: A new paradigm for cell-free regeneration. *Cytotherapy* **18**, 13–24 (2016).
114. Sun, L. *et al.* Safety evaluation of exosomes derived from human umbilical cord mesenchymal stromal cell. *Cytotherapy* **18**, 413–422 (2016).
115. Coumans, F. A. W. *et al.* Methodological Guidelines to Study Extracellular Vesicles. *Circ. Res.* **120**, 1632–1648 (2017).
116. Yu, B., Zhang, X. & Li, X. Exosomes Derived from Mesenchymal Stem Cells. *Int. J. Mol. Sci.* **15**, 4142–4157 (2014).
117. Hartjes, T. A., Mytnyk, S., Jenster, G. W., van Steijn, V. & van Royen, M. E. Extracellular vesicle quantification and characterization: Common methods and emerging approaches. *Bioengineering* **6**, (2019).
118. Sun, L. *et al.* Serum deprivation elevates the levels of microvesicles with different size distributions and selectively enriched proteins in human myeloma cells in vitro. *Acta Pharmacol. Sin.* **35**, 381–383 (2014).
119. Parolini, I. *et al.* Microenvironmental pH is a key factor for exosome traffic in tumor cells. *J. Biol. Chem.* **284**, 34211–34222 (2009).

120. Chen, T., Guo, J., Yang, M., Zhu, X. & Cao, X. Chemokine-Containing Exosomes Are Released from Heat-Stressed Tumor Cells via Lipid Raft-Dependent Pathway and Act as Efficient Tumor Vaccine. *J. Immunol.* **186**, 2219–2228 (2011).
121. Yaghoubi, S. *et al.* How hypoxia regulate exosomes in ischemic diseases and cancer microenvironment? *IUBMB Life* **72**, 1286–1305 (2020).
122. Taylor, J., Azimi, I., Monteith, G. & Bebawy, M. Ca2+ mediates extracellular vesicle biogenesis through alternate pathways in malignancy. *J. Extracell. Vesicles* **9**, (2020).
123. Kim, W. S. *et al.* Comparison of exosomes derived from non-and gamma-irradiated melanoma cancer cells as a potential antigenic and immunogenic source for dendritic cell-based immunotherapeutic vaccine. *Vaccines* **8**, 1–14 (2020).
124. Yoon, J. *et al.* Generation of nanovesicles with sliced cellular membrane fragments for exogenous material delivery. *Biomaterials* **59**, 12–20 (2015).
125. Colao, I. L., Corteling, R., Bracewell, D. & Wall, I. Manufacturing Exosomes: A Promising Therapeutic Platform. *Trends Mol. Med.* **24**, 242–256 (2018).
126. Tirughana, R. *et al.* GMP Production and Scale-Up of Adherent Neural Stem Cells with a Quantum Cell Expansion System. *Mol. Ther. - Methods Clin. Dev.* **10**, 48–56 (2018).
127. Mitchell, J. P., Court, J., Mason, M. D., Tabi, Z. & Clayton, A. Increased exosome production from tumour cell cultures using the Integra CELLine Culture System. *J. Immunol. Methods* **335**, 98–105 (2008).
128. Li, J. *et al.* Serum-free culture alters the quantity and protein composition of neuroblastoma-derived extracellular vesicles. *J. Extracell. Vesicles* **4**, 1–12 (2015).
129. Théry, C. *et al.* Proteomic Analysis of Dendritic Cell-Derived Exosomes: A Secreted Subcellular Compartment Distinct from Apoptotic Vesicles. *J. Immunol.* **166**, 7309–7318 (2001).
130. Wen, Y.-T., Chang, Y.-C., Lin, L.-C. & Liao, P.-C. Collection of in vivo-like liver cell secretome with alternative sample enrichment method using a hollow fiber bioreactor culture system combined with tangential flow filtration for secretomics analysis. *Anal. Chim. Acta* **684**, 81–88 (2011).
131. Jeon, Y., Lee, M. S. & Cheon, Y.-P. Decreased contact inhibition in mouse adipose mesenchymal stem cells. *Dev. Reprod.* **16**, 329–38 (2012).
132. Shelke, G. V., Lässer, C., Gho, Y. S. & Lötvall, J. Importance of exosome depletion protocols to eliminate functional and RNA-containing extracellular vesicles from fetal bovine serum. *J. Extracell. Vesicles* **3**, 1–8 (2014).
133. FiberCellSystems. Available at: https://www.fibercellsystems.com/products/cartridges/. (Accessed: 25th January 2023)
134. The Cell Culture Company. Available at: https://cellculturecompany.com/. (Accessed: 23rd January 2023)
135. Flocel. Available at: https://www.flocel.com/. (Accessed: 23rd January 2023)
136. Terumo. Terumo Quantum. Available at: https://www.terumobct.com/quantum/. (Accessed: 23rd January 2023)
137. Ltd, O. M. Bioreactor Systems by Oxford Mestar. Available at: http://www.oxford-mestar.com/. (Accessed: 23rd January 2023)
138. Coeshott, C., Vang, B., Jones, M. & Nankervis, B. Large-scale expansion and characterization of CD3+ T-cells in the Quantum® Cell Expansion System. *J. Transl. Med.* **17**, 1–13 (2019).
139. Hanley, P. J. *et al.* Efficient manufacturing of therapeutic mesenchymal stromal cells with the use of the Quantum Cell Expansion System. *Cytotherapy* **16**, 1048–1058 (2014).

140. Haack-Sørensen, M. *et al.* Culture expansion of adipose derived stromal cells. A closed automated Quantum Cell Expansion System compared with manual flask-based culture. *J. Transl. Med.* **14**, 1–11 (2016).

141. Paccola Mesquita, F. C., Hochman-Mendez, C., Morrissey, J., Sampaio, L. C. & Taylor, D. A. Laminin as a potent substrate for large-scale expansion of human induced pluripotent stem cells in a closed cell expansion system. *Stem Cells Int.* **2019**, (2019).

142. Allen, A. *et al.* Mesenchymal Stromal Cell Bioreactor for Ex Vivo Reprogramming of Human Immune Cells. *Sci. Rep.* **10**, 1–13 (2020).

143. Usuludin, S. B. M., Cao, X. & Lim, M. Co-culture of stromal and erythroleukemia cells in a perfused hollow fiber bioreactor system as an in vitro bone marrow model for myeloid leukemia. *Biotechnol. Bioeng.* **109**, 1248–1258 (2012).

144. Blaber, E., Sato, K. & Almeida, E. A. C. Stem cell health and tissue regeneration in microgravity. *Stem Cells Dev.* **23**, 73–78 (2014).

145. Mendt, M. *et al.* Generation and testing of clinical-grade exosomes for pancreatic cancer. *JCI insight* **3**, 1–22 (2018).

146. Williams, A. M. *et al.* Mesenchymal Stem Cell-Derived Exosomes Provide Neuroprotection and Improve Long-Term Neurologic Outcomes in a Swine Model of Traumatic Brain Injury and Hemorrhagic Shock. *J. Neurotrauma* **36**, 54–60 (2019).

147. Potter, D. R. *et al.* Mesenchymal stem cell-derived extracellular vesicles attenuate pulmonary vascular permeability and lung injury induced by hemorrhagic shock and trauma. *J. Trauma Acute Care Surg.* **84**, 245–256 (2018).

148. Raposo, G. & Stoorvogel, W. Extracellular vesicles: Exosomes, microvesicles, and friends. *J. Cell Biol.* **200**, 373–383 (2013).

149. Doeppner, T. R. *et al.* Extracellular Vesicles Improve Post-Stroke Neuroregeneration and Prevent Postischemic Immunosuppression. *Stem Cells Transl. Med.* **4**, 1131–1143 (2015).

150. Dismuke, W. M. & Liu, Y. Current Methods to Purify and Characterize Exosomes. in *Mesenchymal Stem Cell Derived Exosomes* doi:10.1016/B978-0-12-800164-6/00012-5

151. Corral-Vázquez, C. *et al.* Cell lines authentication and mycoplasma detection as minimun quality control of cell lines in biobanking. *Cell Tissue Bank.* **18**, 271–280 (2017).

152. Yang, C., Chalasani, G., Ng, Y.-H. & Robbins, P. D. Exosomes Released from Mycoplasma Infected Tumor Cells Activate Inhibitory B Cells. *PLoS One* **7**, e36138 (2012).

153. Quah, B. J. C. & O'Neill, H. C. Mycoplasma contaminants present in exosome preparations induce polyclonal B cell responses. *J. Leukoc. Biol.* **82**, 1070–1082 (2007).

154. Lucchetti, D., Fattorossi, A. & Sgambato, A. Extracellular Vesicles in Oncology: Progress and Pitfalls in the Methods of Isolation and Analysis. *Biotechnol. J.* **1700716**, 1700716 (2018).

155. Gyorgy, Bence, et al. Detection and isolation of cell-derived microparticles are compromised by protein complexes resulting from shared biophysical parameters. *Blood* **117**, 39–49 (2011).

156. Savarimuthu, X. *et al.* Obstacles and opportunities in the functional analysis of extracellular vesicle RNA – an ISEV position paper. *J. Heal. Popul. Nutr.* **24**, 277–281 (2016).

157. Ramirez, M. I. *et al.* Technical challenges of working with extracellular vesicles. *Nanoscale* **10**, 881–906 (2018).

158. Ng, K. S. *et al.* Bioprocess decision support tool for scalable manufacture of extracellular vesicles. *Biotechnol. Bioeng.* **116**, 307–319 (2019).

159. Tauro, B. J. *et al.* Comparison of ultracentrifugation, density gradient separation, and immunoaffinity capture methods for isolating human colon cancer cell line LIM1863-derived exosomes. *Methods* **56**, 293–304 (2012).

160. Webber, J. & Clayton, A. How pure are your vesicles? *J. Extracell. Vesicles* **2**, 1–6 (2013).

161. Greening, D. W., Xu, R., Ji, H., Tauro, B. J. & Simpson, R. J. A Protocol for Exosome Isolation and Characterization: Evaluation of Ultracentrifugation, Density-Gradient Separation, and Immunoaffinity Capture Methods. in 179–209 (Humana Press, New York, NY, 2015). doi:10.1007/978-1-4939-2550-6_15

162. Nordin, J. Z. *et al.* Ultrafiltration with size-exclusion liquid chromatography for high yield isolation of extracellular vesicles preserving intact biophysical and functional properties. *Nanomedicine Nanotechnology, Biol. Med.* **11**, 879–883 (2015).

163. Kanwar, S. S., Dunlay, C. J., Simeone, D. M. & Nagrath, S. Microfluidic device (ExoChip) for on-chip isolation, quantification and characterization of circulating exosomes. *Lab Chip* **14**, 1891–1900 (2014).

164. Clayton, A. *et al.* Analysis of antigen presenting cell derived exosomes, based on immuno-magnetic isolation and flow cytometry. *J. Immunol. Methods* **247**, 163–174 (2001).

165. Mathivanan, S. *et al.* Proteomics analysis of A33 immunoaffinity-purified exosomes released from the human colon tumor cell line LIM1215 reveals a tissue-specific protein signature. *Mol. Cell. Proteomics* **9**, 197–208 (2010).

166. Yoo, C. E. *et al.* A direct extraction method for microRNAs from exosomes captured by immunoaffinity beads. *Anal. Biochem.* **431**, 96–98 (2012).

167. Mercier, S. K. *et al.* The Microvesicle Component of HIV-1 Inocula Modulates Dendritic Cell Infection and Maturation and Enhances Adhesion to and Activation of T Lymphocytes. *PLoS Pathog.* **9**, e1003700 (2013).

168. Koga, K. *et al.* Purification, characterization and biological significance of tumor-derived exosomes. *Anticancer Res.* **25**, 3703–7 (2005).

169. Wiley, R. D. & Gummuluru, S. Immature dendritic cell-derived exosomes can mediate HIV-1 trans infection. *Proc. Natl. Acad. Sci. U. S. A.* **103**, 738–43 (2006).

170. Caby, M.-P., Lankar, D., Vincendeau-Scherrer, C., Raposo, G. & Bonnerot, C. Exosomal-like vesicles are present in human blood plasma. *Int. Immunol.* **17**, 879–887 (2005).

171. Ghosh, A. *et al.* Rapid Isolation of Extracellular Vesicles from Cell Culture and Biological Fluids Using a Synthetic Peptide with Specific Affinity for Heat Shock Proteins. *PLoS One* **9**, e110443 (2014).

172. Sun, D. *et al.* A Novel Nanoparticle Drug Delivery System: The Anti-inflammatory Activity of Curcumin Is Enhanced When Encapsulated in Exosomes. *Mol. Ther.* **18**, 1606–1614 (2010).

173. Kordelas, L. *et al.* MSC-derived exosomes: a novel tool to treat therapy-refractory graft-versus-host disease. *Leukemia* **28**, 970–973 (2014).

174. Lee, C. *et al.* Exosomes mediate the cytoprotective action of mesenchymal stromal cells on hypoxia-induced pulmonary hypertension. *Circulation* **126**, 2601–11 (2012).

175. Van Deun, J. *et al.* The impact of disparate isolation methods for extracellular vesicles on downstream RNA profiling. *J. Extracell. Vesicles* **3**, 1–14 (2014).

176. Rekker, K. *et al.* Comparison of serum exosome isolation methods for microRNA profiling. *Clin. Biochem.* **47**, 135–138 (2014).

177. Alvarez, M. L., Khosroheidari, M., Kanchi Ravi, R. & DiStefano, J. K. Comparison of protein, microRNA, and mRNA yields using different methods of urinary exosome isolation for the discovery of kidney disease

biomarkers. *Kidney Int.* **82**, 1024–1032 (2012).

178. Gallart-Palau, X. *et al.* Extracellular vesicles are rapidly purified from human plasma by PRotein Organic Solvent PRecipitation (PROSPR). *Sci. Rep.* **5**, (2015).
179. van der Pol, E., Böing, A. N., Gool, E. L. & Nieuwland, R. Recent developments in the nomenclature, presence, isolation, detection and clinical impact of extracellular vesicles. *J. Thromb. Haemost.* **14**, 48–56 (2016).
180. Baranyai, T. *et al.* Isolation of exosomes from blood plasma: Qualitative and quantitative comparison of ultracentrifugation and size exclusion chromatography methods. *PLoS One* **10**, 1–13 (2015).
181. Hong, C.-S., Funk, S., Muller, L., Boyiadzis, M. & Whiteside, T. L. Isolation of biologically active and morphologically intact exosomes from plasma of patients with cancer. *J. Extracell. Vesicles* **5**, 29289 (2016).
182. Bo, A. N. *et al.* Single-step isolation of extracellular vesicles by size-exclusion chromatography. *J. Extracell. vesicles* **3**, 1–11 (2014).
183. Gámez-Valero, A. *et al.* Size-Exclusion Chromatography-based isolation minimally alters Extracellular Vesicles' characteristics compared to precipitating agents. *Sci. Rep.* **6**, (2016).
184. Konoshenko, M. Y., Lekchnov, E. A., Vlassov, A. V. & Laktionov, P. P. Isolation of Extracellular Vesicles: General Methodologies and Latest Trends. *Biomed Res. Int.* **2018**, (2018).
185. Kim, K. *et al.* Cyclic tangential flow filtration system for isolation of extracellular vesicles. *APL Bioeng.* **5**, (2021).
186. Han, Z. *et al.* Highly efficient exosome purification from human plasma by tangential flow filtration based microfluidic chip. *Sensors Actuators, B Chem.* **333**, 129563 (2021).
187. Liang, L. G. *et al.* An integrated double-filtration microfluidic device for isolation, enrichment and quantification of urinary extracellular vesicles for detection of bladder cancer. *Sci. Rep.* **7**, 1–10 (2017).
188. Liu, F. *et al.* The Exosome Total Isolation Chip. *ACS Nano* **11**, 10712–10723 (2017).
189. Woo, H. K. *et al.* Exodisc for Rapid, Size-Selective, and Efficient Isolation and Analysis of Nanoscale Extracellular Vesicles from Biological Samples. *ACS Nano* **11**, 1360–1370 (2017).
190. Muller, L., Hong, C.-S., Stolz, D. B., Watkins, S. C. & Whiteside, T. L. Isolation of biologically-active exosomes from human plasma. *J. Immunol. Methods* **411**, 55–65 (2014).
191. Li, P., Kaslan, M., Lee, S. H., Yao, J. & Gao, Z. Progress in Exosome Isolation Techniques. *Theranostics* **7**, 789–804 (2017).
192. Gardiner, C. *et al.* Techniques used for the isolation and characterization of extracellular vesicles: Results of a worldwide survey. *J. Extracell. Vesicles* **5**, (2016).
193. Welton, J. L., Webber, J. P., Botos, L. A., Jones, M. & Clayton, A. Ready-made chromatography columns for extracellular vesicle isolation from plasma. *J. Extracell. Vesicles* **4**, 1–9 (2015).
194. Vergauwen, G. *et al.* Confounding factors of ultrafiltration and protein analysis in extracellular vesicle research. *Sci. Rep.* **7**, 1–12 (2017).
195. Mcnamara, R. P. *et al.* Large-scale , cross-flow based isolation of highly pure and endocytosis-competent extracellular vesicles. *J. Extracell. Vesicles* **8**, (2018).
196. Busatto, S. *et al.* Tangential Flow Filtration for Highly Efficient Concentration of Extracellular Vesicles from Large Volumes of Fluid. *Cells* **7**, 273 (2018).
197. Liangsupree, T., Multia, E. & Riekkola, M. Modern isolation and separation techniques for extracellular vesicles. *J. Chromatogr. A* **1636**, 461773 (2021).
198. Arslan, F. *et al.* Mesenchymal stem cell-derived exosomes increase ATP levels, decrease oxidative stress

and activate PI3K/Akt pathway to enhance myocardial viability and prevent adverse remodeling after myocardial ischemia/reperfusion injury. *Stem Cell Res.* **10**, 301–312 (2013).

199. Musante, L. *et al.* A simplified method to recover urinary vesicles for clinical applications, and sample banking. *Sci. Rep.* **4**, (2014).
200. Moutsatsou, P., Ochs, J., Schmitt, R. H., Hewitt, C. J. & Hanga, M. P. Automation in cell and gene therapy manufacturing: from past to future. *Biotechnol. Lett.* **41**, 1245–1253 (2019).
201. Desjardins-Park, H. E., Foster, D. S. & Longaker, M. T. Fibroblasts and wound healing: An update. *Regenerative Medicine* **13**, 491–495 (2018).
202. Stunova, A. & Vistejnova, L. Dermal fibroblasts—A heterogeneous population with regulatory function in wound healing. *Cytokine and Growth Factor Reviews* **39**, 137–150 (2018).
203. Maarof, M., Lokanathan, Y., Ruszymah, H. I., Saim, A. & Chowdhury, S. R. Proteomic Analysis of Human Dermal Fibroblast Conditioned Medium (DFCM). *Protein J.* **37**, 589–607 (2018).
204. Padeta, I., Nugroho, W. S., Kusindarta, D. L., Fibrianto, Y. H. & Budipitojo, T. Mesenchymal Stem Cell-conditioned Medium Promote the Recovery of Skin Burn Wound. *Asian J. Anim. Vet. Adv.* **12**, 132–141 (2017).
205. Théry, C., Amigorena, S., Raposo, G. & Clayton, A. Isolation and Characterization of Exosomes from Cell Culture Supernatants and Biological Fluids. *Curr. Protoc. Cell Biol.* 1–29 (2006). doi:10.1002/0471143030.cb0322s30
206. Chen, L. *et al.* Conditioned medium from hypoxic bone marrow-derived mesenchymal stem cells enhances wound healing in mice. *PLoS One* **9**, (2014).
207. Walter, M. N. M., Wright, K. T., Fuller, H. R., MacNeil, S. & Johnson, W. E. B. Mesenchymal stem cell-conditioned medium accelerates skin wound healing: An in vitro study of fibroblast and keratinocyte scratch assays. *Exp. Cell Res.* **316**, 1271–1281 (2010).
208. Saheli, M. *et al.* Human mesenchymal stem cells-conditioned medium improves diabetic wound healing mainly through modulating fibroblast behaviors. *Arch. Dermatol. Res.* **312**, 325–336 (2020).
209. Takeuchi, R., Katagiri, W., Endo, S. & Kobayashi, T. Exosomes from conditioned media of bone marrow-derived mesenchymal stem cells promote bone regeneration by enhancing angiogenesis. *PLoS One* **14**, e0225472 (2019).
210. Han, S. K., Chun, K. W., Gye, M. S. & Kim, W. K. The effect of human bone marrow stromal cells and dermal fibroblasts on angiogenesis. *Plast. Reconstr. Surg.* **117**, 829–835 (2006).
211. Lee, C. H., Han, S. K., Choi, W. Il & Kim, W. K. Effect of human bone marrow stromal cells and dermal fibroblasts on collagen synthesis and epithelization. *Ann. Plast. Surg.* **59**, 713–719 (2007).
212. Kim, J. B., Chun, K. W., Han, S. K. & Kim, W. K. Effect of human bone marrow stromal cell allograft on proliferation and collagen synthesis of diabetic fibroblasts in vitro. *J. Plast. Reconstr. Aesthetic Surg.* **63**, 1030–1035 (2010).
213. Han, S. K., Yoon, T. H., Lee, D. G., Lee, M. A. & Kim, W. K. Potential of human bone marrow stromal cells to accelerate wound healing in vitro. *Ann. Plast. Surg.* **55**, 414–419 (2005).
214. Zhang, Y., Liu, Y., Liu, H. & Tang, W. H. Exosomes: Biogenesis, biologic function and clinical potential. *Cell Biosci.* **9**, 1–18 (2019).
215. Hu, S. *et al.* Needle-Free Injection of Exosomes Derived from Human Dermal Fibroblast Spheroids Ameliorates Skin Photoaging. *ACS Nano* **13**, 11273–11282 (2019).
216. Zhang, W. *et al.* Cell-free therapy based on adipose tissue stem cell-derived exosomes promotes wound

healing via the PI3K/Akt signaling pathway. *Exp. Cell Res.* **370**, 333–342 (2018).

217. Zhao, G. *et al.* MSC-derived exosomes attenuate cell death through suppressing AIF nucleus translocation and enhance cutaneous wound healing. *Stem Cell Res. Ther.* **11**, (2020).
218. Hoang, D. H. *et al.* Differential Wound Healing Capacity of Mesenchymal Stem Cell-Derived Exosomes Originated From Bone Marrow, Adipose Tissue and Umbilical Cord Under Serum- and Xeno-Free Condition. *Front. Mol. Biosci.* **7**, 119 (2020).
219. Tsao, Y. S. *et al.* Monitoring Chinese hamster ovary cell culture by the analysis of glucose and lactate metabolism. *J. Biotechnol.* **118**, 316–327 (2005).
220. Cruz, H. J., Freitas, C. M., Alves, P. M., Moreira, J. L. & Carrondo, M. J. T. Effects of ammonia and lactate on growth , metabolism , and productivity of BHK cells°. **27**, 43–52 (2000).
221. Rojewski, M. T. *et al.* GMP-Compliant Isolation and Expansion of Bone Marrow-Derived MSCs in the Closed, Automated Device Quantum Cell Expansion System. *Cell Transplant.* **22**, 1981–2000 (2013).
222. Nold, P., Brendel, C., Neubauer, A., Bein, G. & Hackstein, H. Good manufacturing practice-compliant animal-free expansion of human bone marrow derived mesenchymal stroma cells in a closed hollow-fiber-based bioreactor. *Biochem. Biophys. Res. Commun.* **430**, 325–330 (2013).
223. Haack-Sørensen, M. *et al.* Development of large-scale manufacturing of adipose-derived stromal cells for clinical applications using bioreactors and human platelet lysate. *Scand. J. Clin. Lab. Invest.* **78**, 293–300 (2018).
224. Mizukami, A. *et al.* A Fully-Closed and Automated Hollow Fiber Bioreactor for Clinical-Grade Manufacturing of Human Mesenchymal Stem/Stromal Cells. *Stem Cell Rev. Reports* **14**, 141–143 (2018).
225. Li, M. *et al.* Phenotypic and functional characterization of human bone marrow stromal cells in hollow-fibre bioreactors. *J. Tissue Eng. Regen. Med.* **6**, 369–377 (2012).
226. Yan, L. & Wu, X. Exosomes produced from 3D cultures of umbilical cord mesenchymal stem cells in a hollow-fiber bioreactor show improved osteochondral regeneration activity. *Cell Biol. Toxicol.* (2019). doi:10.1007/s10565-019-09504-5
227. Zhao, H. *et al.* Exosomes from adipose-derived stem cells attenuate adipose inflammation and obesity through polarizing M2 macrophages and beiging in white adipose tissue. *Diabetes* **67**, 235–247 (2018).
228. Jia, Y., Zhu, Y., Qiu, S., Xu, J. & Chai, Y. Exosomes secreted by endothelial progenitor cells accelerate bone regeneration during distraction osteogenesis by stimulating angiogenesis. *Stem Cell Res. Ther.* **10**, 1–13 (2019).
229. Heinemann, M. L. *et al.* Benchtop isolation and characterization of functional exosomes by sequential filtration. *J. Chromatogr. A* **1371**, 125–135 (2014).
230. Erickson, H. P. Size and shape of protein molecules at the nanometer level determined by sedimentation, gel filtration, and electron microscopy. *Biol. Proced. Online* **11**, 32–51 (2009).
231. SterliTECH Tip: What is Molecular Weight Cut-Off (MWCO)? Available at: https://www.sterlitech.com/blog/post/sterlitech-tip:-what-is-molecular-weight-cut-off-mwco. Date accessed: 30 Dec 2022.
232. Pall Laboratory. Choosing the Correct MWCO. Available at: https://www.pall.com/content/dam/pall/laboratory/literature-library/non-gated/PALL_ChooseCorrect MWCO3_21-0317.pdf. Date accessed: 30 Dec 2022.
233. Giacobbo, A., Bernardes, A. M., Rosa, M. J. F. & De Pinho, M. N. Concentration polarization in ultrafiltration/nanofiltration for the recovery of polyphenols from winery wastewaters. *Membranes (Basel).*

8, (2018).

234. Wetterau, G. E., Clark, M. M. & Anselme, C. A dynamic model for predicting fouling effects during the ultrafiltration of a groundwater. *J. Memb. Sci.* **109**, 185–204 (1996).
235. Crozes, G. F., Jacangelo, J. G., Anselme, C. & Laîné, J. M. Impact of ultrafiltration operating conditions on membrane irreversible fouling. *J. Memb. Sci.* **124**, 63–76 (1997).
236. Kang, S. K. & Choo, K. H. Use of MF and UF membranes for reclamation of glass industry wastewater containing colloidal clay and glass particles. *J. Memb. Sci.* **223**, 89–103 (2003).
237. Md Yunos, K. F., Mazlan, N. A., Naim, M. N. M., Baharuddin, A. S. & Hassan, A. R. Ultrafiltration of palm oil mill effluent: Effects of operational pressure and stirring speed on performance and membranes fouling. *Environ. Eng. Res.* **24**, 263–270 (2019).
238. Choi, H., Zhang, K., Dionysiou, D. D., Oerther, D. B. & Sorial, G. A. Influence of cross-flow velocity on membrane performance during filtration of biological suspension. *J. Memb. Sci.* **248**, 189–199 (2005).
239. Field, R. W., Wu, D., Howell, J. A. & Gupta, B. B. Critical flux concept for microfiltration fouling. *J. Memb. Sci.* **100**, 259–272 (1995).
240. Lee, N. H., Amy, G., Croué, J. P. & Buisson, H. Morphological analyses of natural organic matter (NOM) fouling of low-pressure membranes (MF/UF). *J. Memb. Sci.* **261**, 7–16 (2005).
241. Jönsson, A. S. Influence of shear rate on the flux during ultrafiltration of colloidal substances. *J. Memb. Sci.* **79**, 93–99 (1993).
242. Quezada, C., Estay, H., Cassano, A., Troncoso, E. & Ruby-Figueroa, R. Prediction of permeate flux in ultrafiltration processes: A review of modeling approaches. *Membranes (Basel).* **11**, (2021).
243. Jones, G. & Talley, S. K. The viscosity of aqueous solutions as a function of the concentration. *J. Am. Chem. Soc.* **55**, 624–642 (1933).
244. Hoffmann, D. *et al. Purification of new biologicals using membrane-based processes*. *Current Trends and Future Developments on (Bio-) Membranes: Membrane Processes in the Pharmaceutical and Biotechnological Field* (Elsevier Inc., 2018). doi:10.1016/B978-0-12-813606-5.00005-1
245. Lutz, H. Chapter 5 - Configurations. in *Ultrafiltration for Bioprocessing* 77–94 (2015). doi:10.1016/B978-1-907568-46-6/00005-7
246. Takov, K. *et al.* Comparison of small extracellular vesicles isolated from plasma by ultracentrifugation or size- exclusion chromatography : yield , purity and functional potential. *J. Extracell. Vesicles* **8**, (2019).
247. Abramowicz, A. *et al.* Harmonization of exosome isolation from culture supernatants for optimized proteomics analysis. *PLoS One* **13**, 1–15 (2018).
248. Cvjetkovic, A., Lötvall, J. & Lässer, C. The influence of rotor type and centrifugation time on the yield and purity of extracellular vesicles. *J. Extracell. Vesicles* **3**, 1–11 (2014).
249. Li, C. *et al.* Novel scale-up strategy based on three-dimensional shear space for animal cell culture. *Chem. Eng. Sci.* **212**, 115329 (2020).